Report No. CDOT-2013-13
Final Report

LONG-TERM MONITORING OF MECHANICAL PROPERTIES OF FRP REPAIR MATERIALS

Rebecca A. Atadero
Douglas G. Allen
Oscar R. Mata

July 2013

COLORADO DEPARTMENT OF TRANSPORTATION
DTD APPLIED RESEARCH AND INNOVATION BRANCH

The contents of this report reflect the views of the author(s), who is(are) responsible for the facts and accuracy of the data presented herein. The contents do not necessarily reflect the official views of the Colorado Department of Transportation or the Federal Highway Administration. This report does not constitute a standard, specification, or regulation.

Technical Report Documentation Page

1. Report No.	2. Government Accession No.	3. Recipient's Catalog No.
CDOT-2013-13		

4. Title and Subtitle	5. Report Date
LONG-TERM MONITORING OF MECHANICAL PROPERTIES OF FRP REPAIR MATERIALS	July 2013
	6. Performing Organization Code

7. Author(s)	8. Performing Organization Report No.
Dr. Rebecca A. Atadero, Douglas G. Allen, Oscar R. Mata	CDOT-2013-13

9. Performing Organization Name and Address	10. Work Unit No. (TRAIS)
Department of Civil & Environmental Engineering Colorado State University Fort Collins, CO 80521	11. Contract or Grant No. 85.11

12. Sponsoring Agency Name and Address	13. Type of Report and Period Covered
Colorado Department of Transportation - Research 4201 E. Arkansas Ave. Denver, CO 80222	Final
	14. Sponsoring Agency Code

15. Supplementary Notes
Prepared in cooperation with the US Department of Transportation, Federal Highway Administration

16. Abstract
Fiber- reinforced polymer composites (FRP) are an attractive repair option for existing concrete structures. CDOT has used this material on some projects, in particular the repair of the Castlewood Canyon Bridge in 2003. Further use of the material is limited by the lack of data about its long-term performance. Laboratory durability studies have indicated that FRP performs well in conditions such as water and salt water baths, but it is difficult to fully capture field environments in the lab. This project evaluated the condition of the FRP on the Castlewood Canyon Bridge through onsite inspection and pull-off tests, and by bringing FRP back to the labs at CSU to test the tensile strength. Conclusions about the FRP condition are limited by the lack of baseline data, but there does appear to be some deterioration over time. This project also considers the influence of deicing agents on FRP properties through laboratory testing that has been initiated.

Implementation:
Based on results available at this time it is recommended that CDOT monitor the durability of future FRP applications through a more systematic process in which baseline data is collected and maintained and inspections including material testing are conducted at shorter intervals, perhaps every two to three years.

17. Keywords	18. Distribution Statement
Castlewood Canyon Bridge, concrete structures, bridge repair, fiber-reinforced polymer composites (FRP), bond strength, pull-off tests, tensile strength, deicing agents, magnesium chloride	This document is available on the CDOT website http://www.coloradodot.info/programs/research/pdfs

19. Security Classif. (of this report)	20. Security Classif. (of this page)	21. No. of Pages	22. Price
Unclassified	Unclassified	181	

Form DOT F 1700.7 (8-72) Reproduction of completed page authorized

Long-Term Monitoring of Mechanical Properties of FRP Repair Materials

Report No. CDOT 2013-13

Prepared by:

Rebecca A. Atadero, Assistant Professor
Douglas G. Allen, Graduate Research Assistant
Oscar R. Mata, Graduate Research Assistant
Department of Civil & Environmental Engineering
Colorado State University
Fort Collins, CO 80523

Sponsored by:

Colorado Department of Transportation
DTD Applied Research and Innovation Branch
4201 E. Arkansas Ave.
Denver, CO 80222

July 2013

ACKNOWLEDGEMENTS

The authors would like to thank the Colorado Department of Transportation for their assistance and financial support of this project. Funding for this project was also provided through the Mountain Plains Consortium, the USDOT Regional University Transportation Center for Region 8. The authors thank CDOT personnel that helped shape the project through meetings and feedback, including Mike Mohseni, Aziz Khan, Trevor Wang, Matt Greer, Eric Prieve, and William Outcalt. Also, instrumental in the field assessment at the bridge were CDOT personnel Thomas Moss and David Weld. The authors would also like to thank HJ3 Composite Technologies for providing the FRP materials for the repair of the areas damaged areas during the assessment on the bridge, as well as materials for the long-term laboratory testing. Furthermore, HJ3 employees Steve Nunn, George Salustro, and Olley Scholer also provided technical expertise. Lastly, the authors would like to acknowledge Josh Trujillo and Mark Wolfe from Envirotech Services for providing the deicing agents for laboratory testing, and for further assistance on the study including testing of solution concentrations.

EXECUTIVE SUMMARY

Fiber-reinforced polymer composites (FRP) are an attractive repair option for reinforced concrete structures, however their long-term performance in field environments is not well understood. Laboratory durability tests have indicated that FRP generally performs quite well, but these laboratory tests cannot model the synergistic effects that occur when the FRP is in-service on a bridge (or other structure), and agents of interest to CDOT have not been fully considered. This research project was initiated to gain better information about the field performance of FRP.

The project consisted of five research tasks, plus an additional reporting task. Tasks 1-3 were devoted to assessing the present condition of the FRP used to repair the Castlewood Canyon Bridge on State Highway 83 in 2003. Task 4 was a literature review task to determine additional information about questions and concerns related to FRP application posed by CDOT engineers. Task 5 was a laboratory durability study to consider the effects of deicing agents on FRP. Task 6 is the reporting task. This final report has been prepared to satisfy the requirements of this task.

Task 1 required the collection of data about the bridge and its repair and planning for the field assessment. Although many people were contacted, and the project team was able to look through the project box at stored at Region 1, only limited amounts of initial data about the bridge and its repair were collected. A tentative plan for site assessment activities was prepared, including testing locations at the base and crest of the arch.

Task 2 was the field assessment task. This task was completed at the bridge location during July, 2011. The complete extrados of the east arch was inspected for voids between the concrete and FRP using acoustic sounding. Voids that were previously identified during a routine bridge inspection in 2007 had grown significantly larger by the 2011 assessment. Pull-off tests were used to test the bond strength at the base and top of the arch. Pull-off strengths were on average lower and represented different failure modes from pull-off tests conducted at the time of repair. Large debonded regions of FRP were cut from the structure to use in laboratory testing for Task 3. Damaged regions were repaired with new FRP.

In Task 3, materials brought back from the bridge were used for tensile and Differential Scanning Calorimetry (DSC) testing. The tensile tests showed that the FRP strength was well below the specified design strength, but the lack of initial data makes it difficult to tell if the material has deteriorated over time, or if the material started off with lower strengths due to field manufacture techniques. The DSC tests showed that the glass transition temperature of the composites was near the value suggested by the manufacturer.

Task 4 required literature review of topics including fatigue, environmental and chemical exposure, bond behavior, and existing design details and guidance. Literature on topics directly related to Task 1-3 and Task 5 – bond behavior and environmental and chemical exposure – are discussed with the related task. This section of report focuses on fatigue performance of RC members with externally bonded FRP strengthening and existing design guidance.

Task 5 involved laboratory durability testing to determine the effect of deicing agents on FRP. A magnesium chloride based deicer and an alternative deicer were obtained from Envirotech Services. Two types of concrete specimens with bonded FRP were prepared, blocks for pull-off testing and small beams for flexural testing. The specimens were placed in several different exposure environments starting in June 2011. Testing with six months of exposure was conducted in December 2011, and one year tests were conducted in June 2012. Following completion of the durability study, a new section (Section 7.0) was included in this report which discusses the direct tension pull-off test method. After conducting pull-off tests in the field and the laboratory, examination of the results raised questions as far as reliability of this method, and interpretation of results. Therefore, additional research was conducted on this method. Past laboratory and field studies are summarized in Section 7.0, and their results were analyzed.

Implementation

The conclusions drawn from the field assessment of the FRP on the Castlewood Canyon Bridge are limited by the lack of initial data, and the fact that no intermediate testing was conducted between the repair in 2003 and this research project in 2011. The FRP seems to be holding up reasonably well, but the

performance is difficult to quantify. It is recommended that CDOT monitor the durability of future FRP applications through a more systematic process in which baseline data is collected and maintained and inspections including material testing are conducted at shorter intervals, perhaps every two to three years.

The results of the laboratory durability study are not conclusive, as the direct tension pull-off test was found to be subject to high degrees of variability. This type of testing is currently used as a required quality control procedure on FRP repair projects. However, the results of this testing are often difficult to interpret and may be more indicative of the quality of the existing concrete than the FRP repair. For this reason it is also recommended that CDOT consider other forms of quality control such as acoustic sounding for evaluating FRP repairs.

TABLE OF CONTENTS

LIST OF TABLES

LIST OF FIGURES

1.0 INTRODUCTION

Fiber-reinforced polymer composites (FRP) have been proven effective at restoring or increasing the capacity of existing reinforced and prestressed concrete elements and structures. These materials possess several properties that make them an attractive repair option including their light weight, small profile, ability to conform to existing geometries, and durability. Although the materials themselves can be expensive when compared to the materials used in conventional repairs, the overall repair operation can be cost-effective.

Currently, a primary issue limiting the application of FRP to repair transportation structures in Colorado is concern about the long-term performance of FRP repairs. Although FRP has been the subject of numerous durability studies, these studies have generally been conducted through accelerated testing in the lab and there is relatively little information available regarding long-term field performance. In particular, questions exist about the performance of FRP and its bond to concrete in environmental conditions representative of Colorado.

This project was created to study the long-term performance of FRP in field conditions though 1) a field investigation of the FRP used to repair the Castlewood Canyon Bridge in 2003 and 2) a laboratory durability study to consider the effect of deicing agents on FRP. The project also includes a literature review to consider other FRP related questions of CDOT engineers.

The specific tasks included in this project are:

1. Collect Information and Develop Data Collection and Testing Plans for Field Assessment
2. Conduct Testing/Observations on Site and Collect Samples for the Laboratory
3. Laboratory Testing of FRP Samples and Analysis of Data
4. Literature Review on Additional FRP Topics
5. Establish Long-term Testing Program to Consider the Effect of Deicers on FRP
6. Reporting

2.0 TASK 1: COLLECT INFORMATION AND DEVELOP DATA COLLECTION AND TESTING PLANS FOR FIELD ASSESSMENT

2.1 The Castlewood Canyon Bridge

One of the first reinforced concrete arch bridges retrofitted with FRP, the Castlewood Canyon Bridge is located approximately 6.4 km (4 mi) south of Franktown, Colorado on State Highway 83.

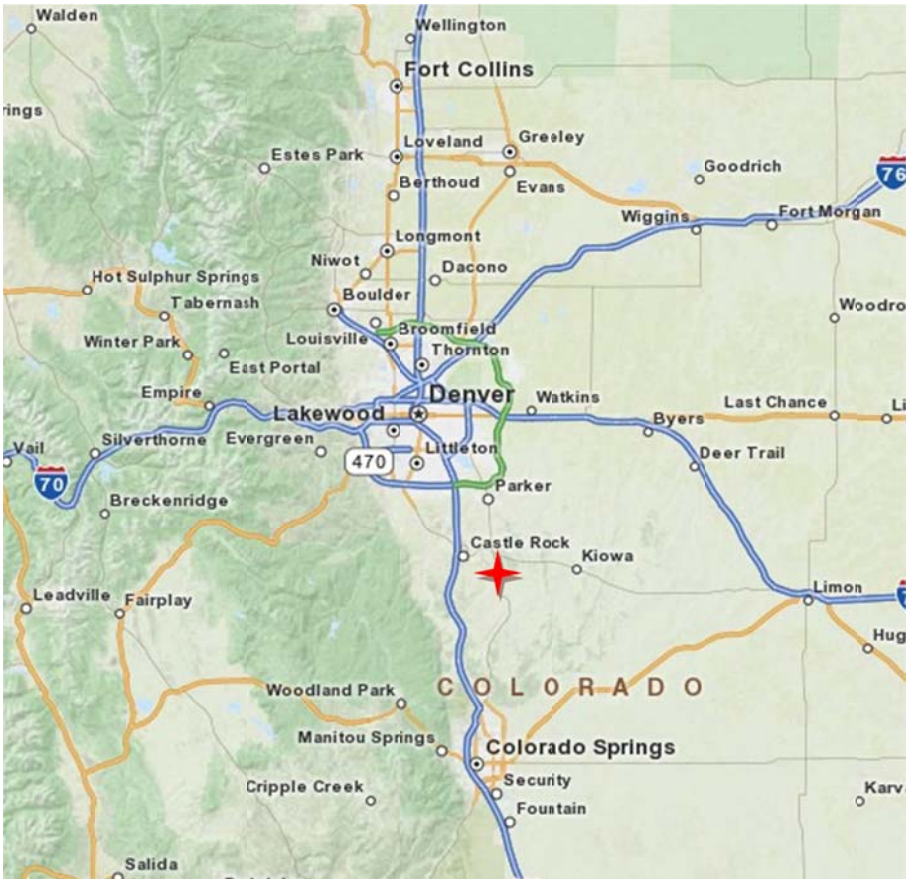

Figure 2.1. Castlewood Canyon Bridge location indicated by the red star

Figure 2.2. Castlewood Canyon Bridge (Mohseni, CDOT)

The Castlewood Canyon Bridge was originally built in 1946 and underwent a major renovation in 2003. The bridge deck and spandrel columns were replaced with precast reinforced concrete members and the existing arches were repaired with CFRP. The identical arches that span approximately 70.1 m (230 ft) in the north-south direction over Cherry Creek were strengthened in shear, flexure, and axially using CFRP. The arch repair also consisted of reinforcing the bases of the arches and wrapping the struts between the arches using a wet-layup application of CFRP fabric.

The arches and their repair comprise the area of focus for this project. At the time of the renovation, in collaboration with the Research Branch of the Colorado Department of Transportation (CDOT), the University of Colorado, Boulder produced a report titled "Evaluation of the FRP-Retrofitted Arches in the Castlewood Canyon Bridge" (Fafach et al., 2005) that included documentation of the arch repair process and results from laboratory durability studies, structural modeling and testing, and instrumentation of the repaired structure. Due to this research effort, significantly more information and details were documented and made available for future study than similar repair/retrofitting/reconstruction projects.

Photographs of the bridge prior to and following the 2003 repair can be seen below in Figures 2.3 and 2.4.

Figure 2.3. Castlewood Canyon Bridge prior to the 2003 repair (Mohseni, CDOT)

Figure 2.4. Castlewood Canyon Bridge after the 2003 repair (Mohseni, CDOT)

For purposes of this report, sections of arch between spandrel columns are referred to as “bays” and their numbering begins at 1 in the first bay between the ground and the 1st spandrel column, ending at 6 which is the middle section at the crest of the arch. North and south are used to denote the two halves of each arch, and the two arches are indicated as west and east, referring to their orientation relative to each other. As an example, the 2SE bay refers to the second bay (between the 1st and 2nd columns) of the east arch on the south end. The majority of the field evaluation in 2011 was conducted on the extrados of the east arch. Below is a plan view of the arches, struts and columns.

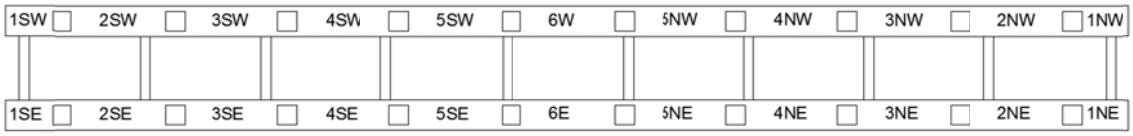

Figure 2.5. Plan view of the arches, struts, and column pedestals showing the bay labeling scheme

2.2 Renovation in 2003

The renovation in 2003 consisted of reinforcing and strengthening the arches and struts with CFRP and replacing the spandrel columns, pier caps, and bridge deck with precast reinforced concrete members.

2.2.1 Replacement of Spandrel Columns, Pier Caps, and Bridge Deck

The renovation began with repairing the base of the arches with Leadline™ CFRP rods and the arches and struts with CFRP fabric using the wet lay-up process. The spandrel columns, pier caps, and bridge deck were replaced between Phases 2 and 3 of the CFRP wet lay-up application on the arches and struts explained below. The bridge deck was widened by about 2.44 m (8 ft) to 13.11 m (43 ft) wide and was systematically replaced with precast reinforced concrete members to prevent unsymmetrical loads on the arches during the renovation, seen below.

Figure 2.6. Systematically replacing the bridge deck (Mohseni, CDOT)

Figure 2.7 is a photograph of spandrel columns being replaced with precast reinforced concrete members on new pedestals adjacent to the original columns.

Figure 2.7. Placing the new spandrel columns adjacent to the existing columns (Mohseni, CDOT)

2.2.2 Repair of Arches and Struts

Prior to repair the concrete arches had severe spalling due to the corrosion of the internal steel reinforcement as seen in the photographs in Figure 2.8.

Figure 2.8. Concrete spalling on arch section prior to repair (Mohseni, CDOT)

Loose concrete, typically no more than the few inches of concrete cover, was removed with 6.8 kg (15 lb.) jack hammers and the exposed steel reinforcement was sandblasted free of rust. Seen below,

the cross-section was restored with shotcrete which included a corrosion inhibitor, Sika FerroGard 903, to prevent further corrosion of the steel reinforcement.

Figure 2.9. Removal of loose concrete using 6.8 kg (15 lbs.) jackhammer and restoring the cross section with shotcrete (Mohseni, CDOT)

The cross-section of the arches tapers in thickness from 1.78 m (70 in) at the base to 1.02 m (40 in) at the peak of the arch, while the width remains constant at 1.93 m (76 in) wide. Once the cross-sections of the arches were restored, FRP was adhered in three phases. Phase 1 consisted of installing longitudinal and transverse CFRP between the arch base and the first spandrel column. More longitudinal CFRP was used on the extrados than the intrados in this area to resist large negative moments generated from a concentrated truck load located at the second spandrel column. The arches were wrapped transversely confining the arches to provide axial and shear strengthening. The transverse wraps alternated between wrapping entirely around the cross-section and wraps that only covered the sides and extrados of the arch. This alternating pattern created intentional areas without FRP on the intrados of the arch that allowed the arches the ability to drain and/or remove humidity or moisture. During Phase 2, longitudinal CFRP wraps were distributed evenly between the extrados and intrados of the remaining arch followed by transverse wraps with the same alternating pattern previously discussed. The transverse wraps were installed on the arches except where the existing columns were and where the replacement columns were going to be located. In Phase 3, these areas were wrapped after the new columns were

installed and the old columns were removed; the struts were also wrapped transversely with the alternating pattern used on the arches concluding the CFRP application.

Figures 2.10 and 2.11 below show photographs of the wet-layup process during Phase 1, and the longitudinal and transverse pattern of CFRP.

Figure 2.10. Fyfe's Tyfo® S Epoxy resin (likely with glass fibers as a filler) being applied to the extrados of an arch and installation of saturated unidirectional CFRP fabric, Tyfo® SCH-41 (Mohseni, CDOT)

Figure 2.11. Longitudinal and transverse CFRP wraps at the base of an arch (Mohseni, CDOT)

The arches and struts were then painted with an exterior acrylic paint to prevent and/or reduce degradation to the resin caused by moisture and UV and to restore the original appearance matching the concrete color.

2.2.3 Initial Values and Quality Control of the Renovation in 2003

As a measure of quality assurance, the contractor of the renovation, Restruction Corporation, was responsible to "obtain suitable documentation from the manufacturer showing results from an independent agency that all materials used in this system meet or exceed the requirements" (CDOT's construction specifications (Revision of Section 602)). The following are some of the codes and reference standards used to define the requirements in CDOT's construction specifications: ACI 440R-96, ACI 318-99, ACI 515R, ACI 546R-96, ASTM D3039, ASTM D4541, ICRI Guideline No. 03730, ICRI Guideline No. 3732, and ICRI Guideline No. 03733.

2.2.3.1 Tensile Properties of CFRP

From CDOT's construction specifications (Revision of Section 602), the number of layers of CFRP necessary was calculated by Fyfe and was to meet the following performance criteria:

- Minimum ultimate rupture strain = 0.006 cm/cm (0.006 inch/inch)
- Resist a force of no less than 320.9 KN per linear meter (22 KIPS per linear ft.), this strength shall be determined at a strain no greater than a usable strain of 0.0043 cm/cm (0.0043 inch/inch).
- The ultimate tensile strength shall be the mean tensile strength of a sample of test specimens (a minimum of 20 replicate test specimens) minus three times the standard deviation.
- The ultimate rupture strain shall be the mean rupture strain of a sample of test specimens (a minimum of 20 replicate test specimens) minus three times the standard deviation.

Restruction was to obtain "suitable documentation" from Fyfe showing results from an independent agency that all materials used in this system met or exceeded these requirements and Restruction was to submit this documentation a minimum of two weeks prior to start of work. Fyfe

published a guarantee of the mechanical tensile properties but, the "suitable documentation" was not recovered but was assumed to exist due to the completion of the project.

Restruction was also required to provide two 30.5 cm x 30.5 cm (12" x 12") sample panels for every 92.9 m^2 (1000 ft^2) of FRP installed to be tested by an independent testing laboratory in accordance with ASTM D3039. The independent testing laboratory was to use one of the two panels to conduct tensile tests and prepare a summary report of all test results. Two panels were initially prepared with one panel held in reserve in case test results on the first panel did not meet specified performance criteria. No documentation of these tests was recovered.

Tensile tests were not conducted in the 2003 study conducted by CU, but values provided by the manufacturer of material properties were included in the CDOT report. These values are tabulated in a table below in Section 4.1.

2.2.3.2 Bond Strength of CFRP

The contractor was to provide a qualified representative on-site to ensure the proper installation of the CFRP. The representative was required to inspect each completed phase of the installation and advise the project engineer regarding repairs and replacements. No documentation of advice or notes was found in regard to this process.

The contractor was required to conduct a minimum of one direct pull-off test per 46.45 m^2 (500 ft^2) of surface of installed FRP to ensure the required minimum tensile strength of 1.38 MPa (200 psi) was satisfied. No documentation of these tests was recovered.

In addition, the contractor accompanied by the engineer and manufacturer's representative, was required to examine all surfaces 24 hours after application of FRP sheets and initial resin cure to check for voids, delaminations and air bubbles. The inspection was accomplished by visual observation and acoustic tapping tests to locate voids or defects. Areas of voids or delaminations can be detected due to the different sound emitted when tapped or when a solid object is slid over the area. Minor areas of voids of less than 38.7 cm^2 (6 in^2) were injected with resin to fill the void and provide a bond between the FRP and the substrate. Voids larger than 38.7 cm^2 (6 in^2) were repaired by removing and re-applying the

required number of layers of CFRP. A void that had been injected with resin directly following the CFRP application can be seen below in Figure 2.12. There was no documentation of this procedure or any information regarding the areas repaired or filled with resin, but it is assumed that this process was satisfactory.

Figure 2.12. Void injected with resin during 2003 renovation (Mohseni, CDOT)

Restruction was also required to utilize an independent testing laboratory, CTC-Geotek, Inc., to perform a minimum of two random field pull-off tests (ASTM 4541) for each day of FRP application. The pull-off tests were intended to ensure the minimum tensile strength of the substrate of 1.38 MPa (200 psi) was satisfied.

A total of 42 pull-off tests were conducted over 5 days, June 10, 13, 30 and July 9 and 17. From Field Observation Reports submitted by CTC-Geotek the following procedures were practiced:

- The pull-off test areas were prepared by core drilling through the composite material and approximately 1 cm (3/8”) into existing concrete.
- A 5.7 cm (2 ¼”) diameter core barrel was used in conjunction with a Hilti High Speed core rig
- 5.1 cm (2”) diameter pucks were placed using Devcon 10.34 MPa (1500 psi) fast-set epoxy

Tests were performed on both sides and on the extrados of the arches in the following bays: 1SE, 1SW, 1NW, 4NE, 4NW, 5SE, 5SW, 5NE, 5NW, 6E, 6W. The pull-off test locations can be seen below in Figure 2.13.

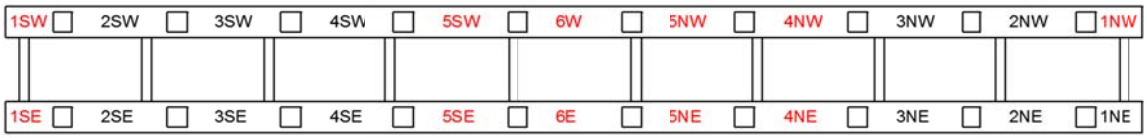

Figure 2.13. Pull-off test locations from 2003 denoted in red

A complete summary of the pull-off test results can be found in Appendix B. CTC-Geotek described the failure modes in a field observation report. The failure modes were converted to be consistent with the failure modes described in ASTM D7522, which is a standard specifically for FRP bonded to concrete substrate. This standard published in July 2009, was not available at the time of the tests conducted in 2003. Failure modes defined in ASTM D7522 are tabulated below.

Table 2.1. ASTM D7522 Failure Modes

Failure Mode	Description
A	Bonding adhesive failure at loading fixture
B	Cohesive failure in FRP laminate
C	Adhesive failure at FRP/adhesive interface
D	Cohesive failure adhesive
E	Adhesive failure at FRP/concrete interface
F	Mixed Mode E and Mode G
G	Cohesive failure in concrete substrate

Pull-off tests with failure modes other than Mode G are considered to be premature failures and are not desirable. Only one test from 2003 was not satisfactory with a pull-off strength of 1.32 MPa (191 psi), but was due to failure Mode A, and therefore was not of concern. Quantities of the different failure modes are tabulated in Table 2.2 below.

Table 2.2. Failure Modes of the pull-off tests conducted in 2003

42 Tests	Failure Modes of 2003 Pull-off tests							
	A	B	C	D	E	F	G	NA
Quantity	9	0	0	0	2	3	25	3
Percentage	21.4	0	0	0	4.8	7.1	59.5	7.1

After having a number of pull-off tests with a failure Mode A, the pull-off technique was altered to prevent the premature failure of subsequent tests. The tests with failure modes E and F failed at strength values higher than the minimum 1.38 MPa (200 psi) and, therefore it can be deduced that the tensile strength of the substrate also exceeded 1.38 MPa (200 psi). Further discussion of the results and subsequent pull-off tests resumes in Section 3.3.

2.3 Biannual Bridge Inspections

Biannual bridge inspections were conducted on the Castlewood Canyon Bridge following the renovation in 2005, 2007, and 2009. The 2011 bridge inspection had not yet occurred at the time of the field assessment in July 2011. The conditions of the CFRP material and its bond were evaluated as a component of these bridge inspections. These evaluations consisted of visual inspections and acoustic tapping tests of areas easily accessible which included the extrados and bases of the arches. The boundary of defects in the CFRP were outlined and dated with a “permanent” marker.

In discussing defects or voids in the CFRP composite system, it is necessary to further differentiate between the type of defect and the time of occurrence. The term “void” will be used to denote an area lacking a bond at some interface between the surface of the CFRP and the substrate, but with no distinction of when it developed. The term “unbonded” will refer to areas in which the FRP failed to bond to the substrate at the time of repair. The term “debonded” will be used to denote that at some point following the repair the FRP lost the bond to the substrate that it once had, and “delamination” will refer to a loss of bond between layers of CFRP. Voids found during the bridge inspections were denoted using familiar terminology of bridge inspectors as “DELAM” should be considered as voids and not delaminations. Bond loss between reinforcing steel and the concrete cover is often referred to as a

"delamination" by bridge inspectors. Cracks and other imperfections in the CFRP composite will be referred to as defects.

Assuming the tap tests performed directly after the repair were thorough and the FRP was bonded to the substrate at all locations following the repair procedure, any voids found during the bridge inspections were created during service and such debonded areas should be monitored to detect any additional damage that may occur. Debonded areas may increase in quantity or size over time and therefore careful documentation is necessary to evaluate the FRP system accurately.

Markings made with a permanent marker on the bridge from the 2007 bridge inspection were barely visible at the time of the 2011 field assessment. Depending on the exposure from moisture and sun, markings on the bridge can exist for only a relatively short time with respect to the life span of the bridge. Below are three photographs of the areas identified from June 2007, two of which were barely visible at the time of the July 2011 visit. There were no markings found on the east arch from the inspections in 2005 and 2009. In addition to the three voids, three cracks in the CFRP were also identified in 2007, one of which can be seen below.

Figure 2.14. Outlined in permanent marker are identified areas of debonding between the FRP and the substrate developed in the structure between inspections in 2007 and 2011. Faintly denoted in the bottom of the photographs (enclosed in red circles) are previously found voids identified with "DELAM 07" and lines distinguishing the boundaries of the voids.

Figure 2.15. Enclosed in permanent marker are identified areas of debonded areas between the FRP and the substrate from 2011 and June, 2007. Notice in this more protected bay of the structure the markings from 2007 are more clearly visible.

Figure 2.16. Crack identified in 2007

It is possible that additional markings on the bridge have become too faded to be recognized. The only other documentation of such markings are only briefly mentioned in bridge inspection report as "some areas of delams." This makes quantification of number and size of voids difficult to track over time. In addition, the development of debonded areas may appear more extreme under more meticulous and closer inspection.

2.4 Planning Tests and Locations

Planning for a field assessment to evaluate the durability of the CFRP application on the bridge began in the fall of 2010. Following literature review, evaluation techniques suitable for the Castlewood Canyon Bridge project were chosen to evaluate the durability of the FRP system. Pull-off tests, tensile tests, and differential scanning calorimetry (DSC) were chosen as the primary methods to evaluate the durability of the FRP application. The pull-off tests indicate values of bond strength which is essential to the performance of FRP composites. Tensile tests provide mechanical properties of the composite material. DSC tests evaluate the glass transition temperature of the composite which can significantly vary depending on the wet lay-up process and the exposure to moisture. Visual inspection, acoustic tapping tests, and thermal imaging were selected as identification methods to identify areas of voids and visible defects.

Two general locations, the crest and base of the arches, were locations of interest prior to the field assessment. The two locations have different exposures and stresses that could potentially affect the durability of the FRP application. The crest of the arch has less exposure than the base of the arch to moisture from precipitation such as driving rains and drifting snow due to the protection of the overhanging deck. However, because the crest of the arch is located closer to the bridge deck it is also more susceptible to moisture draining from the deck as well as deicing agents. The crest of the arch is also more protected from the sun and consequentially experiences lower thermal stresses than the base of the arch. As a typical arch structure, the base of the arch, in general, has larger stresses due to the self-weight of the arch as well as those generated from service loads. The differences between these two locations provide a variety of conditions that are known to have an impact on the durability of FRP composites.

In addition to conducting the tests described above at these two different locations, the effect of the two different substrates - concrete and shotcrete - on the bond and material properties was also an area of interest. However, it was not possible to identify whether the substrate was concrete or shotcrete at a particular location because the areas where shotcrete was applied during the repair in 2003 were not

documented other than in coincidental photographs documenting the progress of the project. Therefore, the effect of the different substrates was not determined in this assessment.

Conduct of the identification and testing methods was planned for the extrados of the arch for two reasons. The extradoses of the arches were easily accessed and navigated. Secondly, from the modeling in the CU study, this is an area that could potentially experience high stresses due to concentrated truck loads over the second spandrel column. Due to limited time and safety equipment the east arch was arbitrarily chosen as the primary arch of focus for the field assessment.

Due to conditions at the bridge site, the north end of the arches was chosen for access and as the location to conduct pull-off tests at the base of the arch. Particular locations to conduct pull-off tests were established in areas where there were no voids found using the thermal imaging infrared camera or tap tests.

Different techniques for pull-off tests were explored in the laboratory to ensure testing procedures accurately represented bridge conditions. Experiments with wet core drilling, dry core drilling, cleaning, sanding, epoxying, and cure times helped improve the pull-off test methods used in the field. Dry drilling caused too much heat and presumably exceeded the glass transition temperature of the epoxy between the FRP and the substrate and caused the FRP bond to prematurely fail. Drilling after the pucks were adhered to the FRP benefitted the starting of the coring, but presented difficulties due to the heat generated from friction whether the core drilling was wet or dry. The core drilling was more successful using a jig that provided the guidance to start the coring rather than the adhered puck. Wet core drilling introduced moisture and created problems in the adhesion of the pucks to the FRP. Drying and cleaning the adhesion surface with compressed air and alcohol provided the best method for adhesion after wet core drilling. Sanding the pucks with 40 grit sandpaper and a similar cleaning technique provided the preparation for sufficient bonds. Thorough mixing of the two-part epoxy and a minimum cure time of 1 hour were also critical to a successful pull-off test.

Tensile and DSC tests require equipment in the laboratory; therefore samples had to be collected from the bridge to be brought back to the lab for testing. Specimen sizes of CFRP strips approximately

2.5 cm (1”) wide and 20.3 cm (8”) long were required for the tensile test while samples for the DSC tests are 15 mg of finely ground particles or powder. The strips were planned to be collected from the outside corner of the arches in the locations of interest with the use of an abrasive cut-off wheel mounted on a right angle grinder and masonry chisel, and the DSC samples could easily be provided from material from the other tests or samples collected.

Experiments in the laboratory prior to the site visit with the infrared camera proved to be beneficial in learning the capabilities and ranges of thermal detection of the camera. Information in regard to surfaces could be received when a temperature differential existed. Because of the delicate nature of the information held in the transient state, it was anticipated that using the camera at different times of day would have significant benefits and drawbacks that would be difficult to predict. It was determined that it would be beneficial to have a preliminary site visit to establish the most effective thermal camera techniques.

A preliminary site visit would also provide an opportunity to establish transportation, parking, arch access, and safety procedures, as well as general familiarity with the project. Necessary equipment to conduct the field assessment included the following: gas-powered generator, air-compressor, hoses, extension cords, drill, grinder, ice, safety equipment, repair CFRP materials, and paint. Planning for the setup of this necessary equipment could also be accomplished by a preliminary site visit.

3.0 TASK 2: CONDUCT TESTING/OBSERVATIONS ON SITE AND COLLECT SAMPLES FOR THE LABORATORY

3.1 Preliminary Site Visit

Prior to the site visit, a Special Use Permit was acquired from the Colorado Department of Transportation (CDOT) to inform the necessary parties of the planned activities and to outline procedures and liability. On the 6th of July 2011, the field assessment of the durability of the FRP repair began with an orientation visit to the bridge. CDOT personnel present at the preliminary site visit included Thomas Moss, a bridge inspector for CDOT, and CDOT Research Staff, David Weld. Mr. Weld provided high-visibility safety vests, parking recommendations, assistance in maintaining proper procedure for roadside activity, and supervision. The north side of the bridge was used for parking and access to the arches. Parking off the shoulder was recommended to eliminate the need for lane-closures.

Mr. Weld was present for the duration of the field assessment as per CDOT policy. Mr. Moss provided guidance to the access of the arches, safety equipment (e.g. safety harnesses, lanyards, and safety ropes), and installation of the safety apparatus on the eastern arch. Mr. Moss demonstrated the proper technique to use the safety equipment. In addition Mr. Moss recounted previous bridge inspections and assisted in locating the previously identified areas of flaws in the FRP repair.

Once the safety rope system was installed on the east arch, a thermal imaging infrared camera, FLIR ThermaCAM™ E4, coupled with the use of a tap test were used to identify areas of voids between the CFRP and the substrate (either concrete or shotcrete) of the arch. Heating, cooling, and the effects of solar radiation on the surface of the arches were also explored in order to optimize the use of the thermal camera in detecting voids. Both thermal imaging and tap tests were used to confirm the existence of voids while the acoustic tapping test was more precise in determining the size and shape of the voids.

The thermal camera was used to identify areas where there was a significant temperature differential. In theory, the concrete or substrate acts as a “thermal sink” pulling heat applied to the surface through the CFRP in areas that are well bonded. Voids between the CFRP and the substrate would not allow the heat to conduct as quickly resulting in a “hot pocket” in the void. Cooling the surface would

also work in a similar manner. Multiple external sources of heat and cold were considered prior to the site visit: liquid nitrogen, liquid carbon dioxide, heat blankets, electric iron, heat gun etc. For various reasons these candidates were deemed unfit for the project. Liquid nitrogen and liquid carbon dioxide would provide temperatures of 78 K (-319˚ F) and 195 K (-109 ˚F) respectively. Because the coefficient of thermal expansion of CFRP and concrete differ of up to an order of magnitude, externally applying extreme temperatures would introduce thermal stresses possibly compromising the bond between the two materials. Therefore, it was reasoned that any heating or cooling to create a temperature differential should be limited to a moderate change relative to the ambient temperature. The electric iron and heat gun would both require electricity, and would not have significant advantages compared to a handheld propane heater. The use of heat blankets would have provided a more controllable uniformly heated area, but blankets large enough to justify their use would have been too heavy and cumbersome to handle in traversing the arches.

A handheld propane heater was used to supply an external heat source. Initially, the surface of the CFRP registered a constant temperature in the thermal camera due to the heating, followed by a transient state in which the substrate would pull the applied heat at well bonded areas but not in areas of voids. This method proved to be fairly time intensive including applying the heat and waiting for the transient state to occur. A 929 cm^2 (1 ft^2) section required approximately 3 minutes and the area of the extrados of only one arch exceeded 148.6 m^2 (1600 ft^2). In addition, it was difficult to apply the heat uniformly, resulting in thermal images containing transient temperature differentials due to the application of the heat not necessarily due to the area of voids.

Following the same philosophy as the externally applied heat an alternative technique of externally applying ice water to create a temperature differential was also tested. Using this technique the voids appear to the thermal camera as pockets of cold regions because the substrate conducts heat back to the CFRP in areas that are well bonded. This method was not effective either. Applying the ice water was easier than applying heat when considering large areas, but the transient state was delayed longer until the water on the surface was totally removed. In addition, the uniform contact time and contact area of the ice

water to the surface of the arch was difficult to control causing temperature differentials during the transient state that were due to the external application rather than areas of voids.

After trying the propane heater and ice water during the preliminary site visit, it was determined that solar radiation and no other externally applied sources of heat or cold other than that of the sun would be used for the final assessment. The effectiveness of using solar radiation proved to be highly sensitive to the intensity and duration of the exposure to sun or lack thereof. Thermal images from areas of the arch that had been shaded from the sun for long periods of time were more effective at locating areas of voids than areas that were transitioning in or out of direct sunlight.

Detection of areas of voids was much quicker with the thermal camera than the tap test technique, but the tap test technique was unmistakable in detecting voids. Depending on the recent thermal history, the thermal camera would produce images that would suggest areas of voids that may or may not actually represent areas of voids. The tap test not only was used to find areas of voids and confirm areas of voids found by the infrared camera, but also to identify the size and shapes of the voids.

The preliminary site visit provided the following conclusions:

- Parking and access would be at the north end of the arches
- Thomas Moss would set-up a similar safety system extending the entire length of the arch for the field assessment on July 11th 2011
- The extradoses and east arch would be accessible and the primary focus of the field assessment
- Quantity, size, and shape of voids would be detected by the coupled use of the thermal camera and acoustic tapping tests
- The thermal camera would rely solely on solar radiation for void detection
- The bridge deck replaced in 2003 was continuous and waterproof with no expansion joints or areas of leakage. The bridge deck appeared to be protecting the arches from any exposure to deicing agents

3.2 Void Detection

The week-long field assessment of the durability of CFRP began with detecting voids on July 11, 2011. It was important to detect any areas of voids not only to evaluate the condition of the CFRP bond to the substrate globally but also in order to avoid these areas when conducting pull-off tests.

Thermal imaging and acoustic tapping techniques established from the preliminary site visit were employed to discover the existing voids on the extrados of the entire east arch as well as the 1st bay on the north end of the west arch. In areas where the solar radiation was not ideal, acoustic tapping tests were relied upon to detect voids. In most areas, the thermal camera was more time efficient in detecting voids, but the acoustic tapping test method was more thorough in detecting voids.

A typical thermal image of voids, shown below in Figure 3.1, provided the temperature of the location of the cross hairs in the upper right hand corner of the image, a color-coded temperature scale on the right side of the image, and the time, e (emissivity), and Trefl (the reflected ambient temperature) at the bottom of the figure.

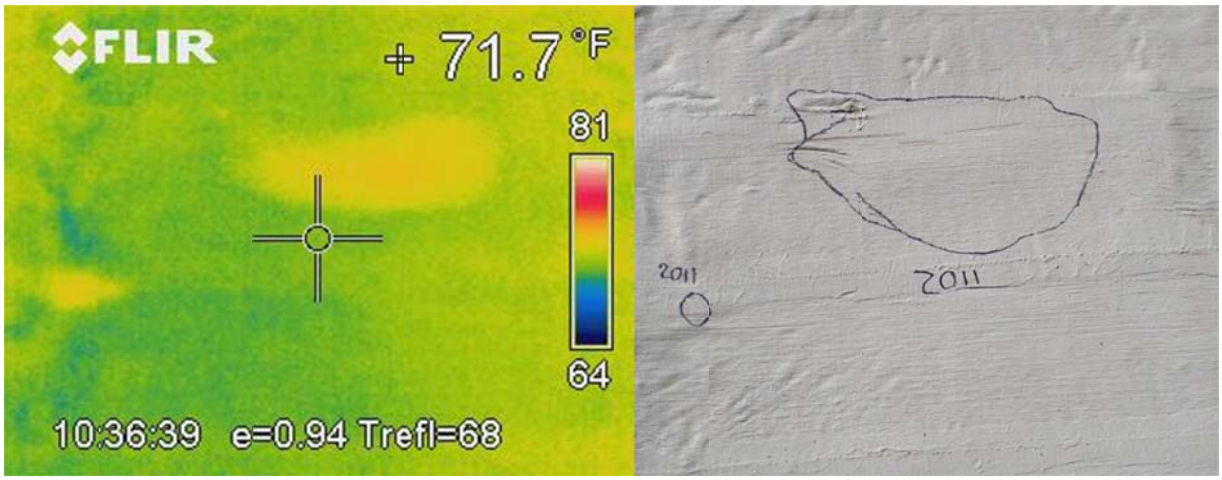

Figure 3.1. Photograph and thermal image from an infrared camera of two voids, (appearing yellow), found in 2011 on the 1st bay on the north side of the east arch

The images above are of two voids found in the 1st bay on the north end of the east arch. The area of the larger void was one of two areas eventually removed from the arch and is referred to as the

"smaller" patch removed from the arch. Note the horizontal or transverse cracks enclosed in the red oval near the top of the void in Figure 3.2.

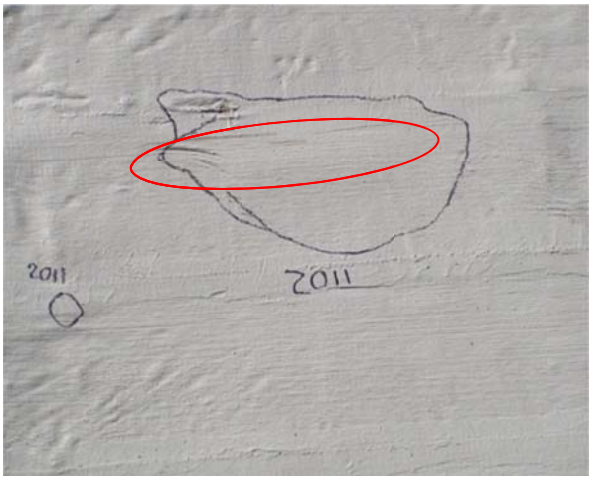

Figure 3.2. Two identified voids during the 2011 inspection, visible cracks in CFRP

All three voids identified during the biannual inspection in 2007 had grown in size and all voids found in the 2011 field assessment that were not previously identified presumably developed in the time between the 2007 bridge inspection and the 2011 field assessment. It was not possible to determine whether the crack identified in 2007 had grown in size; the physical markings on the bridge only indicated the crack existed at the time of the 2007 bridge inspection. In terms of documentation, in addition to the physical markings left on the bridge from both the 2007 bridge inspection and 2011 field assessment, locations and sizes of voids found on the extrados of the east arch are tabulated in Appendix A. There were 28 voids, 3 cracks, and 1 rust spot found during the 2011 field assessment. The voids ranged in area from less than 26 cm^2 (4 in^2) to 9876 cm^2 (1530 in^2) averaging approximately 580 cm^2 (90.3 in^2). Photographs of the identified areas on the arches can also be found in Appendix A as well as thermal images of voids.

3.3 Pull-off Tests

Multiple sources for pull-off test recommendations or standards have been published including the International Concrete Repair Institute (ICRI) Guideline No. 03739 (2004), the Army Corps of Engineers Technical Report REMR-CS-61 (1999), ACI 503R (1993), and ASTM D7522 (2009). Unfortunately some of these reports can be inconsistent. For instance, the Army Corps of Engineers states in their technical report "The important issue associated with pull-off tests is the depth of the core drilling into the existing concrete" adding, "ignoring the effect of drilling depth may be one of the main causes of difficulties in reproducing and comparing test results." Unfortunately, the other three sources have differing recommendations in regard to the core drilling depth into the substrate. ICRI recommends core drilling a minimum depth of 25 mm (1") into the existing substrate, while ASTM D7522 requires core drilling between 6 mm (0.25") and 12 mm (0.5") into the substrate. ACI 503R recommends "core drill through the coating and down barely into the subsurface."

Previous pull-off tests described above in Section 2.2.3.2 were conducted by CTC-Geotek directly following the repair in 2003 and for the sake of comparing test results, the testing procedure used by CTC-Geotek was replicated as closely as possible. The testing procedure was also intended to be consistent with the majority of the guidelines and recommendations made by the sources above where possible. While each of these guidelines is respected, the default testing technique was that of ASTM D7522.

As previously discussed, it is essential that the CFRP is well bonded to the arches in order to transfer stresses. To test the bond strength a pull-off tester, Proceq Dyna Z 16, was attached to a 50 mm (2") diameter aluminum puck which was adhered with a 5-minute, 2500 psi, two-part epoxy, Devcon S-210, to the surface of CFRP. The pull-off tester output the force applied to the puck via digital manometer. The digital manometer was also capable of outputting the stress that was applied by the puck to the bond, based on the area of the 50 mm (2") diameter puck.

Three separate sets of nine pull-off tests were performed during the field assessment in 2011. The first set of nine were located on the extrados of the base of the east arch at the north end, the second set

was located on the extrados of the base of the west arch at the north end, and the final set was located on the extrados of the center or crest of the east arch. These locations are depicted in red lettering in Figure 3.20 below.

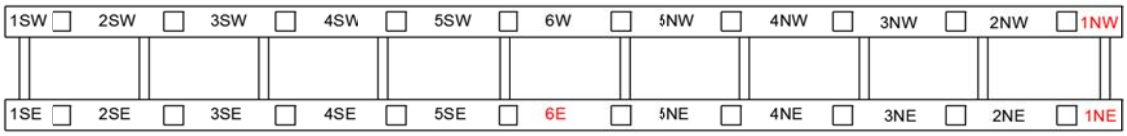

Figure 3.3. Pull-off test locations highlighted in red

A 5.7 cm (2 ¼”) outside diameter Husqvarna diamond coring bit was used in a Type DM-225 Husqvarna core drill. This drill is intended for wet-drilling and has an attachment for a typical garden hose. Due to the remote location of the Castlewood Canyon Bridge, a pressurized water source was not available. If the core drilling was completed dry without the use of externally applied water, damage to the bit as well as damage to the core would have been caused by excessive heat. Therefore, ice cubes were placed inside the 36.8 cm (14 ½”) cylindrical shaft of the 5.7 cm (2 ¼”) outside diameter coring barrel to provide available water for drilling as well as cooling for both the bit and core.

A 2.5 cm x 14 cm x 91.4 cm (1” X 5 ½” X 36”) wood board with a 5.7 cm (2 ¼”) diameter hole was used as a jig to start the holes, as there was no center drill arbor as there are with hole saws. Starting a core hole is the most difficult part of the process and was made much easier by the use of a jig, seen in Figure 3.5. In addition to being dangerous, coring without the use of a jig or center drill arbor could result in damage to the surface due to the coring bit unintentionally translating laterally, seen in Figure 3.4.

Figure 3.4. Damage caused by core bit without the use of the jig

Many core drills are bolted to the surface in which they are to core for these reasons. Below is a photograph of a core hole being started using the jig described above.

Figure 3.5. Starting a core hole using a wooden jig

Once the core hole was established using the jig, the jig was removed and the remainder of the coring process was completed. The core depth of 1 cm (3/8”) into the substrate was consistent with that of previous pull-off tests conducted by CTC-Geotek.

Adding torsional stresses to the circular area of CFRP and substrate inside the cored circle was inevitable due to the drilling process. These stresses were minimized by using a less aggressive drill bit with diamonds instead of a coring bit which has more aggressive carbide teeth for instance. Wet drilling by use of the ice also reduced stresses by adding water which created a slurry that removed displaced debris while using the finer particles to aid the diamonds in the cutting process. In one instance out of the 27 cored locations, the stresses induced by the drilling were enough to fail the cored section at the interface between the CFRP and the substrate. Figure 3.6 illustrates this occurrence.

Figure 3.6. The core drilling location that failed due to torsional stresses during the core drilling process, bay 1NW

In anticipation of applying a two-part epoxy to adhere pull-off pucks, remaining moisture and standing water was removed from the cored areas using compressed air and nozzle seen below in Figure 3.7.

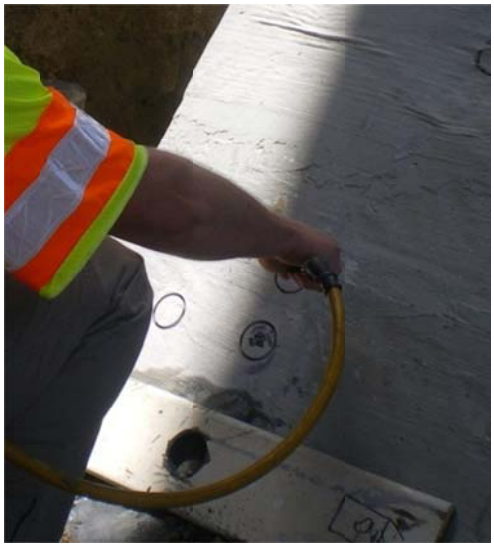

Figure 3.7. Removing water and debris from core cuts

The pull-off tests were intended to test the adhesion or bond between the FRP and substrate; therefore the acrylic paint layer was removed using a right angle grinder and masonry grinding disc to eliminate any premature failure of bond that may occur at the paint/CFRP interface. Additionally, this procedure also created a rougher surface increasing the surface area, improving the likelihood of strong bond between the puck and the CFRP. However, stresses from friction and heat from both the drilling and the grinding procedures could have influenced the results of the pull-off tests. This process is represented in Figure 3.8 below.

Figure 3.8. Removing the acrylic paint later before adhering the aluminum pucks

The areas with paint removed were then cleaned of debris and dust in preparation for the adhesion of the 2” diameter, 1” thick aluminum pucks. Compressed air and nozzle were used once again with the additional use of 70% isopropyl alcohol as a quickly evaporating cleaning agent. The prepared surfaces are in figures below.

Figure 3.9. Prepared areas for the adhesion of aluminum pucks for pull-off tests and a close-up of a prepared surface

The aluminum pucks were also prepared prior to adhering them to the CFRP. Each puck was sanded with 40 grit sandpaper, cleaned with 70% isopropyl alcohol, and then blow-dried using the compressed air and nozzle. Figure 3.10 are photographs contrasting aluminum pucks before and after sanding with 40 grit sandpaper and pucks being thoroughly cleaned.

Figure 3.10. Aluminum pucks before and after sanding with 40 grit sandpaper and preparing the aluminum pucks way up high on the arch

Once both the aluminum pucks and CFRP surfaces were prepared and cleaned, the pucks were adhered to the CFRP at the cored locations with epoxy. This rapid setting epoxy achieved full strength in one hour, making it ideal for field work. The aluminum pucks were allowed approximately 3 hours before the pull-off tests commenced.

The pull-off tests were conducted in the same chronological order as the pucks were adhered. In the center of the aluminum pucks a threaded hole allowed for a spherical headed bolt to be threaded hand-tight into the puck. The pull-off tester was then moved into place to engage the spherical head of the bolt threaded into the puck. The pull-off tester was then leveled parallel with the testing surface and the digital manometer was zeroed and the pull-off test started. Smooth continuous rotations of a hand-crank applied an upward force on the puck until failure. Figures below show adhered pucks, the spherical headed bolt threaded into a puck, the pull-off tester being placed, the pull-off test with a reading from the digital manometer, and removing the puck following the test from the pull-off tester.

Figure 3.11. Adhered aluminum pucks for pull-off tests

Figure 3.12. Spherical headed bolt threaded into puck and placing the pull-off tester to engage the spherical headed bolt

Figure 3.13. Conducting a pull-off test with the digital manometer reading and removing the tested puck from the pull-off tester

The maximum stress applied and failure modes of the tests were recorded in accordance with ASTM D7522. The results of the pull-off tests can be found with the results from CTC-Geotek tests in tables in Appendix B. Failure modes A, B, E, F, and G as defined above in Table 2.1 occurred during the testing. Representative photographs of these different failure modes are shown below.

Figure 3.14. Failure Mode A: bonding adhesive failure at loading fixture (on left), failure Mode E: adhesive failure at CFRP/substrate adhesive interface (on right)

Figure 3.15. Failure Modes B and F: cohesive failure in FRP laminate, and mixed cohesive failure in substrate and adhesive failure at the adhesive/substrate interface, respectively (on left), failure Mode G: cohesive failure in concrete substrate (on right)

Two pull-off tests were not able to be recorded due to technical difficulties. One of the tests failed during the preparation process of core drilling and the other test had a puck with faulty threads that would not allow for the spherical headed bolt to be engaged. These tests are represented as not available, NA, in the tables and plots. A summary of the failure modes for the 27 pull-off tests from 2011 and the 42 pull-off tests from 2003 are below in Table 3.1 and Figure 3.16.

Table 3.1. Summary of Failure Modes for the Pull-off Tests

42 Tests	Failure Modes of 2003 Pull-off tests							
	A	B	C	D	E	F	G	NA
Quantity	9	0	0	0	2	3	25	3
Percentage	21.4	0.0	0.0	0.0	4.8	7.1	59.5	7.1
27 Tests	Failure Modes of 2011 Pull-off tests							
	A	B	C	D	E	F	G	NA
Quantity	2	2	0	0	7	8	8	2
Percentage	7.4	7.4	0.0	0.0	25.9	29.6	29.6	7.4

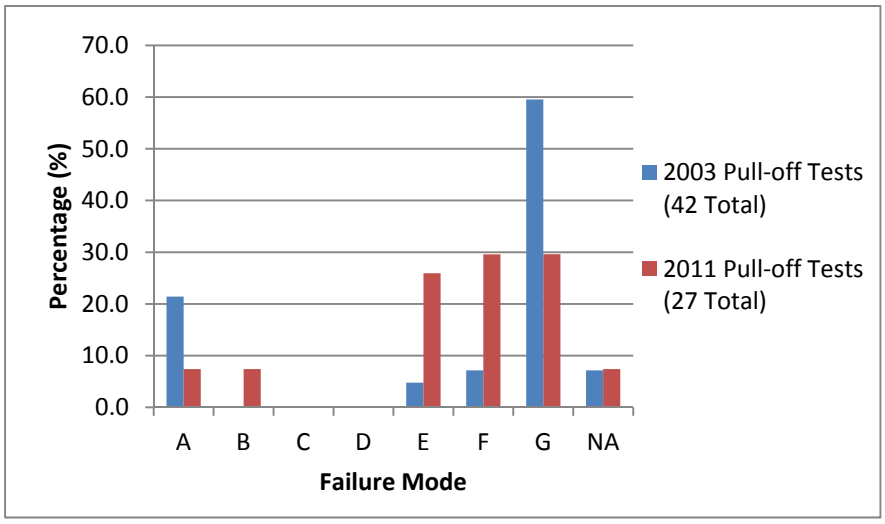

Figure 3.16. Failure modes of pull-off tests from 2003 and 2011

The number of failure Modes E, F, and G are roughly equal in number with only approximately 7% of the specimens failing in each of the A, B, and NA Modes for the tests conducted in 2011. From Figure 3.16 it is apparent that the high percentage of failure Mode G from 2003, significantly decreased to the evenly distributed Modes E, F, and G of the 2011 test results. Mode B was a failure mode that did not occur in 2003, but did in 2011 twice out of 27 tests. An increase in percentage of failure Modes B, E, and F indicates that other interfaces other than within the substrate are weaker and controlling. Failure Mode B is, according to ASTM D7522, "an indication of poor through-thickness properties of the FRP. Such failures may be due to incomplete wet-out of the fibers or plies comprising the laminate. Such failures may also result from environmental degradation of the FRP material itself." The term "wet-out" is

referring to the quality of the CFRP composite material and whether the fibers were fully saturated in epoxy during the wet lay-up process. Failure Mode E is an indication of poor adhesion properties and Mode F is a commonly observed mixed failure mode that is believed to initially fail in the cohesion in the substrate, followed by propagation to the adhesive interface. Different substrates at the location of the pull-off tests of 2003 and 2011 could have influenced both the failure mode and results of the pull-off tests. It is reasonable to consider that the tensile strength of concrete could have improved marginally since 2003 due to continued curing especially if the substrate was shotcrete rather than the original concrete. However, even in the case of shotcrete as the substrate this improvement or increase in strength would be fairly marginal. Comparing bond strengths of the 2003 and 2011 tests of only failure Mode G tests would be a reasonable evaluation of this possible strength gain of the substrate if the testing processes and substrates were identical or had very little variation. Below is a table with strengths of failure Mode G for comparison.

Table 3.2. Pull-off Test Results of Failure Mode G Tests

	Average		Maximum		Minimum		Sample Size
	MPa	psi	MPa	psi	MPa	psi	
2003	2.92	423	4.12	597	1.50	217	25
2011	2.07	300	3.81	553	0.13	19	8

According to the values in Table 3.2, the tensile strength of the substrate decreased or became weaker over time which makes little physical sense. Average, maximum, and minimum strength values all decreased from 2003 to 2011. The minimum test value of 2011 may have been so low due to imperfections during the core drilling process that completely failed one specimen with a failure Mode E. The two low values could have also been due to areas of poorly mixed concrete. The average value of the 2011 tests was significantly influenced by the one low value because of the small sample size. The difference in values of tensile strength of the substrate is likely due to the imperfections of the testing process and local characteristics of the substrate rather than an accurate representation of the changes in material properties of the substrate globally.

Of the 27 pull-off tests conducted in 2011, nine tests, two of which were failure Mode G, failed to meet the 200 psi minimum requirement of CDOT's construction specifications (Revision of Section 602). Six of the nine tests that had strengths less than 200 psi had failure Mode E. This failure mode is a failure at the interface between the CFRP and the substrate. A relatively thick layer of resin was used to smooth the surface of the substrate at the time of the CFRP repair. The thick "filler" resin varied in thickness and in color. These pull-off tests with low values all appeared to have very similar failure modes and strengths as well as appearance of the failure plane. Only one of the 42 tests conducted in 2003 failed to exceed 200 psi. Below are two figures displaying the distribution of pull-off strengths and probability density functions based on a normal distribution of pull-off strengths.

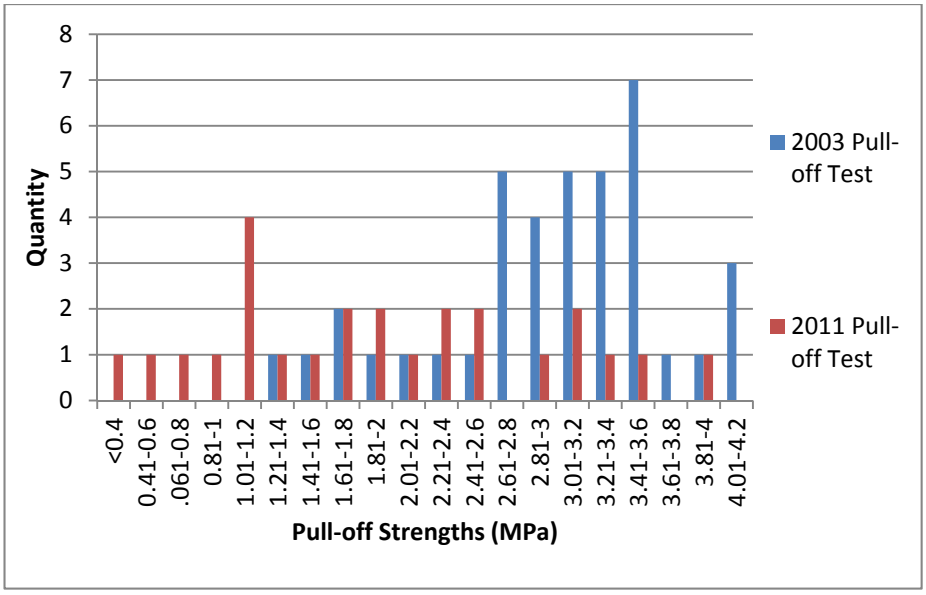

Figure 3.17. Histogram of pull-off test strength

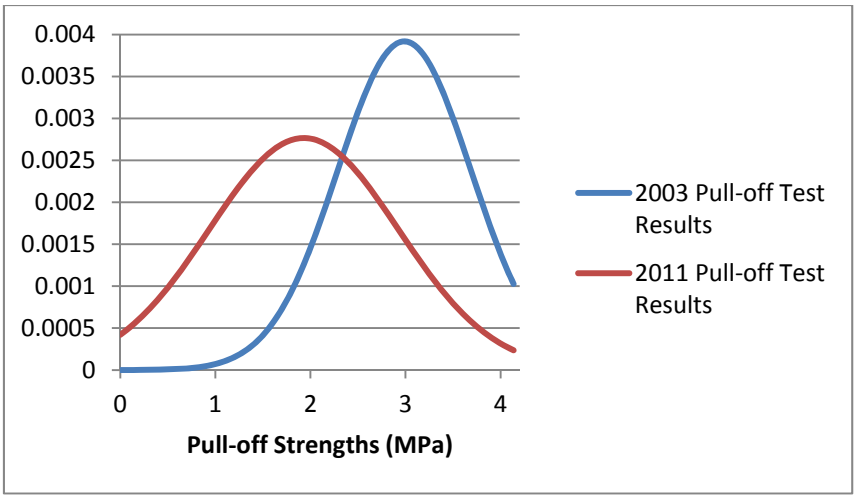

Figure 3.18. PDF of pull-off test results

The lower, wider, curve of the 2011 PDF in Figure 3.18 gives evidence that the standard deviation increased from 2003 to 2011. The data was fit with a normal distribution for the creation of the PDF and statistical analysis. In addition from 2003 to 2011 the mean lowered, shifting to the left. If the influence of the testing procedure could be disregarded, the larger variance of the 2011 results would likely represent the varying conditions in which the CFRP was exposed. The decrease in the mean from 2.98 to 1.93 from 2003 to 2011 gives indication of an overall decrease in the bond strength of the CFRP to the concrete. This indicates a possible durability concern for long-term applications.

The detection of voids, void sizes, and the bond strength evaluation provide several different types of evidence that consistently showed there are some issues in regard to the durability of the CFRP. The increase in number of voids, increase in size of existing voids, change in distribution of failure modes, decrease in average bond strength with more inadequate strength values, and increase in variance of bond strengths all indicate deterioration of the CFRP composite. It would be prudent to monitor the durability and performance of the CFRP composite closely and consistently to try and accurately quantify the development of the degradation.

3.4 Collecting Specimens for Laboratory Testing

The original plan was to remove strips of CFRP from the exterior corner of the extrados of the arch to provide the specimens for the tensile testing and DSC testing in the laboratory. After detecting

voids on the extrados of the east arch, it was determined that it would be beneficial to remove two large voids found rather than remove strips of FRP that were intact. Three reasons contributed to this decision. Intact or well-bonded CFRP would not have to be removed from the arch for the laboratory testing. This would preserve the strength the CFRP was providing to the bridge and it would significantly reduce the necessary efforts of trying to remove intact CFRP by chipping or cutting concrete and avoiding causing damage to the CFRP. Secondly, inspection of the substrate would be possible by the removal of larger areas of CFRP. Lastly, repairing areas of voids would improve the performance of the CFRP retrofit by allowing stresses to be transferred from the substrate to the CFRP via the bond which it lacked at the time of removal. Below in Figure 3.19 is a plan view drawn to scale of the locations of the patches removed.

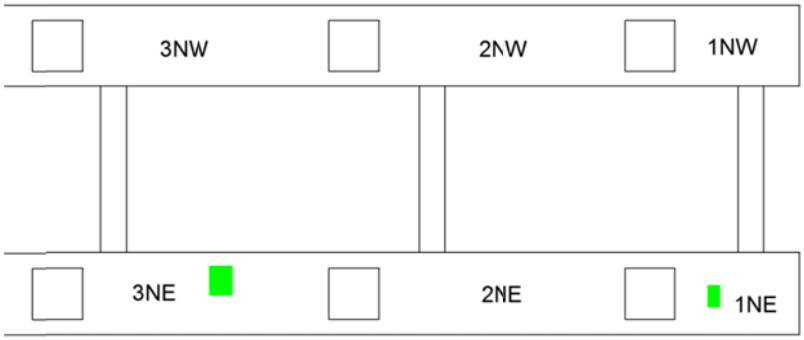

Figure 3.19. Areas removed are highlighted in green

The smaller of the two voids, approximately 28 cm x 51 cm (11" x 20") in size, was removed from the extrados of the 1st bay on the north end of the east arch. This void had a previously identified crack running in the transverse direction on the arch. A right angle-grinder mounted with 11.4 cm (4 ½") masonry cutting wheel was used to cut through the CFRP layer in a rectangular shape enclosing the area of the void. Once the CFRP was removed, it was reasoned that this area of CFRP was at one time bonded to the substrate, because the crack previously seen in the surface of the CFRP was also present in the substrate. It was likely that the concrete cracked due to service loads or shrinkage. It is possible the crack was present before the CFRP was applied and the crack opened more causing the CFRP to crack. According to CDOT's construction specifications, cracks in the substrate larger than 1.5 mm (0.06 in) in width were to be pressure injected with epoxy resin prior to the application of the CFRP. When the

concrete cracked or the crack widened due to internal tension, the same strain was imposed on the CFRP to cause cracking there as well. A local bond would have been necessary to impose the same strain to the CFRP. Once the CFRP became cracked, water and moisture was able to penetrate the CFRP layer and subsequent freeze/thaw cycles not only opened the crack more, but debonding of the CFRP from the substrate also occurred. The debonded area increased over time due to freeze/thaw cycles and temperature fluctuations. The unidirectional CFRP fabric was more susceptible to cracks in the transverse direction because the carbon fibers were aligned in this same direction and no, or very few, fibers had to rupture. The ultimate tensile strength 90 degrees to the primary fibers of Tyfo® SCH-41, according to Fyfe, is approximately 4.6% of the ultimate tensile strength in the direction of the primary fibers.

Upon cutting the lower edge of the CFRP rectangle, water exited the cut at the bottom of the void revealing standing water at the interface between the CFRP and substrate. Photographs of the void and the removal of the CFRP layer are shown in Figures 3.20, 3.21 and 3.22 below.

Figure 3.20. Void in CFRP with transverse crack identified with red arrows and cutting the perimeter of the void in the CFRP

Figure 3.21. Water exiting the void area directly after the lower cut through the CFRP was completed

Figure 3.22. Cracks in the substrate were transmitted through the CFRP and notice the smooth texture and blue and white color of the underside of the CFRP

It is worth noting the condition of the underside of the CFRP panel removed. It is blue and white in color and smooth in texture. This smooth texture is the underside of a thick layer of resin referred to as a “filler resin” used to smooth the rough surface of the substrate. There are no pieces of the substrate adhered to the CFRP panel, which when compared to the other area removed would strengthen an argument that this area was never well bonded to the substrate. The transmitted crack and the smooth

surface provide contradictory indications as to the quality of bond over time. The transmitted crack indicates a strong bond existed at one time and the smooth textured underside of the CFRP indicates that this area may have never been well bonded.

The second void was removed from the 3rd bay on the north end of the east arch. A rectangular section of the CFRP was removed with the same procedure previously described. Photographs of the area of the void and the removal of the CFRP rectangle are in Figure 3.23 below. There was no standing water or evident moisture in this larger void area, but there was significant pieces of the substrate adhered to the underside of the CFRP patch removed.

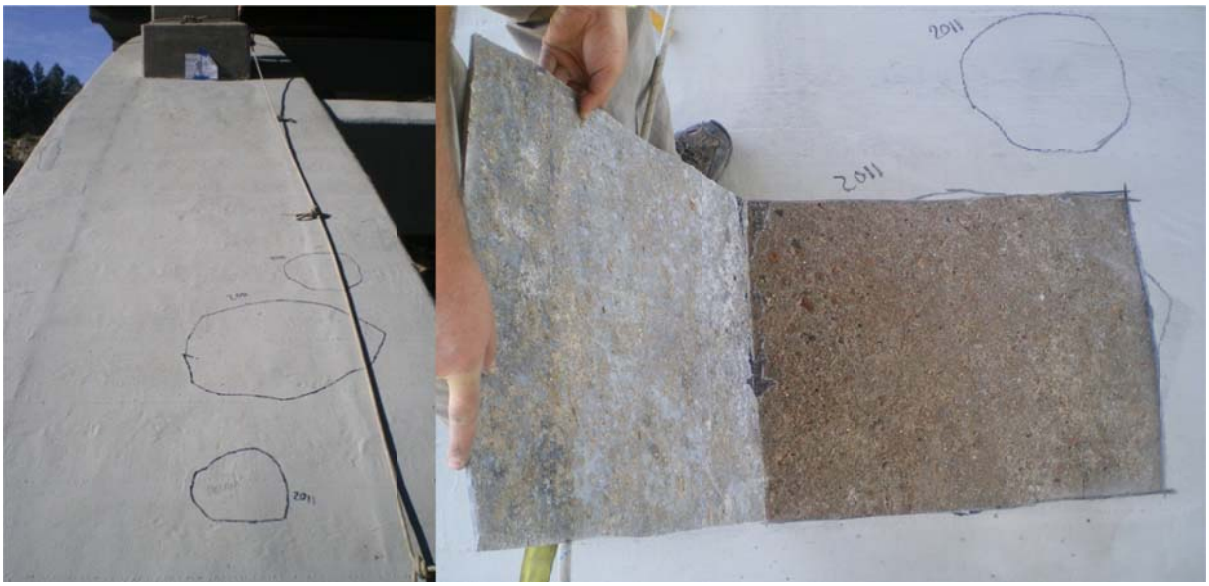

Figure 3.23. Voids found in the 3rd bay on the north end of the east arch and removal of the CFRP of the largest void

Both sections of CFRP removed from the arch were taken to the laboratories at CSU for tensile tests and differential scanning calorimetry tests. These tests and their results are discussed in Section 4.0.

3.5 CFRP Repair

Due to the pull-off tests, a total of 27 – 57.15 mm (2 ¼") diameter holes of varying depths, depending on the failure mode, were created on the arch. These areas were filled with epoxy to replace the cross-sectional area. Initially, the same epoxy used to adhere the aluminum pucks to the CFRP was used to fill the holes created from the pull-off tests. Due to the inclined angle, this epoxy, which is less

viscous before curing, would slump and run down slope on the locations near the base of the arches. This was undesirable and a more viscous epoxy, 3000 psi Loctite epoxy gel, was used to fill the holes created from the pull-off tests. These filled holes of varying depths can be seen below.

Figure 3.24. Epoxy filled holes following the pull-off tests

Once the holes were filled with epoxy, the 3 areas of pull-off tests and the 2 areas of removed CFRP (debonded regions) were prepared for a repair process. First these areas were washed using a non-toxic, biodegradable, soap and water, then they were cleaned with 70% Isopropyl alcohol to remove any remaining soap film. CFRP patches must overlap a minimum of 6”; therefore primer was applied to the affected areas of the arches plus a minimum of 6” in each direction. The primer used for the repair was a two part epoxy made by HJ3, STRONGHOLD Primer Epoxy (STR-BW-200A). The mix ratio was 2 parts of the PC-200 Primer Resin, Part “A”, to 1 part of the PC-200 Primer Hardener, Part “B”. Once the two-part epoxy was well mixed, the primer was distributed to the repair areas using 9” rollers as seen in the photograph below.

Figure 3.25. Applying a primer coat to the areas for repair

Following the recommendation of HJ3, the primer was allowed to cure for 24 hours before the repair process was continued. The CFRP material, comparable to that of the CFRP fabric used during the 2003 repair, was also provided by HJ3. HJ3 provided both CF-516 Uniaxial Carbon Fabric and CF-528 Biaxial Carbon Fabric for the repair. Below is a table with material properties of the existing material made by Fyfe and the comparable repair material made by HJ3.

Table 3.3. Material Properties of the Existing and Repair Materials

Material Properties of Uniaxial Carbon Fabric						
Date of Information	Manufacturer	Product	Tensile Strength MPa (ksi)		Modulus of Elasticity GPa (ksi)	
			Typical Values	Design Values	Typical Values	Design Values
2003 (CDOT Report*)	Fyfe	Tyfo® SCH-41	876 (127)	745 (108)	72.4 (10500)	61.5 (8900)
2011	HJ3	CF-516	1034 (150)	818 (119)	85.4 (12380)	71.9 (10433)

The CFRP fabric was saturated by applying a well-mixed two part epoxy, two parts of HJ3 SRS-400-A Resin and one part HJ3 SRS-400-B Hardener, to both sides of the fabric. The two part epoxy was also applied to the repair areas identical to that of the primer. The saturated fabric was then placed on the arch and the use of hand pressure and rollers eliminated air bubbles and pockets between the fabric and

the substrate. Unidirectional CFRP fabric was used to repair the area where the patches were removed. Proper alignment of the fiber direction in the transverse direction was necessary to repair the transverse wraps. The pull-off tests were conducted closer to the edge of the arches damaging both transverse and longitudinal sections. Therefore, biaxial patches were used to repair these areas. This process is represented in the photographs below. Following the CFRP repair, 24 hours was allowed for curing before the areas were painted

Figure 3.26. Allocating fabric for repair and applying the second layer of CFRP to the area of pull-off tests on the east arch

Figure 3.27. The repaired sections on the north end of the arches

4.0 TASK 3: LABORATORY TESTING OF FRP SAMPLES AND ANALYSIS OF DATA

4.1 Tensile Tests

The two rectangular pieces of CFRP that were removed from the Castlewood Canyon Bridge were taken back to Colorado State University for testing. The panels, approximately 55.9 cm x 71.1 cm (22" x 28") and 27.9 cm x 50.8 cm (11" x 20"), were cut using a band saw into strips 2.5 cm (1") wide by 21.6 cm (8.5") long. The cuts were made to isolate areas of CFRP that were only one layer thick, and the 21.6 cm (8.5") direction was required to be parallel with the direction of the fibers. Twelve samples from each area were tested at the Foothills campus of CSU at the Engineering Research Center using a United universal testing machine in accordance with ASTM D3039M-08 except the alignment procedures with the strain gauges and tabs were not used. For each test the failure mode, ultimate strength and modulus of elasticity was recorded.

The thickness of the CFRP strips varied significantly due to the rough contour of the adhered side of the CFRP. As previously discussed in sections 3.2.4 and 3.2.5, a thick filler resin was applied to smooth the surface of the substrate prior to adhering the CFRP fabric to the arches. A photograph of the rough texture is below.

Figure 4.1. The rough contour of a tensile test strip of CFRP

The tensile strength and modulus should be dominated by the fibers, and thus the built up addition of filler resin was not considered as the thickness, but rather the manufacturer's data of 1.02 mm (0.04") for the thickness per layer was used to calculate the area of the specimens. Before the testing began, an extensometer was placed in the mid-section of the specimen and was removed during the testing when the load reached 8896 N (2000 lb.) for most specimens.

Three letter failure codes were used in accordance to ASTM D3039. The first letter signifies failure type, the second identifies failure area, and the third refers to the location of failure. A summary of the codes and their respective failure modes are tabulated in Table 4.1.

Table 4.1. ASTM D3039 Letter Codes for Failure Modes

First Character		Second Character		Third Character	
Failure Type	Code	Failure Area	Code	Failure Location	Code
Angled	A	Inside grip/tab	I	Bottom	B
edge Delamination	D	At grip/tab	A	Top	T
Grip/tab	G	<1W from grip/tab	W	Left	L
Lateral	L	Gage	G	Right	R
Multi-mode	M	Multiple areas	M	Middle	M
long Splitting	S	Various	V	Various	V
explosive	X	Unknown	U	Unknown	U
Other	O				

Ideally, the specimens would fail in the area of the extensometer away from the grips. Photographs of the failed tensile test specimens displaying varying combination of failure modes are shown in Figures 4.2 and 4.3. Note the striking difference in appearance of the underside of the CFRP sections removed.

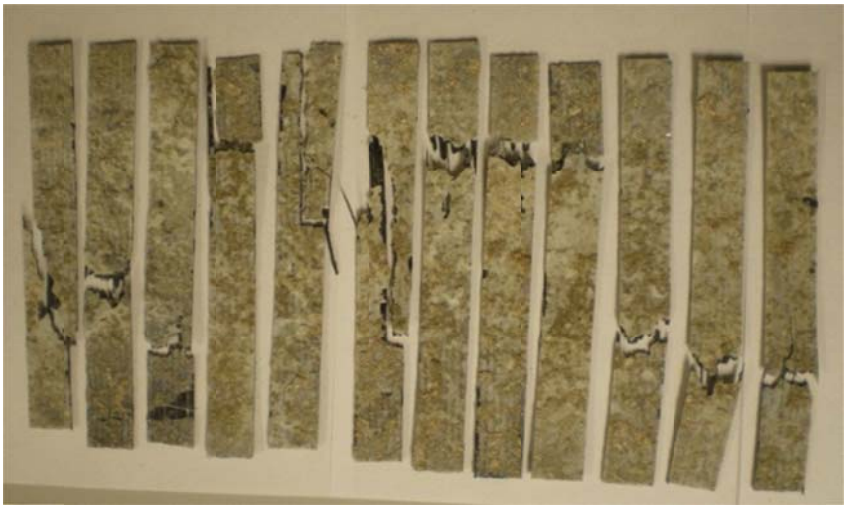

Figure 4.2. Failed tensile test specimens from the large void removed from bay 3NE, note the oatmeal appearance

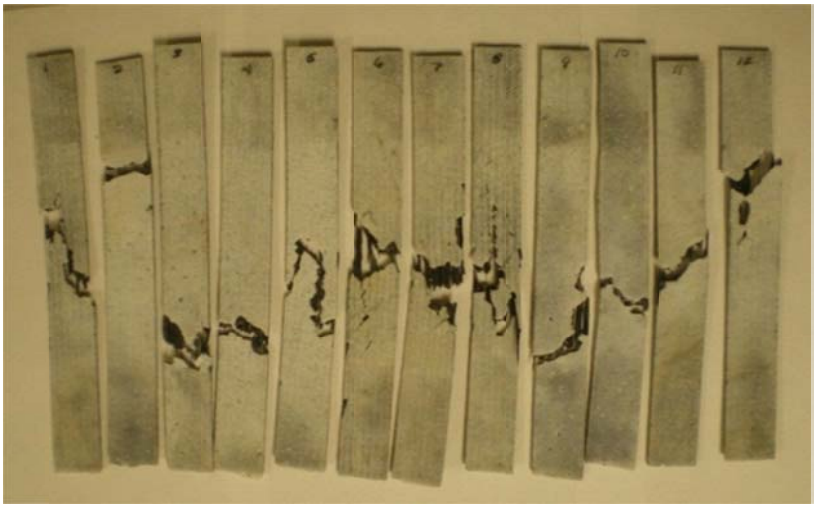

Figure 4.3. Failed tensile test specimens from the small void removed from bay 1NE, note the milky appearance

Test results can be found in Appendix C. The modulus of elasticity was not calculated due to difficulties with the extensometer during three of the 24 tensile tests. Bar charts in Figures 4.4 and 4.5 display the distribution of values of tensile strength and modulus of elasticity of the tensile tests.

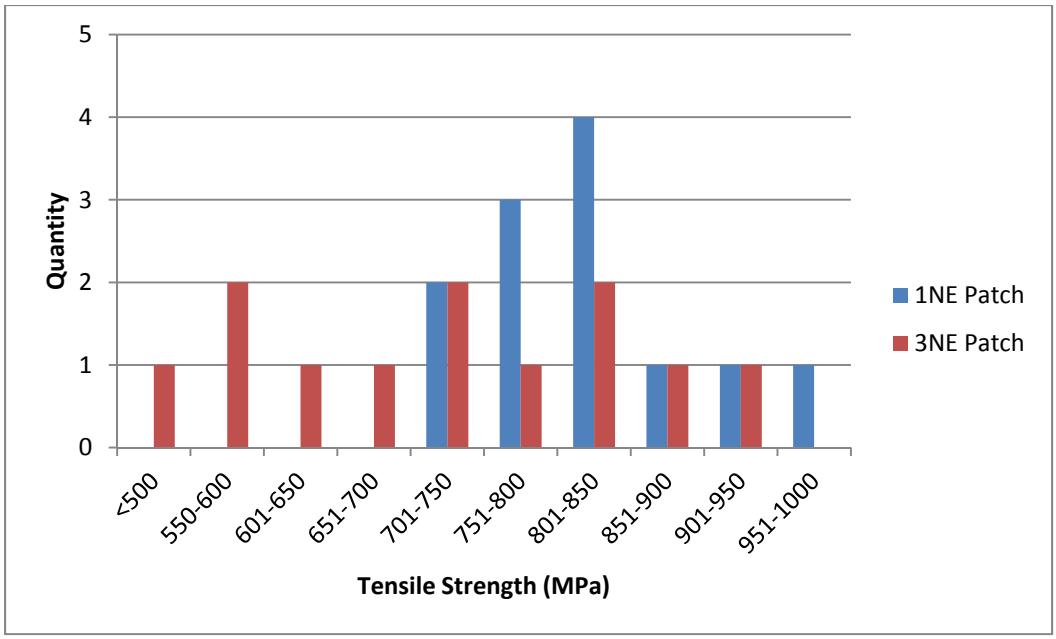

Figure 4.4. Distribution of tensile strength results

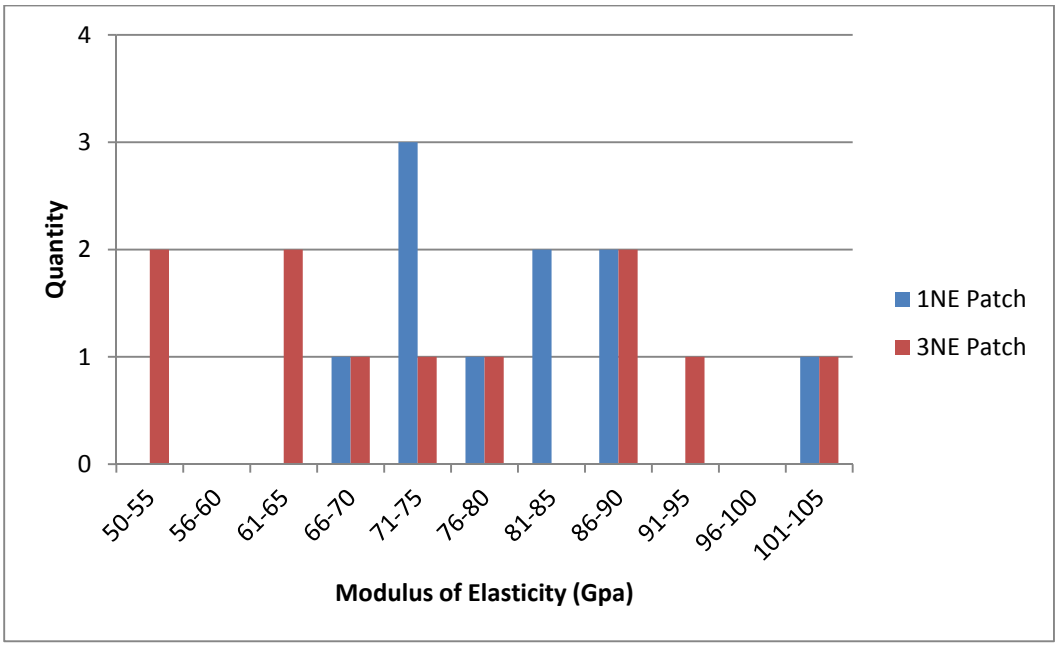

Figure 4.5. Distribution of modulus of elasticity results

Material properties of the CFRP used in 2003 are tabulated below for comparison purposes. These values are considered the initial values before any degradation has occurred.

Table 4.2. Material Properties of 2003 CFRP

Material Properties of Uniaxial Carbon Fabric						
Date of Information	Manufacturer	Product	Tensile Strength MPa (ksi)		Modulus of Elasticity GPa (ksi)	
			Typical Values	Design Values	Typical Values	Design Values
2003	Fyfe	Tyfo® SCH-41	876 (127)	745 (108)	72.4 (10500)	61.5 (8900)

A graphical representation of the test values relative to the manufacturer's values reported in the CDOT report are the probability density functions shown in Figures 4.6, 4.7, 4.8, and 4.9. The typical values and design values given by the manufacturer are represented as dashed lines in the plots below. The design tensile strengths are typically some percentile of a distribution while the modulus of elasticity is usually the mean. For instance, from the CDOT specification, "the ultimate tensile strength shall be the mean tensile strength of a sample of test specimens minus three times the standard deviation." Statistically, this would correspond to a percentile of 0.14 which is very restrictive. This CDOT specification also required a minimum of 20 specimens to determine material properties. This would result in combining the samples from the small and large patch totaling 24 specimens, resulting in a usable ultimate tensile strength of 288.2 MPa (41.8 ksi). These values referred to as "CDOT design values" are in the table below and represented as solid vertical lines in the plots below for each set of samples as well as all the tests combined. A common statistical reference used in other guidelines is the 5^{th} percentile which is also depicted as a solid vertical line in Figure 4.7 below. To determine the 5^{th} percentile, 1.645 times the standard deviation was subtracted from the mean.

The probability density functions assuming normal distributions were generated using the statistics in Table 4.3 below. The vertical axis for the probability density functions is relative to the horizontal axis; the area under the curve equals unity.

Table 4.3. Statistics from the Tensile Samples

	Modulus of Elasticity (GPa)			Ultimate Tensile Strength (MPa)		
	1NE	3NE	Total	1NE	3NE	Total
Mean	81.1	74.0	77.3	820.5	688.2	754.4
Standard Deviation	10.7	16.3	14.1	79.3	186.2	155.4
CDOT Design Tensile Strength				582.5	129.6	288.2
5th Percentile				690.0	381.9	498.8

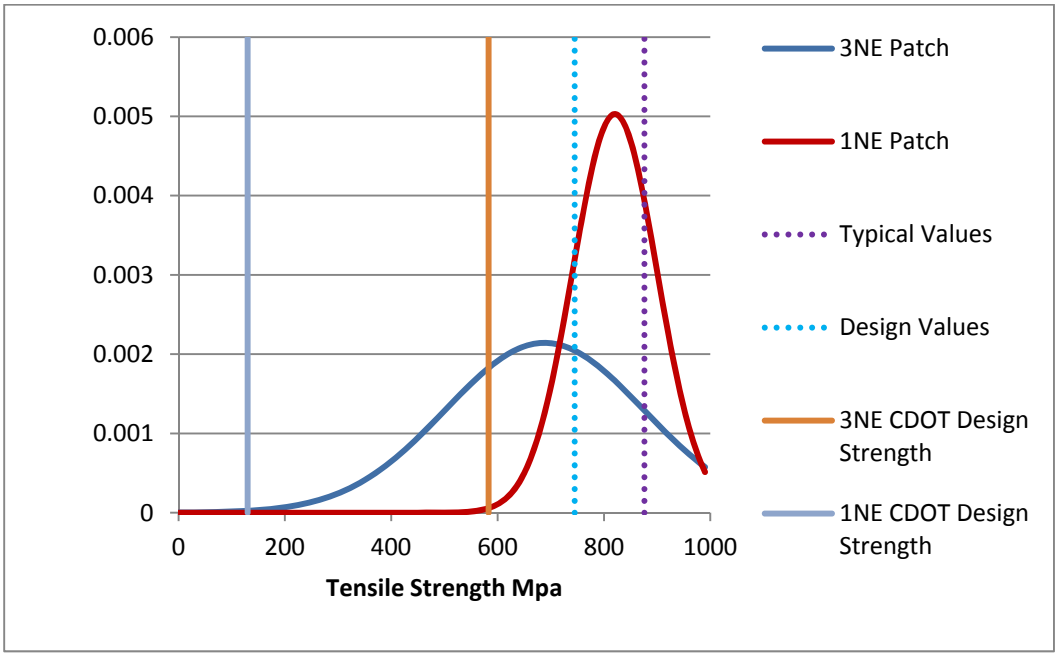

Figure 4.6. Probability density function of the two samples, tensile strengths

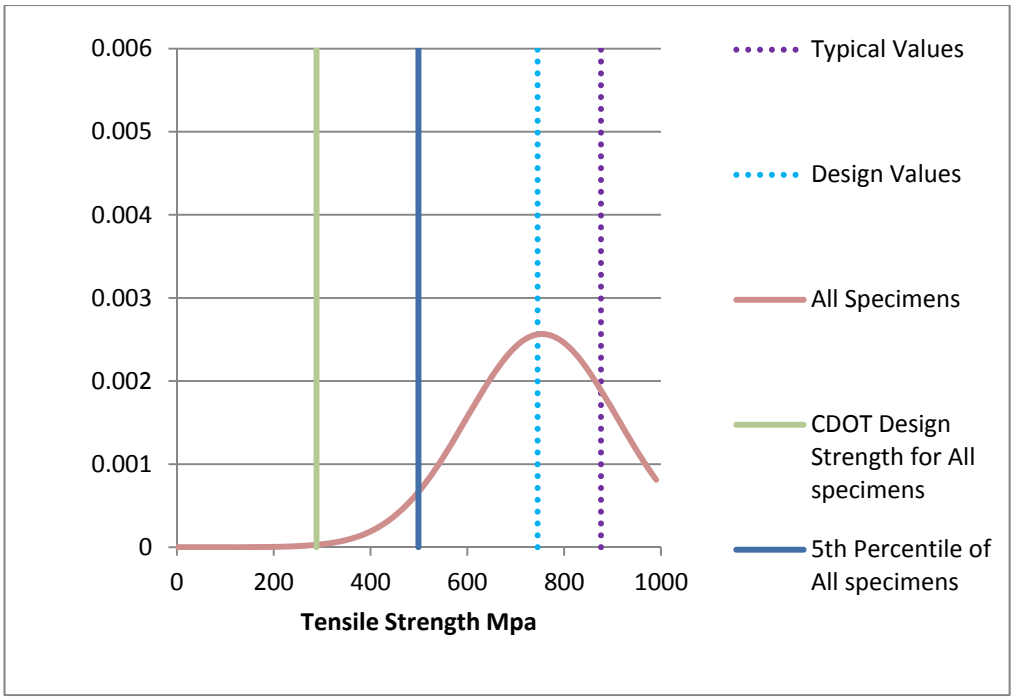

Figure 4.7. Probability density function of all tensile tests

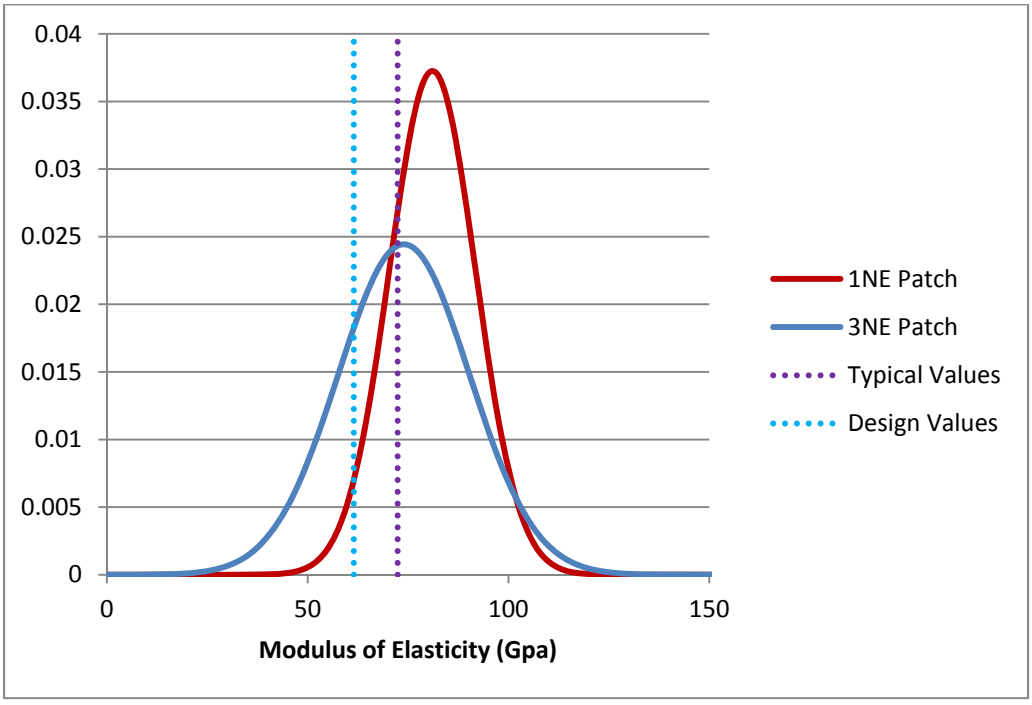

Figure 4.8. Probability density function of the two samples, modulus of elasticity

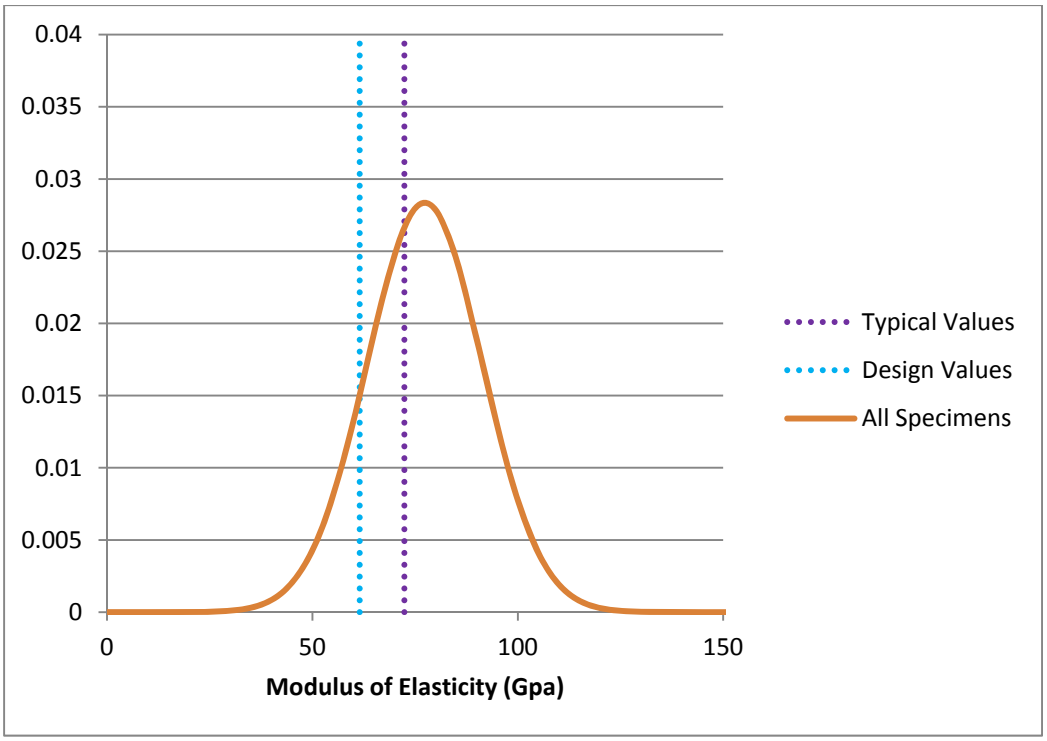

Figure 4.9. Probability density function of all modulus of elasticity samples

Looking at the location of these values in Figure 4.7 above, there is a very concerning discrepancy between the values of tensile strength provided by the manufacturer and the values generated from the tensile tests. The values of modulus of elasticity are fairly representative of the values provided by the manufacturer.

By assuming the stress versus strain response of the CFRP was linear until failure, the rupture strain was found by dividing the ultimate tensile strength by the modulus of elasticity, which was the chord modulus of 0.0043 strain or less. CDOT's construction specifications (Revision of Section 602) required a minimum rupture strain of 0.006 cm/cm. The rupture strain of the material at the time of repair was identified in the CDOT report as being 0.012 cm/cm for both the typical and design value.

Table 4.4. Tyfo SCH-41 Rupture Strain Values

Date of Information	Rupture Strain	
	Typical Values	Design Values
2003 (CDOT Report)	0.012	0.012
2011 Testing (Revision of Section 602)	0.0098	0.00308

Similar to the tensile strengths, CDOT's construction specifications (Revision of Section 602) required "the ultimate rupture strain shall be the mean rupture strain of a sample of tests specimens minus three times the standard deviation." A table of these values is below.

Table 4.5. Rupture Strain Values from the 2011 Tensile Tests

Rupture Strain	
Mean	0.00981
Standard Deviation	0.00224
CDOT Design Rupture Strain	0.00308
5th Percentile	0.00612

The 5th percentile value in the table above would satisfy the minimum rupture strain requirement of CDOT's construction specifications (Revision of Section 602), but the "CDOT Design rupture strain" calculated per CDOT's construction specifications (Revision of Section 602) is not adequate. A visual representation of this can be found in the probability density function in the figure below.

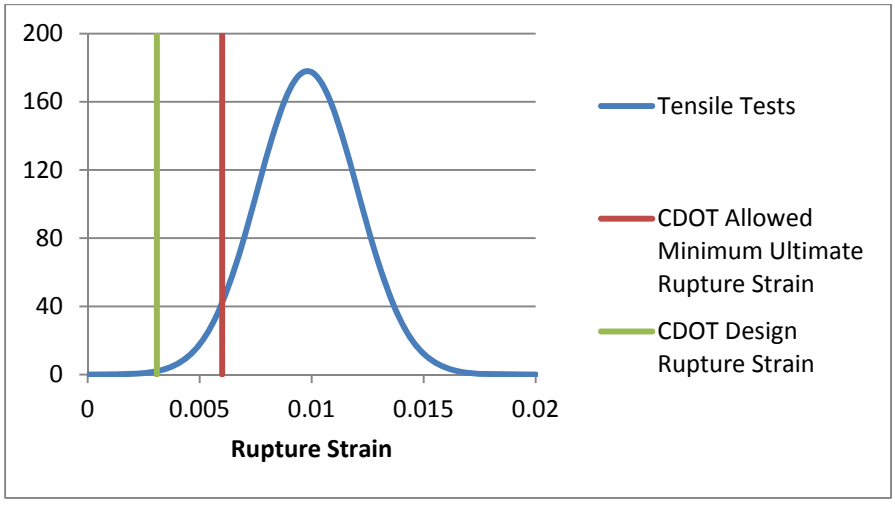

Figure 4.10. Probability density function of the rupture strain of all tensile tests

In summary, the tensile strengths were significantly lower than the values reported by the manufacturer, Fyfe and required by CDOT. It is difficult to determine whether these values are due to poor workmanship during the 2003 repair or degradation. Initial values at the time of repair would help make this differentiation if the samples tested in 2003 were representative of the material on the bridge. No results from such tension tests were recovered for comparison. The modulus of elasticity values were reasonably close to reported values considering the sample size. The rupture strain, similar to the tensile strength, had values lower than acceptable design values according to CDOT's construction specifications (Revision of Section 602).

4.2 Differential Scanning Calorimetry (DSC)

Dr. Radford at the Motorsport Engineering Research Center on the Foothills campus of Colorado State University provided the guidance and equipment to conduct the DSC analysis. After material was allocated for tensile tests from the patches removed from the bays 1NE and 3NE, the remaining material was used for DSC. Samples of CFRP and the filler resin were tested using a Seiko SSC/5200 DSC testing machine. Testing specimens consisted of 15 mg of small particles. Specimens consisting of smaller particles are more desirable because there will be better contact between the specimen and the aluminum pan containing the specimen resulting in better accuracy and fewer resulting artifacts.

Available water acts as a plasticizer to the resin and can cause the glass transition temperature to decrease. By the time the specimens were removed from the bridge and then transported to and tested in the lab, the moisture content of the specimens was likely more representative of the relative humidity of the lab environment than their condition during service. Therefore, the lowering of the glass transition temperature due to higher water content was not detected, but likely existed on-site especially in the case of the section removed from bay 1NE where water drained from the area in which the patch was removed.

The specimens of the CFRP material were prepared in two ways. The first of method was by grinding the material and collecting the debris from this process. The advantage of this procedure was that very small particles could be created quickly which resulted in better contact to the aluminum pan. The disadvantage was heat was introduced to the sample which may have exceeded the thermal history of the

material causing some post-curing, resulting in T_g higher than what the actual T_g was during service. The second technique used in preparing specimens of CFRP was mincing or dicing the material into small pieces with the use of a knife. The advantage of this technique was no additional heat was introduced to the specimen; the disadvantage was the time-intensive preparation and the larger pieces would have less contact with the aluminum pan. This second technique was also used for the preparation of samples of the "filler" resin. Unmeasured specimens can be seen in a photograph in the figure below.

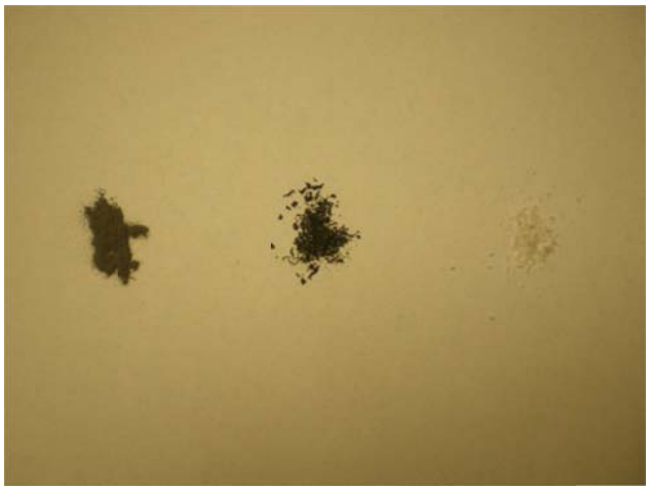

Figure 4.11. Ground CFRP, diced CFRP, and diced filler resin

A maximum of 15 mg was used for each DSC evaluation. The reactive material was only the resin of the composite and the percentage of resin to fiber was unknown. If the amount of constituents of the composite was known, additional information such as the amount of energy absorbed could be calculated by the hysteresis of the DSC test. The CFRP material likely had a lower percentage of reactive material, resin, than the filler resin and therefore smaller specimen sizes of the filler resin were sufficient in providing ample reactive material.

Each specimen was placed in an aluminum pan and an aluminum top was crimped in place to the bottom pan to enclose the specimen. The specimen was then inserted into the DSC testing machine, the mass of the specimen was entered into the software and the DSC was started. Liquid Nitrogen was used to cool the specimen to -30˚C and the temperature was held until the DSC returned to equilibrium. The derivative of DSC, DDSC, was used to determine the beginning, middle, and end of transient states. The

beginning and end of transient states had DDSC values of zero and the middle of the transient state was often considered the maximum absolute value of the DDSC between the zero values.

Figure 4.12. DSC specimen chamber and DSC with liquid nitrogen

Once the specimen was held at -30˚C for approximately 5 minutes, a pre-programmed temperature versus time environment was created in the testing chamber. Starting at -30˚C, the DSC established a baseline and a built-in furnace provided the heat flow to the specimen's chamber. This constant increase in temperature, 10˚C/min, continued for approximately 15 minutes until a temperature of approximately 130˚C was achieved.

The temperature of 130˚C was held for approximately one minute to allow the specimen to reach equilibrium in its transition from being endothermic to exothermic. Liquid Nitrogen was then used to cool or drop the temperature of the specimen at a constant rate back to the approximate room temperature of 20˚C. During this returning of temperature, the DSC displayed similar behavior as before with an initial baseline, followed by a transient state, returning to a baseline below that of the previous baseline. This transition also represents the glass transition temperature; however the heating process up to 130˚C likely cured the epoxy resin in a post-curing process resulting in an increase to the glass transition temperature. Below is a plot graphically showing the temperature versus time relationship of the specimen chamber during the DSC test.

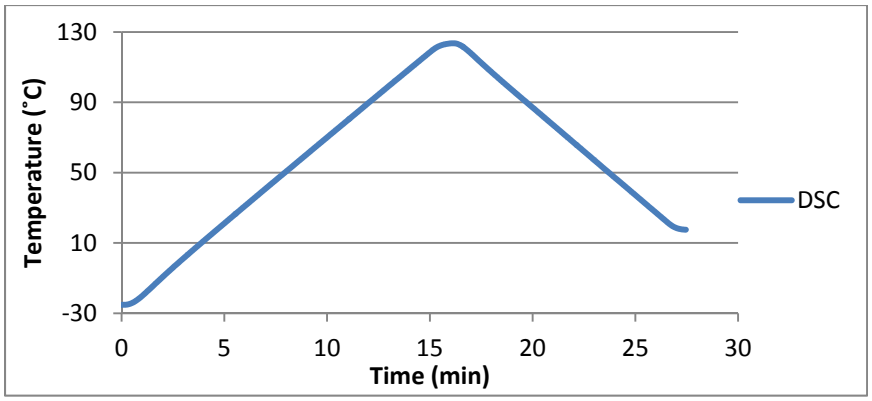

Figure 4.13. Temperature vs. time of the DSC analysis for the round CFRP1 specimen

The first specimen tested was of the ground CFRP material. The DSC curve is in the plot below. The glass transition temperatures are two points identified in the plot.

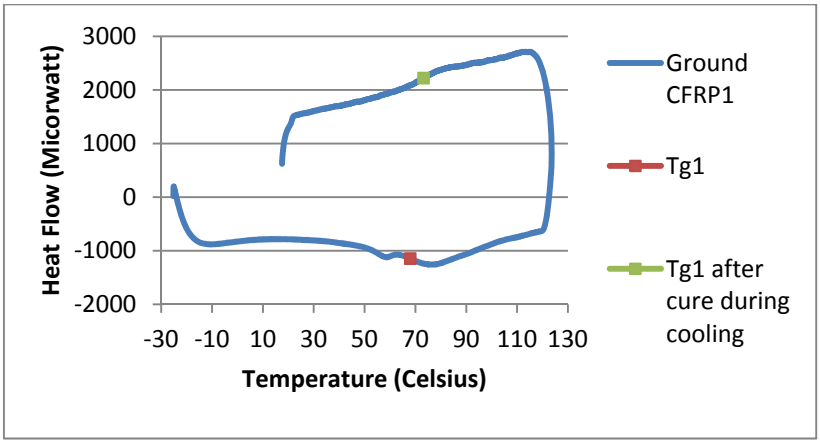

Figure 4.14. Ground CFRP specimen

During heating the glass transition temperature, Tg, was 67.95˚C, while during the cooling process the Tg was 73.19˚C. This increase in Tg is due to the curing process caused by the heating up to 130˚C. The glass transition temperature of the CFRP composite was expected to be between 60˚C and 82˚C as quoted by the manufacturer as being the design value and typical test value respectively. The highest temperature of the composites thermal history was probably not much greater than 40˚C, which explains the additional curing and the upwards shift in the Tg during the heating process up to 130˚C.

The same testing procedure was conducted for a second time on the same specimen because "differences between the first and second heating curves can be very informative" (Mettler Toledo, 2000).

Two reasons in particular justified this decision. Firstly, it was of interest to explore the influence the heating process has on the specimen and its glass transition temperature due to post-curing. Secondly, if the erratic behavior disappears it would be considered an artifact and less significant in the first test as opposed to a descriptor of a material property such as Tg. This specimen was referred to as Ground CFRP1A and its plot is below.

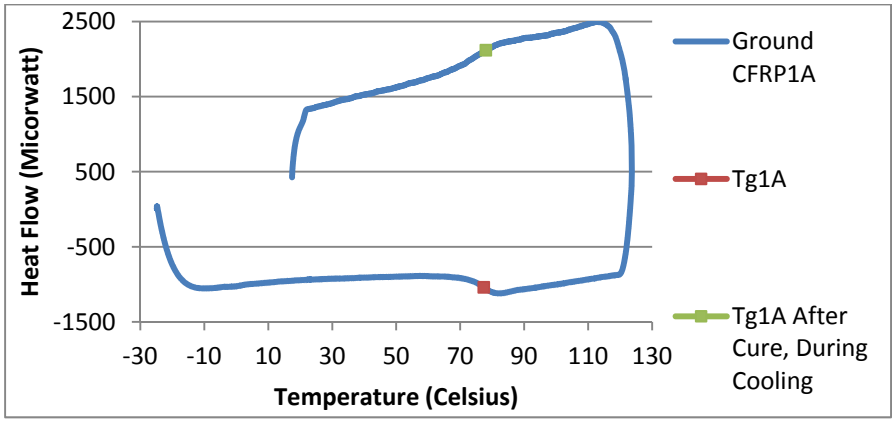

Figure 4.15. Ground CFRP1A

The erratic or irreversible behavior does not exist in the classic behavior of the DSC curve in the plot above. The behavior during heating and cooling are reversible and look identical. Subtracting the Ground CFRP1A curve from the Ground CFRP1 curve would yield an area that represents irreversible behavior.

The two glass transition temperatures were found to be 77.38˚C and 78.02˚C for the heating and cooling processes respectively. The second time the specimen was heated to 130˚C the T_g increased by a much smaller amount due to the post-curing that occurred during the first test. The closer a specimen gets to being fully cured, the smaller the influence additional heat will have on T_g. Additionally, there is a relatively small shift in the T_g that is due to the different processes of heating and cooling that should be considered when comparing the T_{gs} found during the heating and cooling processes. During the heating the T_g is shifted to the right and during the cooling the T_g is shifted to the left; the glass transition temperature should be taken as the average of the two values found during the heating and cooling

processes if no significant curing occurred during the heating process. A plot of the heat-cool-reheat-cool process is in the figure below.

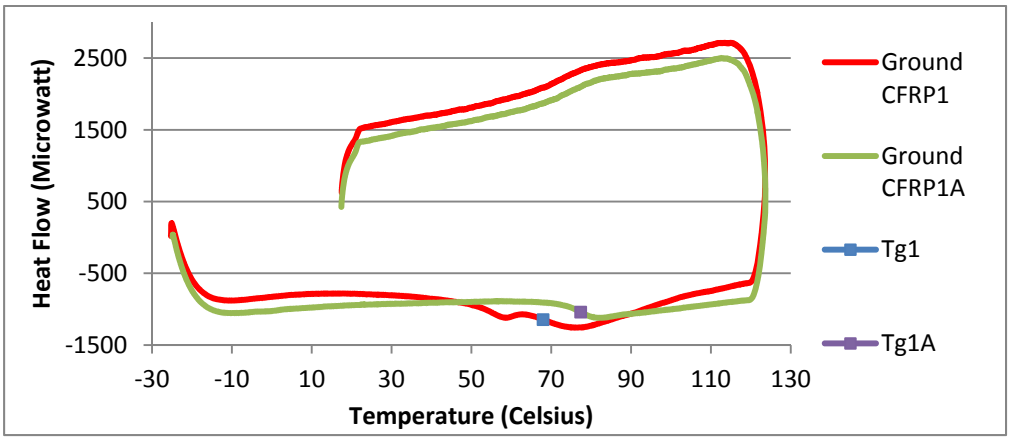

Figure 4.16. Heat-cool-reheat-cool of the same specimen

DSC is not usually approached as though the data or results are random variables with corresponding distributions and therefore multiple tests are not usually conducted. However, a second test of ground CFRP was conducted to compare the T_gs and the presence of erratic or irreversible behavior. This specimen was Ground CFRP2 and its plots are below.

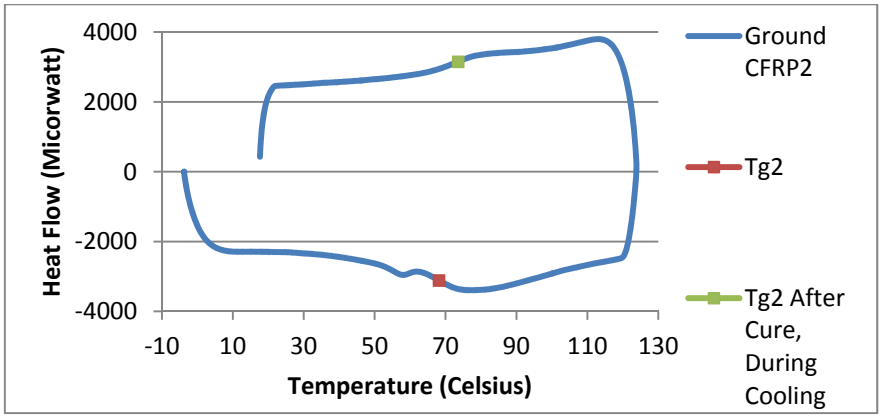

Figure 4.17. Ground CFRP2

The T_{gs} were very close to that of Ground CFRP1, 68.13˚C and 73.56˚C respectively, as was the general response and presence of the irreversible behavior. Diced CFRP was also analyzed as opposed to the ground CFRP. The diced CFRP had slightly lower values of T_g, possibly due to the heat added to the ground specimens but the difference was fairly marginal. All three plots are combined in the figure below.

To reduce the test time and conserve liquid nitrogen, the start temperature was changed to from -30˚C to -10˚C for the Ground CFRP2 test.

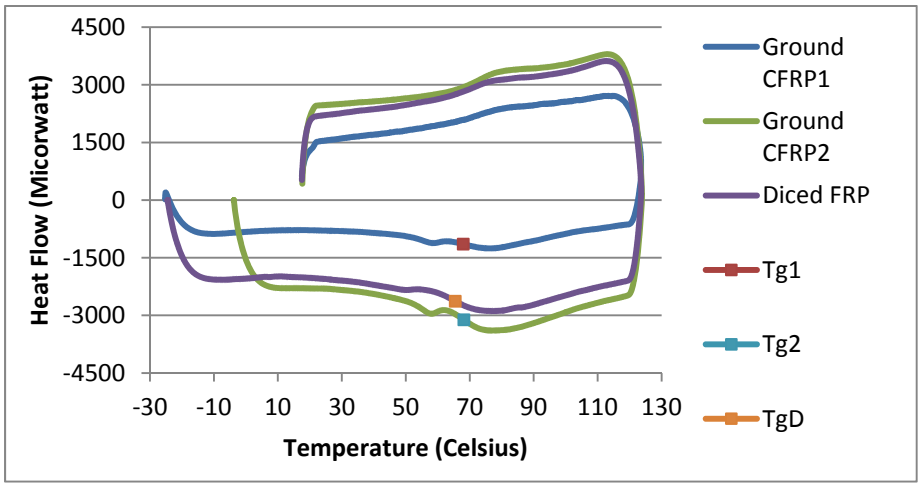

Figure 4.18. Ground and diced CFRP DSC results

The vertical shift in the DSC curves is due to the amount of reactive material within each specimen. The percentage of reactive material was likely very similar among the CFRP specimens but the different specimen sizes resulted in this vertical shift.

Two different types of filler resin were used in the DSC analysis. The specimens labeled “Filler Resin1” and “Filler Resin2” were made from the thick white filler resin found on the patch removed from bay 1NE. The specimen labeled “Bonded Filler Resin” was created from diced filler resin that was more translucent and less thick and white which came from a section of CFRP that was well-bonded to the substrate.

The first filler resin tested was Filler Resin1, which resulted in a DSC curve that had erratic behavior early in the test that was presumed to be irreversible behavior. The plot of this curve is in the figure below.

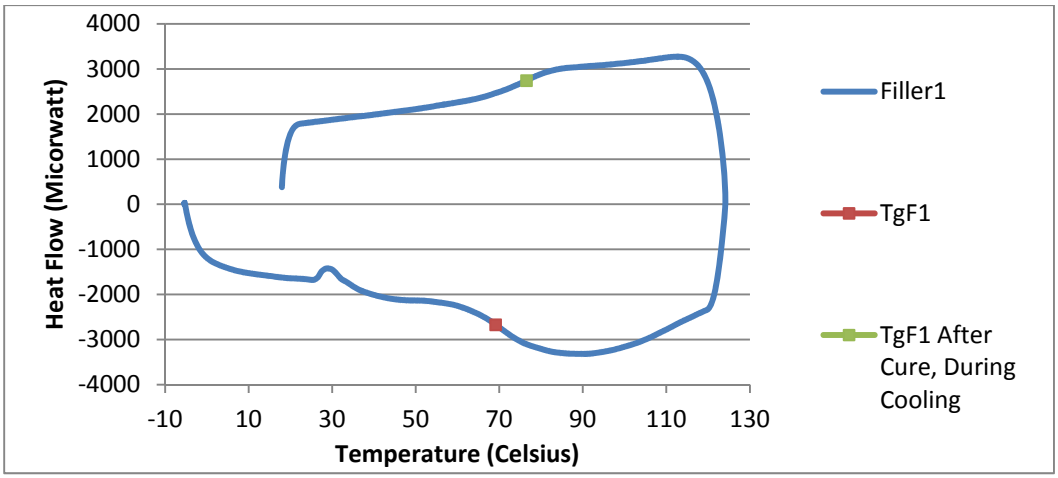

Figure 4.19. Filler resin1 DSC curve

Due to the erratic behavior near 30˚C during heating, it was decided to re-run this analysis with a new specimen, but to heat the specimen up to 40˚C then return the specimen to -10˚C and restart the DSC test. This would hopefully remove any irreversible behaviors without post-curing the specimen and consequently increasing the Tg. The erratic behavior was not however present in the second sample labeled Filler Resin2. The start temperature was moved back to -30˚C for the analysis of Filler Resin2 and Bonded Filler Resin. The plot is below.

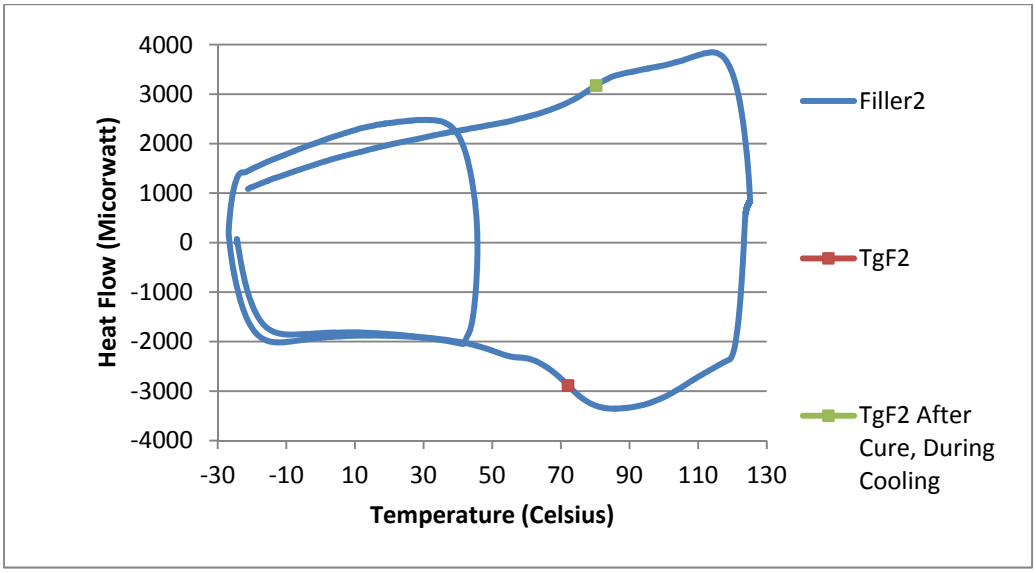

Figure 4.20. Filler resin2

The Bonded Filler Resin specimen was prepared similar to the other Filler Resin Specimens, but resulted in significantly different behavior and a higher T_g value. The T_g values are tabulated below the plots of the Bonded Filler Resin and the plot of all three Filler Resins.

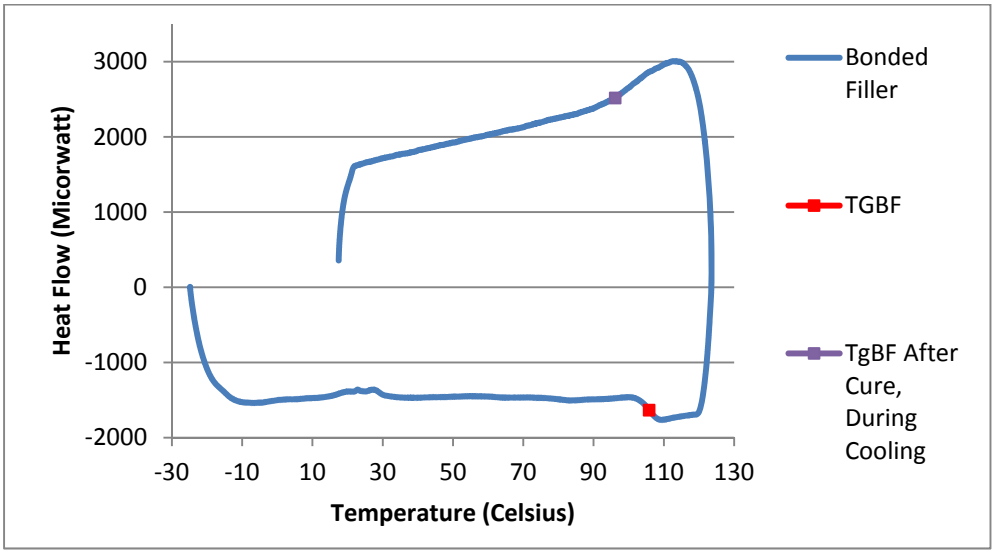

Figure 4.21. Bonded filler resin DSC curve

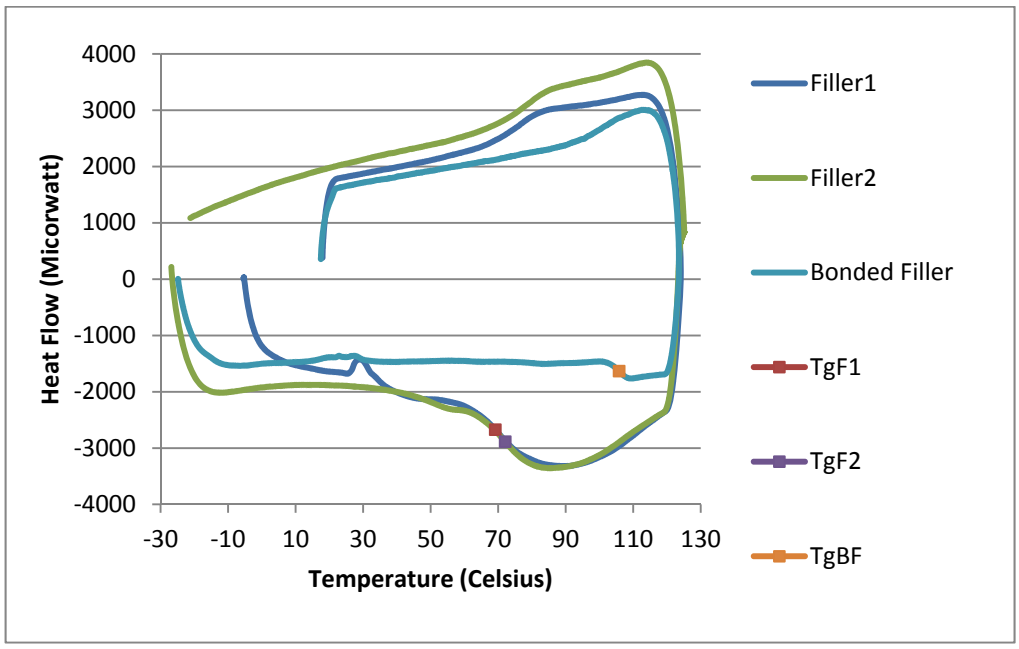

Figure 4.22. Filler resin DSC results

Table 4.6. Glass Transition Temperatures of CFRP and Filler Resins

	T_g	T_g, After Cure During Cooling
Ground CFRP1	67.95	73.19
Ground CFRP1A	77.38	78.02
Ground CFRP2	68.13	73.56
Diced CFRP	65.43	72.33
Filler Resin1	69.14	76.51
Filler Resin2	72.08	80.27
Bonded Filler Resin	105.83	96.15

The response of the Bonded Filler Resin is somewhat peculiar. It is possible that the milky white filler resin had higher water content, acting as a plasticizer reducing the T_g of the Filler Resin1 and Filler Resin2 specimens. As previously mentioned, even though there was water in direct contact to the CFRP patch of Filler Resin1 and Filler Resin2, by the time the material was tested, the moisture content was likely the same for all the specimens and very similar to that of the environment. All filler resins likely had similar if not the same curing conditions also making the higher T_g of the Bonded Filler Resin somewhat surprising.

All specimens had T_g values over the manufacturer's value of 60˚C which is well above any temperatures that the material could reach during service. The results other than the Bonded Filler Resin seemed reasonable and similar materials produced similar results. The T_g values measured at the laboratory were probably higher than the actual values of the material in contact with moisture on the arches of the bridge.

4.3 Summary of Field Assessment and Laboratory Testing

To summarize the test results and findings from the field assessment and laboratory testing, voids, pull-off tests, physical characteristics of the specimens collected, tensile tests, and DSC all contribute to the evaluation of the durability of the CFRP. All of these findings represent the extrados of the east arch and bay 1NW.

- The number of voids identified increased from 3 to 28

- Previous voids found (3) had an average increase in size by approximately 400%
- Filler Resin appeared thick, white, and smooth for some pull-off tests (6 of the 9 that were inadequate strength and failure Mode E) and the 1NE patch removed
- Pull-off test failure modes were distributed differently than 2003 results with more failure Modes B, E, and F
- Pull-off tests results of 2011 had a lower mean and higher standard deviation than the 2003 results
- 33% (9 of 27) of pull-off tests in 2011 were below the minimum 1.38 MPa (200 psi) compared to 2.4% (1 of 42) in 2003
- Ultimate tensile strengths were significantly lower than manufacturer's data, mean value of 754.4 MPa was above manufacturer's design value of 745 MPa, but CDOT construction specifications required the mean minus 3 standard deviations resulting in ultimate tensile strength of 288.2 MPa, and 5^{th} percentile was 498.8 MPa
- Rupture strains were significantly lower than specified minimum, specified minimum rupture strain was 0.006, mean was sufficient at 0.00981 but CDOT construction specifications required the mean minus 3 standard deviations resulting in 0.00308, 5^{th} percentile was adequate at 0.00612.
- Modulus of Elasticity values were representative of the manufacturer's data, mean of 77.3 GPa met the manufacturer's design value of 61.5 GPa
- Glass transition temperatures of both the CFRP and Filler Resins exceeded the manufacturer's value of 60°C.
- Physical phenomena causing irreversible behavior of DSC was not fully understood
- More data points for all tests (initial values and additional points upon every evaluation) would provide more insight into trends, durability thresholds, and performance

- Initial values of tensile tests, T_g, and bond strengths coupled with thorough void identification could help identify poor workmanship or quality

The increase in number and size of voids may be due to poor documentation of the past or there may be definite cause for concern. The pull-off test may have provided more of an insight into testing technique than bond strength. The unsatisfactory results of ultimate tensile strength and rupture strain are due in part to the stringent demands of the CDOT specifications. The modulus of elasticity, 5^{th} percentile of rupture strain, mean of ultimate tensile strength, and glass transition temperatures were all satisfactory. Based on these results there appears to be some deterioration, but a more detailed test program would be needed to thoroughly characterize the deterioration.

5.0 TASK 4: LITERATURE REVIEW ON ADDITIONAL FRP TOPICS

Topics requested by CDOT included: fatigue, durability under environmental and chemical exposure, bond behavior, and existing design details and guidance. Bond behavior and testing is addressed in Section 6.0.

5.1 Fatigue of Concrete Beams with Externally Bonded FRP Strengthening

The effect of fatigue loading on FRP repair was identified as a topic of interest to CDOT engineers because transportation structures such as bridges will generally be subject to fatigue loads. A thorough review of existing work studying the fatigue performance of concrete beams strengthened with externally bonded fiber-reinforced polymer composites was published by Kim and Heffernan in 2008. This review provides a valuable introduction to the topic. Both reinforced and prestressed concrete beams of various sizes were considered. For some studies considered by this review the test beams were taken from decommissioned bridges (Rosenboom and Rizkalla, 2006) or constructed based on scaling a full-scale bridge elements (Aidoo, Haries and Petrou, 2004).

Concrete beams with externally bonded FRP subject to fatigue loads will most often fail due to fracture of the steel reinforcing bars followed quickly by debonding of the FRP from the concrete (Kim and Heffernan, 2008). Thus, although the fatigue performance of FRPs (especially carbon) is often described as one of their advantages, when it is used as external reinforcement fatigue performance may be limited by the properties of the existing structure, the reinforcing steel in particular. When FRP is applied as an external strengthening mechanism, tensile loads are shared between the steel and FRP, and the stresses in the steel are lower for a beam with externally bonded FRP than one without. Thus the application of FRP would be expected to extend the fatigue life of the strengthened structure by reducing the level of stress in the reinforcing steel. In their analysis of existing work Kim and Heffernan found that most studies reached this conclusion (2008). The amount of increase can vary widely depending on the specific loading conditions and quantities such as the amount of steel and FRP. In the work surveyed fatigue lives for strengthened beams ranged from 2.1-95 times the fatigue life of unstrengthened control

beams (Kim and Heffernan, 2008). For load ranges between 30 and 50 percent of the yield strength of the reinforcement, fatigue damage did not seem to be accumulating. Beams strengthened with FRP also showed higher flexural stiffness and reduced crack widths, which may further benefit the fatigue performance of the steel reinforcement (Kim and Heffernan, 2008).

With respect to design of external FRP strengthening for fatigue, the review by Kim and Heffernan (2008) considered existing design guidance and identified issues that merit designer consideration. Fatigue is generally addressed only in a limited way in existing guidelines for the design of externally bonded FRP. Recognizing that the fatigue life is generally controlled by the reinforcing steel documents such as the ISIS Canada and *fib* guidelines recommend limitations on the stress range in the steel. ACI-440.2R-02 limits the stress in the FRP in order to prevent both creep and fatigue failure, but several studies pointed out that this limit did not correspond to the actual failure mode of beams failing due to fatigue and Kim and Heffernan (2008) suggested that the ACI 440 provisions be revised. A revised version of ACI 440.2R was released in 2008 without changes to way fatigue is considered. Design of FRP strengthening for a structure subject to fatigue loading should consider: 1) limiting the stress range in the reinforcing steel (existing limits from ACI 215 and the AASHTO LRFD manual should be applicable); 2)making the bonded area between the concrete and FRP as large as possible by selecting wider and longer dimensions for the FRP as opposed to shorter and thicker dimensions; 3) the effect of sustained load levels and the load level for which the structure was originally designed.

Kim and Heffernan (2008) conclude their review by identifying a list of seven areas meriting further research:

1. Detailed explanation of the progressive debonding at the concrete/FRP interface;
2. A method to predict the redistribution of stress in a strengthened cross-section is needed to better predict the fatigue life assuming fracture of the reinforcing steel as the controlling limit state;
3. Development of better anchorage systems to prevent debonding failure of the FRP;
4. Detailed design guidelines are still needed, especially considering the effect of the existing condition of a structure before the application of FRP strengthening;

5. Consideration of slabs – i.e. bridge decks;
6. More experimental work considering different load ranges and frequencies and more realistically representing actual bridge loading;
7. Investigation of applications of FRP in the field using.

In the years since this review was published, research on the fatigue performance of externally bonded FRP strengthening and repair schemes has continued. In most of the studies considered by Kim and Heffernan (2008), the beams were undamaged before the FRP was applied, but there were individual examples of corrosion, pre-cracking of the concrete, and cyclic loading before the FRP was applied. More recent research has continued to investigate these types specimens which are more representative of field conditions. Al-Hammoud, Soudki and Topper (2011) tested a series of 30 beams where corrosion was induced in the reinforcing steel and the beams were then repaired with CFRP. The combination of corrosion and fatigue is an important case to consider because 1) this combination is a common occurrence on structures such as bridges which are subject to cyclic loading and winter application of deicing chemicals, and 2) corrosion hurts fatigue performance by creating pits in the rebar, reducing the cross-sectional area of the rebar, and causing cracking of the concrete. This study considered three different load ranges : 47, 57, and 72% of the static load capacity of the beams, as well as the amount of corrosion and the amount of FRP used for repair. They found that a single sheet of FRP applied to a beam with medium corrosion levels (7.05-9.05% mass loss) was able to extend the fatigue life to that of an uncorroded beam without FRP. The FRP was also beneficial to the fatigue life of highly corroded beams (10-14.3% mass loss), although these beams still had a shorter fatigue life than the undamaged, unrepaired control beam.

Davalos et.al. (2010) also induced corrosion in a series of beams and tested the beams under static and cyclic loads. However, this series of tests was intended to evaluate the effectiveness of different anchorage schemes. Three different types of strengthening configurations were tested. The first configuration only had the FRP sheet in the tension zone, the second configuration used two U-shaped

stirrups of FRP applied close to the outer quarter points of the span, and the third configuration used eight evenly spaced U-wraps. The beams were not tested to failure, but the deflection and stiffness were monitored at increments of 250,000 cycles up to two million cycles. All of the strengthening configurations showed a significant loss in stiffness during the first 250,000 cycles. Although there was some variation between duplicate specimens which complicated interpretation of results, the beams with some anchorage (either two or eight U-wraps) had lower deflections when loaded in the serviceability range and there appeared to be some advantage with respect to permanent deflections.

While most existing work considers fatigue performance of beams with FRP applied for flexural strengthening. Dong, Wang and Guan (2012) looked at the fatigue performance with FRP applied as shear reinforcement. Performance of beams with strips of CFRP and GFRP applied vertically on the sides of the beam in the shear span were compared. Vertically arranged GFRP was also compared to diagonal GFRP strips. Both types of FRP were found to offer significant enhancement of load capacity and lower deflections. The FRP strengthened beams also showed fewer cracks with a wider crack spacing. After one million fatigue cycles the stiffness of the CFRP showed a greater degree of degradation than the GFRP.

Ongoing work has also been aimed at developing or evaluating models for the prediction of fatigue life. Meneghetti et. al. (2011) used fatigue testing results available in the literature as well as the author's own work to fit regression models relating the variation in stress in the reinforcing steel to the Log of the number of cycles. Two models were created, one for FRP strengthened beams and one for un-strengthened beams. Although the models reasonably fit the data upon which they were based, the authors note that in real beams which might have significant deterioration before the FRP is applied the existing condition of the rebar will be unknown and the FRP reinforcement may not be as effective at extending the fatigue life. Gordon and Cheng (2011) collected several existing models relating the stress range to fatigue life (S-N curves) presented in the literature and fit additional S-N models to results of fatigue tests by other researchers. In some cases, due to the available published data, they developed P-N curves relating the applied load to the fatigue life. They then evaluated the predictive ability of these

different models, and concluded that none of the models were particularly accurate and emphasized the need for further research including parametric studies to evaluate how different variables in terms of the specimen and the loading conditions affect fatigue life.

The importance of fatigue performance for RC beams strengthened with externally bonded FRP has clearly been acknowledged, and through numerous studies progress has been made in understanding the behavior of these beams. However, there is still a significant amount of work to be done. The research conducted since the literature review of Kim and Heffernan (2008) has yet to fully address the areas they identified for further research. Of particular importance is the need for better models for predicting fatigue life and design guidance. In most practical applications FRP will be applied to a structure that has already been subject to a significant amount of cyclic loading and which is likely showing signs of deterioration such as cracking, or perhaps corrosion. Designers need guidance allowing them to predict the effect of an FRP strengthening application on extending the fatigue life of an existing structure and indicating how different design choices such as amount of FRP, will affect that prediction.

5.2 FRP Durability under Environmental and Chemical Exposure

Tan et al. (2011) explains that "though the main factors affecting durability and failure mechanism of concrete have been fully investigated, few studies on the durability of FRP reinforced structures have been taken" and "factors affecting the durability of FRP reinforced structures should be analyzed." Tan et al. (2011) defines the term "durability" as:

> "the given structure under conditions of normal designing, constructing, serving and maintaining can continue to perform its intended functions during the specified or traditionally expected service life, in spite of structural performance deteriorating with time."

Similarly, the Civil Engineering Research Foundation (CERF) and the Market Development Alliance (MDA) of the FRP Composites Industry in collaboration with Karbhari et al. (2000) defined the term "durability" with respect to fiber-reinforced polymer composites as "the ability to resist cracking, oxidation, chemical degradation, delamination, wear, and/or, the effects of foreign object damage for a specified period of time, under the appropriate load conditions, under specified environmental conditions" in their study of "Critical Gaps in Durability Data for FRP Composites in Civil Infrastructure." The term

"durability" used throughout this thesis will be inclusive of both definitions provided above by Tan et al. (2011) and Karbhari et al. (2000).

FRP materials have potentially high overall durability, however, Karbhari et al. (2000) notes that "there is evidence of rapid degradation of specific types of FRP composites when exposed to certain environments" and "actual data on durability is sparse, not well documented, and in cases where available – not easily accessible to the civil engineer." Karbhari et al. (2000) continues that there is a "wealth of contradictory data published in a variety of venues" resulting from the "reporting of data without sufficient detail of the actual materials used, use of different forms of materials and processing techniques, and even changes in the materials systems with time" (Karbhari et al. 2000). Seven years later, Chen et al. (2007) agrees "although a number of durability studies on FRP have been reported by various researchers, no general conclusions are possible as researchers used different testing procedures and conditions. In some cases, even conflicting results have been reported."

The durability of an FRP composite is compromised if the material properties of the FRP appreciably change or if the bond between layers of FRP or between the FRP and its substrate becomes weak or is lost altogether. Karbhari and Ghosh (2009) identify the critical components of the performance of externally applied FRP, stating "since the composite element is bonded onto the concrete substrate the efficacy of the rehabilitation scheme depends on the combined action of the entire system with emphasis on the integrity and durability of the bond between the FRP and concrete." Karbhari and Ghosh (2009) add "the performance characteristics of the substrate, FRP, adhesive/resin forming the bond and the interfaces can all be deteriorated by environmental exposure and hence there is a need to assess its effect on these materials and on the bond itself." Byars et al. (2003) agrees contributing "changes in mechanical properties such as Young's modulus, tensile and interlaminar shear strengths and bond strength are the best indicators of changes in the performance of FRP."

Manufacturing, material components (fiber and resin types), environmental conditions, and the quality of the application process all contribute to the durability of an FRP composite. Prefabrication and wet layup are the two primary manufacturing processes for strengthening applications of FRP. The wet

layup process utilizes an “ambient temperature cure resin system” (Karbhari and Ghosh, 2009) which has the advantage of conforming to irregular shapes or areas of uneven geometry reducing unbonded areas, but it may deteriorate faster than prefabricated bars or strips. As described by Karbhari and Ghosh (2009) these prefabricated materials are based on “well characterized high-temperature and controlled condition cure resin/adhesive systems used for long–term durable bonds in the aerospace industry.” Durability of FRP depends intrinsically on the choice of constituent materials, methods and conditions of processing, and surrounding environmental conditions through their service lives (Karbhari, 2003).

Karbhari et al. (2000) and Karbhari et al. (2003) identify identical environmental conditions of primary importance pertaining to the durability of internal and external applications of FRP: “moisture/solution, alkali, thermal (including temperature cycling and freeze-thaw), creep and relaxation, fatigue, ultraviolet, and fire.” Coinciding with Karbhari et al., Byars et al. (2003) considered similar environmental conditions that may affect the durability of FRP: “moisture, chlorides, alkali, stress, temperature, UV actions, carbonation and acid attack.” Numerous laboratory tests of the durability of FRP have been conducted.

Previous laboratory studies have investigated the durability of both glass fiber-reinforced polymers (GFRP) and carbon fiber-reinforced polymers (CFRP). From these studies, it has been identified that different fiber types are susceptible or vulnerable to different conditions. Karbhari and Ghosh (2009) found that “glass fiber-reinforced system undergoes slightly greater moisture initiated deterioration than the carbon fiber-reinforced system.” Fiber types can be optimized depending on the requirements of the FRP application such as in Stallings (2000) study where GFRP was used for shear strengthening and CFRP was used for flexural strengthening of bridge girders in Alabama. The stronger, more expensive CFRP was used where durability was more critical because the flexural strength was controlling, while the weaker, less expensive GFRP plates were used to confine the flexural cracks and to add stiffness, reducing deflections.

The durability of fiber types alone is unfortunately not a comprehensive study of the durability of FRP. Karbhari (2003) addresses this complexity stating “Although carbon fibers are generally considered

to be inert to most environmental influences likely to be faced in civil infrastructure applications the inertness does not apply to the fibre-matrix bond and the matrix itself, both of which can in fact be significantly deteriorated by environmental exposure."

5.2.1 Accelerated Aging

Through rigorous durability studies Karbhari (2000) anticipates "appropriately designed and fabricated, these systems can provide longer lifetimes and lower maintenance than equivalent structures fabricated from conventional materials." To further understand the development of degradation, multiple lab tests have been conducted to determine the effects of various conditions on the durability of GFRP and CFRP composites. Externally bonded FRP applications are typically subject to certain environmental exposures in which CFRP has proven to be much more durable than GFRP. A multitude of lab tests have been conducted in which the normal ageing process is sped up called accelerated ageing. The following are a few examples.

Typical accelerated aging techniques include exposing specimens, sometimes alternating exposures, to varying solutions and temperatures. As an example, Chen et al. (2007) conducted accelerated aging tests by elevating the temperatures of specimens while cycling wet and dry (WD) and freezing and thawing (FT) in solutions representative of expected environments. Chen et al. (2007) used 5 different solutions in their study consisting of: tap water "to simulate high humidity and used as a reference environment," solutions with varying amounts of sodium hydroxide, potassium hydroxide, and calcium hydroxide with pH values of 13.6 and 12.7, a simulation of ocean water consisting of sodium chloride and sodium sulfate, and finally a solution emulating concrete pore water contaminated with deicing agents containing sodium chloride and potassium hydroxide with a pH of 13. "Elevated temperatures of 40 ˚C and 60 ˚C were used to accelerate the attack of simulated environments on FRP bars, since the degradation rate mainly depends on diffusion rate and chemical reaction rate, both of which can be accelerated by elevated temperatures" (Chen et al., 2007). The first four solutions were subject to nine WD cycles which "consisted of four days of immersion at 60 ˚C followed by four days of drying at 20 ˚C" (Chen et al., 2007). All five solutions were subject to FT cycles which "consisted of 30

min of soaking at 20 ˚C, 90 min of ramping from 20 to -20 ˚C, 30 min of soaking at -20 ˚C, and finally 90 min of ramping from -20 to 20 ˚C" (Chen et al., 2007). Durability performance was measured by the change in tensile and interlaminar shear strengths after exposures. Bond strengths were also evaluated through use of pullout tests. Chen (2007) concluded "strength loss resulted from the accelerated exposure of both bare and embedded GFRP bars, including bond strength, especially for solutions at 60˚C. In contrast CFRP bars displayed excellent durability performance."

Hu et al. (2007) conducted a study exposing specimens to the aggressive environmental conditions of: fast freeze-thaw cycling, alkaline immersion, water immersion, and wet-thermal exposure. This study also concluded: "CFRP specimens subjected to aggressive environments showed good durability with no significant degradation in tensile strength and modulus, however, GFRP specimens exhibited a little decrease in mechanical property after aggressive environments exposure."

Ghosh et al. (2005) also used 5 different exposures in the evaluation of bond strength durability by the use of pull-off tests. "Eleven different composite systems, six carbon fabric systems, one glass fabric system and four pultruded carbon strip systems, were bonded to the surface of concrete blocks using epoxy resin systems" (Ghosh, 2005). Five different exposure conditions in addition to a set of specimens kept at room temperature were evaluated at 6, 12, and 18 months. Ghosh (2005) concluded "only two systems showed susceptibility to these exposure conditions. In terms of overall performance, two carbon fabric/epoxy resin composite systems showed good bond strength retentions under all the exposure conditions studied." Confirming what Karbhari (2000) ascertained Ghosh (2005) advised "a judicious selection of the composite system based on its performance specific to its application condition will be necessary for optimization and long-term integrity of such strengthening/rehabilitation."

Durability tests conducted in laboratories using accelerated aging techniques and extreme exposures to determine the long-term durability of FRP composites have often shown promising results. Though useful, these efforts have not satisfied the concern about the long-term performance, or durability, of FRP strengthened reinforced concrete structures in the field. This difference was explained by Karbhari (2003) as an "apparent dichotomy between 'real-world' applications and laboratory data" that is currently

accounted for through the use of safety factors in design. Moreover, perhaps providing some of the reasoning why this dichotomy exists Karbhari et al. (2003) states “synergistic effects (i.e., effects resulting from the combination of multiple environmental conditions, both in the absence and presence of load) are known to exacerbate individual effects.”

Reay et al. (2006) pointed out “Studies on field applications of FRP materials have been limited, and many of those that have been performed have not provided the type of real-time, long-term durability data needed to better understand the effects of environmental conditions on FRP materials.”

5.2.2 Field Evaluations

A review of literature was conducted to identify existing examples of field evaluation. There were not that many examples identified. Nineteen highway bridges were repaired with 11,000 meters of bonded FRP plates in the Republic of Macedonia in 2001 and 2002 (Crawford 2008). American Concrete Institute (ACI) 440.2R (2000) was used for the design of the FRP repair. Evaluation of these bridges was conducted to establish a baseline for investigation of durability. Load tests were conducted on 3 of the bridges prior to and following the repair. These load tests were considered “trial testing” and were done to confirm and verify mathematical models, the FRP repair, and to provide data for comparison with future tests. The trial test consisted of static and dynamic load of a 102 ton, 9 axle heavy commercial vehicle. Strain gauges on reinforcing steel prior to the repair were replaced with strain gauges on the FRP in similar locations following the repair. The trial test was a success and “strongly supported the provisions of ACI 440 (2000),” and “fully justified the suitability of FRP system for strengthening of bridges” (Crawford, 2008). The study developed a valuable model for FRP system inspection which is outlined below:

- Define bridge performance standards and criteria
    - Establish base-line condition for the bridges, i.e. at completion of FRP application
    - Define bridge performance (loading) standard
- Inspection
    - Establish inspection criteria, procedures, protocols
    - Set inspection frequency, measuring points, data collection requirements
- Data Collection and Analysis
    - Collect inspection data, record in national data base

    - Perform data analysis to identify types of deterioration and rate of deterioration
- FRP-System Bridge Maintenance
    - Set maintenance criteria and standards for bridges and FRP systems
    - Prescribe FRP-maintenance protocols and procedures
- Load Testing and Certification
    - Perform bridge load testing, up to 100 tons, every 8-10 years
    - Certify bridge load capacity for national authorities

Crawford (2008) did an excellent job describing durability, environments that threaten durability, debonding mechanisms, and design, but this study provided no data other than the initial values from the load tests prior to and following the repair. This study does not provide any inspection criteria, procedure, or protocol nor does it recommend inspection frequency, measuring points, or data collection methods. In addition, this paper has failed to describe how to set maintenance criteria or maintenance protocols and procedures. This study has presented a large group of bridges with known baseline values of load tests, and have set the stage for a durability study, but neglected to give any specific guidance as to how or what future durability studies should consist of other than load tests "up to 100 tons, every 8-10 years."

Barlow (2005) outlines the history of the use of FRP with five case studies in the northwest region of the United States. In 1993, "the northwestern United States spearheaded the bold use of these materials" despite the fact that "initial research was done in other states and parts of the world" (Barlow, 2005). The case studies included 2 bridges, a library, a courthouse, and a treatment plant. Quality control of the FRP applications on the bridges as well as the courthouse and library were monitored by tension test panels that were made simultaneous to the installation. In the cases of the bridges, the test panels were retained by their respective agencies, WSDOT and ODOT. Independent testing prior to the repair provided the quality assurance of the projects. The owner of the courthouse retained the test panels and an independent testing laboratory performed "periodic special inspection." The application on the courthouse also included pull-off tests in accordance with ASTM D4541 to verify the bond strength of the FRP to the substrate.

The anticipation of test panels with these projects was innovative and much needed. From this study, no information in regard to degradation over time or durability was provided. It is unknown as to whether or not subsequent pull-off tests were conducted or if the test panels were used. It was also unclear

as to what conditions or environments the test panels were stored. Perhaps the test panels are intended to be tested in the future, but without utilizing these samples with premeditated frequency it is uncertain as to how helpful, if at all, the resulting data will be to understanding the durability of FRP. To fully understand the development of degradation it is necessary to collect more data points over time with additional samples and their respective environments.

Hag-Elsafi et al. (2004) conducted an "in-service evaluation" of an FRP repaired bridge in New York. In November, 1999, a T-beam bridge, Wynantskill Creek Bridge was strengthened to increase the shear and flexural capacities using the FRP wet layup process. The FRP repair was also intended to contain freeze-thaw cracking. Prior to and directly following the FRP repair, instrumentation was installed and load tests were conducted to find the change in stiffness or performance of the repaired bridge. The bridge was in service for approximately 2 years before an additional load test was conducted in November, 2001. There was no detection of deterioration of the strengthened bridge in the 2 years of service through measures of strain caused from the load test or from infrared thermography. Figures were included of the repaired T-beam bridge as well as a figure of an infrared Thermographic image of the repaired bridge (Hag-Elsafi et al., 2004).

"The changes in beam stiffness during the three tests are very small," however smaller strains were consistently recorded for the 2001 test, "although some of the strains were within the variations normally associated with instrumentation" (Hag-Elsafi et al., 2004). Hag-Elsafi et al. (2004) concluded that from the data collected and subsequent analysis considering transverse load distribution, effective flange width and neutral axis locations established from strain gauge measures and thermographic imaging that there was "absence of any signs of deterioration in the retrofit system after two years in service."

It is reasonable to believe that the repaired T-beam bridge could be in service until 2030 or longer. This study confirms that the FRP repaired bridge proved to be durable and resilient to the conditions between November, 1999 and November, 2001. It did not however, anticipate any follow up evaluations in which further valuable data and information of performance could be gathered. It is

unreasonable to forecast 30 years of durability based on two years of exposure, especially considering the variance of conditions the bridge can be exposed from year to year.

Saenz et al. (2004) conducted a durability study of FRP composites exposed to "single, dual and multi-variable environmental exposures." The study combined GFRP and CFRP with epoxy-resin and urethane-resin matrices for a total of 4 combinations of FRP composites. The single exposure specimens were isolated in a dry dark environment to undergo "natural aging" or non-accelerated exposure evaluated at 450 and 900 days. The dual exposures were subject to the combination of "accelerated freeze-thaw cycling in salt water" for 112 and 162 cycles of exposure. The multi-variable environmental exposure, also considered "naturally exposed" consisted of aging the specimens at the State Street Bridge location on I-80 in Salt Lake City, Utah and evaluated at 365 and 730 days of exposure. The purpose of the single and dual environmental exposures was to decouple the degradation due to natural aging with the degradation due to the accelerated freeze-thaw cycles in the saline solution. The purpose of the specimens "naturally exposed" was to identify degradation due to typical environmental exposures at bridge locations.

Zhang (2002) also contributed a durability study of FRP aged in a natural setting. Tensile, ring, and lap slice tests were conducted and it was determined that the "naturally exposed" units showed no degradation after the 365 days of exposure. The specimens with urethane-resin matrix showed "significant loss in interlaminar shear strength after freezing and thawing exposure" while specimens with epoxy-resin matrix "showed a significant increase after freezing and thawing exposure."

Reay and Pantelides (2006) conducted a similar durability study in regard to the State Street Bridge and considered the CFRP retrofit "effective after 3 years of service." Following three years of exposure, "nondestructive evaluation was conducted through strain gauges, tiltmeters, thermocouples, and humidity sensors installed on the bridge bents for real-time health monitoring." "Destructive tests were performed to determine the ultimate tensile strength, hoop strength, concrete confinement enhancement, and bond-to-concrete capacity of the CFRP." In addition, thermography was used to detect voids, or unbonded areas, between the FRP and the concrete substrate.

During the repairs (east bents in August of 2000 and west bents in June of 2001), three types of tests were conducted as quality assurance measures: tensile tests, fiber volume tests, and glass transition temperature tests. Specimens were also created at the time of the FRP repair for future tests consisting of tensile tests, composite rings, confined concrete cylinders, and pull-off tests. The specimens were stored in 3 different locations: "on top of the cap beam at the State Street Bridge, inside a cage located at ground level between two columns of the State Street Bridge, and in an isolated area of the Structures Laboratory at the University of Utah" (Reay and Pantelides, 2003). The specimens were tested at approximately six month intervals of 18, 24, and 30 months. In addition to the specimens created at the time of repair a section of the side of the cap beam was prepared with a patch for future tensile tests. Half of the patch was covered with an "ultraviolet protective coating" (Reay and Pantelides, 2003) and the other half unprotected. Some degradation of the FRP due to the environment was found through the destructive tests. Reay and Pantelides (2003) concluded "Destructive tests of CFRP composite tensile coupons, rings, and CFRP composite-to-concrete bond specimens have shown that specimens stored in the laboratory, generally give higher ultimate strength capacity than those stored at the bridge."

Both of these studies were innovative in sample selection and storage, but it is unclear as to why the Saenz et al. (2004) study evaluated specimens at differing times. It makes the comparison more difficult when the "single exposure" specimens were evaluated at 450 and 900 days, while the other specimens were evaluated at 365 and 730 days. It is also difficult to compare the exposures when the environment at the bridge was not quantified in ways such as number of freeze/thaw cycles, precipitation, applications of deicing agents etc.

In addition to the destructive and non-destructive tests, in June of 2003, multiple voids of varying shapes and sizes were located on the southeast bent of the State Street Bridge using thermographic imaging. Because no thermographic images were taken directly after the retrofit, it was not possible to determine whether the voids or bond flaws existed at the time of the repair or if they developed during service. Six months later in December, 2003 thermographic images were taken and compared with the images collected in June, 2003 and no significant changes in size or shape were found. Reay and

Pantelides (2003) concluded “More sophisticated methods are required to determine quantitatively the size and any enlargements of the voids.”

Thermographic imaging at the time of the repair or retrofit would have been an excellent means to provide quality control of the installation of FRP and it would have helped to quantify the degradation of the bond during service. Additionally it would be beneficial to have an object of known size that appears distinctly such as a hot or cold coin to reference for size.

5.3 Existing Design Guidance

5.3.1 National Cooperative Highway Research Program

Several reports prepared by NCHRP studies are particularly relevant as they focus on design for bridges. The first two reports include a discussion of design considerations, sample design provisions, and design examples. The examples are listed below. The third report may be helpful in writing CDOT construction specifications. These reports can be obtained as PDFs free from the NCHRP website, http://www.trb.org/NCHRP/NCHRP.aspx

NCHRP Report 655 Recommended Guide Specification for the Design of Bonded FRP Systems for Repair and Strengthening of Concrete Bridge Elements
6 Examples:

- Calculation of the characteristic value of the strength of an FRP reinforcement system
- Flexural strengthening of a T-beam in an unstressed condition
- Flexural strengthening of a T-beam in a stressed condition
- Shear strengthening of a T-beam using U-jacket FRP reinforcement
- Shear strengthening of a rectangular beam using complete wrapping FRP reinforcing system
- Strengthening of an axially loaded circular column

NCHRP Report 678 Design of FRP Systems for Strengthening Concrete Girders in Shear

6 Examples:

- RC T-beam without internal transverse steel reinforcement strengthened with FRP in U-wrap configuration without anchorage systems

- RC T-beam without internal transverse steel reinforcement strengthened with FRP in U-wrap configuration with an anchorage system
- RC T-beam with internal transverse steel reinforcement strengthened with FRP in U-wrap configuration without anchorage systems
- RC T-beam with internal transverse steel reinforcement strengthened with FRP in U-wrap configuration with an anchorage system
- PC I-beam with internal transverse steel reinforcement strengthened with FRP in U-wrap configuration without anchorage systems
- PC I-beam with internal transverse steel reinforcement strengthened with FRP in U-wrap configuration with an anchorage system

NCHRP 514: Bonded Repair and Retrofit of Concrete Structures Using FRP Composites -- Recommended Construction Specifications and Process Control Manual

5.3.2 American Concrete Institute

The ACI guideline is not specific to bridges, but still provides a number of valuable examples.

ACI 440.2R-08 Guide for the Design and Construction of Externally Bonded FRP Systems for Strengthening Concrete Structures

Part 5 Design Examples

9 Examples:

- Calculation of FRP system tensile properties
- Comparison of FRP systems' tensile properties
- Flexural strengthening of an interior reinforced concrete beam with FRP laminates
- Flexural strengthening of an interior reinforced concrete beam with NSM FRP bars
- Flexural strengthening of an interior prestressed concrete beam with FRP laminates
- Shear strengthening of an interior T-beam
- Shear strengthening of an exterior column

- Strengthening of a noncircular concrete column for axial load increase
- Strengthening of a noncircular concrete column for increase in axial and bending forces

5.3.3 Concrete Society Committee (UK)

Although this is a slightly older guideline the design flow charts may be helpful to designers working with FRP for the first time.

Technical Report 55. Design guidance for strengthening concrete structures using fibre composite materials
Design Flow Charts

- Flow chart of assessment process (pg. 4)
- Flow chart of strengthening members in flexure (Chapter 6)
- Flow chart of shear strengthening (Chapter 7)
- Flow chart of strengthening axially loaded members (Chapter 8)

6.0 TASK 5: ESTABLISH LONG-TERM TESTING PLAN

6.1 Importance of FRP – Concrete Bond Durability

The use of carbon fiber-reinforced Polymers (CFRP) has progressively gained popularity in the reinforcement of aging and deteriorating concrete structures. Other than cost, the reason why this repair method has not yet been more widely used in the field is due to the lack of knowledge about the long-term behavior of the CFRP material itself and of the bond between the CFRP and concrete. A strong bond is vital for proper transfer of stresses between the concrete and the reinforcement. If a structural element is poorly reinforced with CFRP, premature debonding is likely to occur, leading to failure of the structure at load capacities much lower than what the reinforcement was designed to provide (Karbhari & Ghosh, 2009). In addition, environmental exposure may significantly affect the bond performance over time. Natural conditions such as rapid temperature changes, fires, snow and rain, as well as manmade conditions including application of deicing salts on roads and bridges, are some of the factors involved in the deterioration of a bond.

Over the years, research has been conducted to study the behavior of the bond between FRP and concrete using different testing methods and testing exposures. The following sections of this chapter provide descriptions of the various methods used by previous researchers to test bond, and reviews durability studies that have been conducted in the past.

6.2 Bond Tests

The strength and behavior of the bond between CFRP and concrete can be determined through various testing methods, depending on the nature of the study. Factors such as size, geometry, and quantity of specimens are taken into consideration when choosing an appropriate bond test. Sections 6.2.1 through 6.2.5 describe the different bond testing methods that were evaluated, and the various reasons why two methods were specifically chosen for the purposes of the durability study, described later in this Section 6.0.

6.2.1 Direct Shear Tests

Previous studies have employed direct shear tests in order to test bond strength under pure shear. Pan and Leung (2007) used direct shear tests to "study the crack-induced debonding failure in reinforced concrete members flexurally strengthened with FRP composites". Figure 6.1 illustrates a direct shear test using a simple diagram. For testing procedures, the concrete specimen, already bonded with the FRP composite, was placed vertically on the material testing system. In order to perform direct shear on the bond, a steel frame was designed to hold the specimen in its vertical position. When aligned properly, the concrete specimen was held in place, while the FRP plate was subjected to an upward tensile force, causing direct shear between the concrete beam and the composite (Pan & Leung, 2007). The primary disadvantage of this method is the complexity of having to build a custom frame to hold the specimen in place. The slightest error in alignment could have caused eccentricity on the specimen which would have decreased the accuracy of the results. For this reason, direct shear tests were not used in this study.

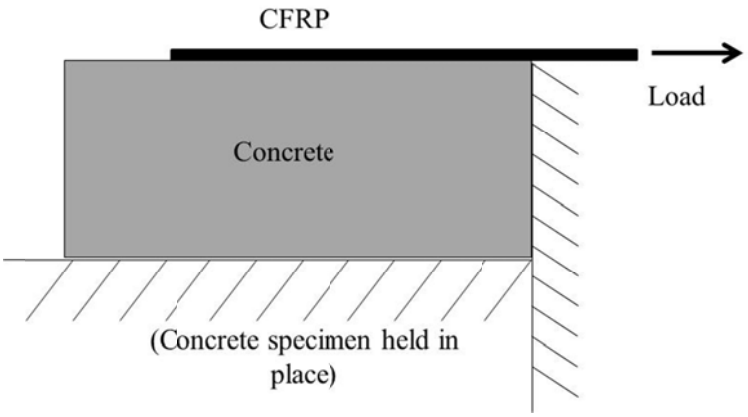

Figure 6.1 Direct shear test representation

6.2.2 Double- Face Shear Tests

Double shear tests have some similarity with single shear tests in the sense that they both determine the strength of the CFRP-concrete bond under pure shear. However, double shear tests have two bonded regions being tested at the same time. More specifically, two blocks of concrete of the same type and dimensions are attached together by two strips of CFRP on opposite sides. Testing of these specimens has been conducted in different ways. Ko and Sato (2007) performed a study in which a steel

bar was internally fixed in the concrete block, and cut in the middle to allow the stress to be distributed into the concrete and the composite. Uniaxial tension was applied by gripping the steel bar, and measurements were recorded with the use of strain gauges. (Ko & Sato, 2007). In addition, a variation of a double-face shear test can consist of pushing two specimens away from each other. Both types put the CFRP-concrete bond in pure shear. Figure 6.2 shows the two different kinds of double- face shear tests. The main issue that was noticed with this test type was making sure that both concrete blocks were properly aligned when the two FRP sheets were bonded. Also, handling of the specimens seemed difficult, particularly when moving them was necessary. As a result, double shear tests were not conducted in this study.

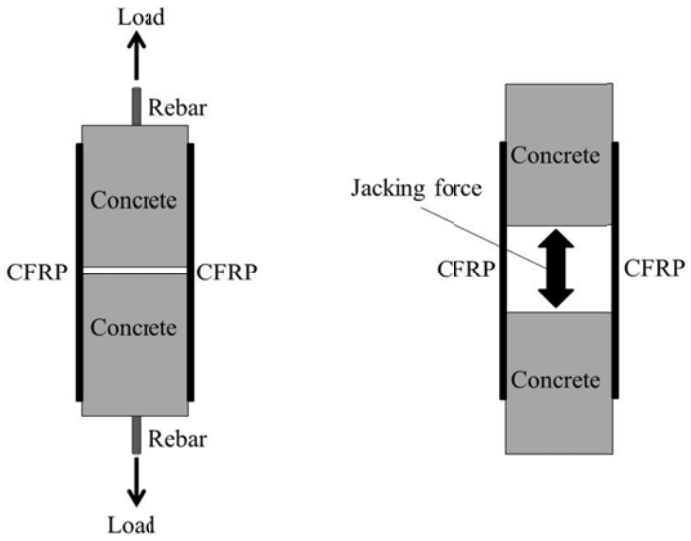

Figure 6.2. Types of double-face shear tests

6.2.3 Direct Tension Pull-off Tests

The pull-off test is a test method that determines the greatest tension force (applied perpendicular to the bond) that the FRP-concrete bond can resist. The method consists of adhesively bonding a metallic circular loading fixture, also referred to as a dolly or puck, to the surface being tested. The dolly contains a threaded hole in the center that allows for attachment of the fixed alignment adhesion testing device, also known as a pull-off tester. Once attached, the tester slowly applies tension to the bond until a partial

or full detachment of the dolly is witnessed, at which point the load is regarded as maximum bond force. Figure 6.3 illustrates a pull-off test scenario.

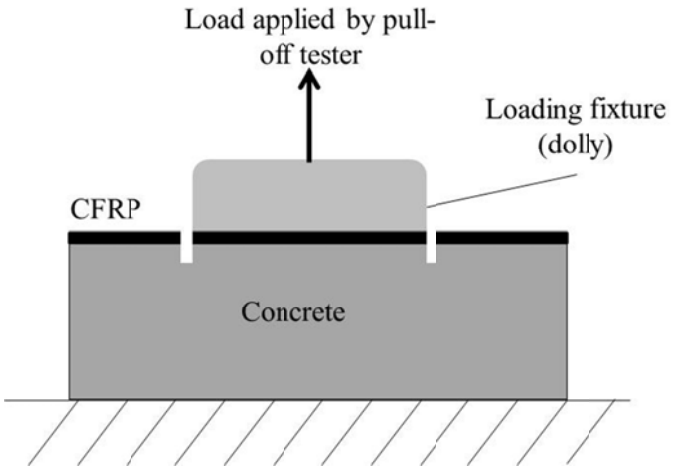

Figure 6.3. Pull-off test representation

The main instruments needed to perform pull-off tests consist of the pull-off tester, loading fixtures (dollies), epoxy adhesive to attach the dollies to the surface, and a core drill or circular hole cutter. The circular hole cutter is used to isolate the area being tested from the rest of the surface. This hole must be the same diameter as the loading fixture, commonly taken as 50 mm (2.0 in). These instruments are shown in Figure 6.4.

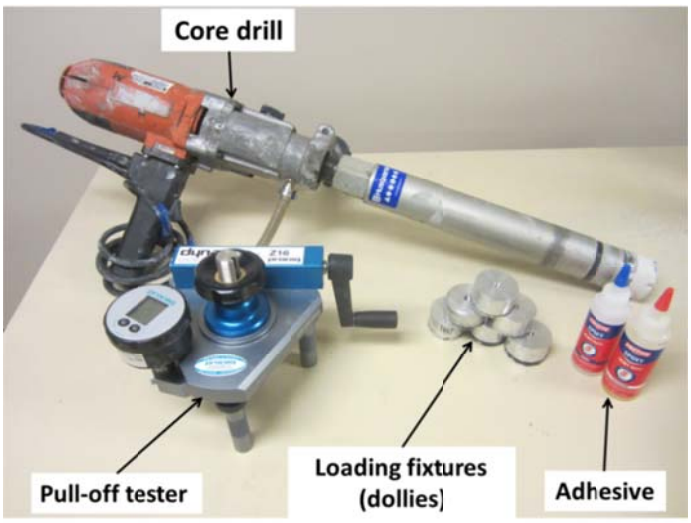

Figure 6.4. Instruments needed to conduct pull-off tests

Prior to 2009, the standard used as guidance for pull-off tests was ASTM D4541. This standard was primarily created as a test method for the pull-off strength of coatings. However, due to similarities in specimen preparation and testing procedures, the standard was used by previous studies as a method for testing pull-off strength of FRP materials bonded to concrete. With the increase in popularity of this specific test application, ASTM D7522/D7522M was created in 2009, specifically to determine the pull-off strength of FRP bonded to concrete. The standard is applicable to both wet lay-up and shop-fabricated or pultruted laminates bonded to concrete. The test cannot be classified as non-destructive, but due to its relatively small scale, surface repairs are minimal.

The maximum force recorded during each pull-off test is used to calculate the pull-off bond strength, as shown in Equation 6.1, where σ_p is the pull-off strength, F_p is the maximum pull-off force, and D is the diameter of the dolly.

Equation 6.1

$$\sigma_p = \frac{4F_p}{\pi D^2}$$

Following completion of the test, different failure characteristics may be witnessed at the bond surfaces. ASTM D7522/D7522 (2009) classifies these failure modes into seven types, labeled from Mode A through Mode G. These failure modes are summarized in Table 6.1.

Table 6.1. Pull-off Test Failure Modes (ASTM D7522/D7522M, 2009)

Failure Mode	Failure Type	Causes of Failure
A	Bonding adhesive failure at dolly	Improper adhesive bonding of dolly. Not an acceptable failure mode.
B	Cohesive failure in FRP	Improper saturation of the FRP, environmental degradation.
C	Adhesive failure at FRP/adhesive interface	Contamination of adhesive during application, incomplete adhesive cure.
D	Cohesive failure adhesive	Contamination of adhesive, incomplete cure, environmental damage of material.
E	Adhesive failure at FRP/concrete interface	Contamination of adhesive during application, incomplete adhesive cure.
F	Failure mode E and G combined	Inconsistent FRP-concrete adhesion. Failure is partly adhesive and partly on substrate
G	Cohesive failure in concrete substrate	Proper adhesion of FRP-concrete. Desirable failure mode

Figure 6.5 shows the interfaces which these seven failure modes represent. The image is not to scale. The adhesive and FRP layers have been magnified for clarity.

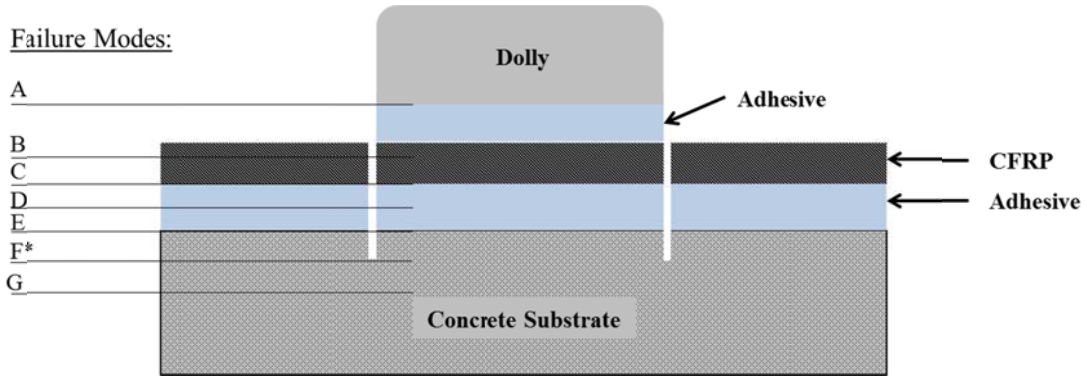

Figure 6.5. Pull-off test failure modes. Mode F failure represents a combination of Mode E and Mode G failures

For the purposes of the durability study conducted in this research, a variety of environmental scenarios were considered, which made it necessary to fabricate a large number of specimens. In addition, convenient handling of the specimens was needed, especially for the groups that underwent wet-dry cycles and freeze-thaw cycles. As a result, due the low cost, small scale, and convenient procedures, pull-off tests were chosen as the primary test method.

6.2.4 Three-Point Beam Bending Tests

Beam bending tests represent the second FRP-concrete bond test method chosen for this study. In relation to pull-off strength tests, bending tests provide a more realistic behavior of the FRP concrete bond when subject to flexural loads. Gartner, Douglas, Dolan, and Hamilton (2011) recently presented a study in which this new bond test method is introduced. The authors wanted a new testing procedure that was simple to perform, easy to understand, and that could allow for fabrication of a large number of specimens for statistical validation. Their test method was primarily based on ASTM C78/C78M (2010), a standard test method for the flexural strength of concrete.

Three modifications were made by Gartner et. al. (2011) to ASTM C78 in order to adapt the test method for determining bond strength between CFRP and concrete: a saw cut was added at the midspan

of the beams, CFRP sheets were added to the tension face, and loading was modified from four-point bending to three point bending. The test is based on flexure because as tension develops at the bottom of the beam where the CFRP is located, shear stresses develop to transfer forces between the concrete and FRP. Three-point bending puts the bond in shear, and allows for calculation of the bond shear strength. Three-point bending was also used because with this loading configuration there is less chance of a concrete shear failure outside of the CFRP reinforcement area, helping to ensure that the test actually measures bond strength. The saw cut is placed at midspan to ensure that failure starts to develop at the top of the cut, which forces the CFRP reinforcement to fully mobilize its development length. The development length represents the length of the composite that undergoes the bond shear strength during loading; more specifically, it constitutes the length starting from the edge of the saw cut to the end of the carbon fabric, as shown in Figure 6.6.

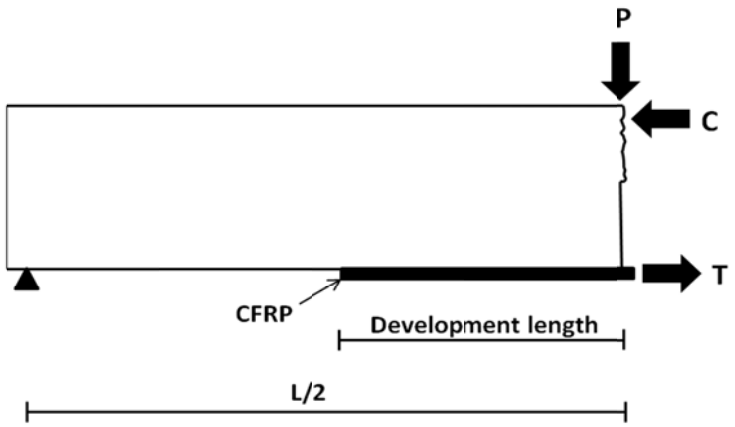

Figure 6.6. Development length and forces under three-point bending. This figure shows half of the beam. P is the load applied at midspan, T is the tension force generated at the bottom of the beam, and C is the compression force at the top of the beam.

As mentioned in Section 6.2.3, pull-off tests were chosen as the primary test method. Pull-off tests, however, apply the load perpendicular to the surface. When the FRP repair is in service, perfectly perpendicular loads are never experienced by an FRP-concrete bond, meaning it can be difficult to understand what the test results actually mean in terms of structural performance, As a result, three-point beam bending tests were chosen as a supplementary test method for this research study, since it provides a more realistic scenario of the behavior of FRP reinforcement on actual concrete structural members.

6.3 Testing Plan Overview

The purpose of this study was to evaluate the behavior of the bond between the concrete and the CFRP when subjected to various environmental scenarios. These environmental conditions include freeze-thaw and wet-dry cycles, as well as immersion in deicing agents over two testing stages. The testing stages consisted of keeping the specimens exposed to these scenarios over a period of 6 months, and 12 months. Section 3.3 describes the stages in more detail.

In order to test the bond between the CFRP and concrete, various testing methods were evaluated with the purpose of finding a test that was most suitable for this study. Tests such as single shear and double face shear were considered. However, these types of tests showed to have some inconveniences in relation to the goal of this study. Since various environmental scenarios were considered, a large amount of specimens was needed. Therefore, practical specimen sizes were necessary for easy handling of the blocks, as well as lower cost for materials and testing devices. As a result, two different testing methods were chosen: pull-off tests, and small three-point bending tests.

6.4 Environmental Exposure Scenarios

During the winter months in Colorado and other northern regions, roads and bridges are faced with various adverse weather conditions that may affect their performance over time. These conditions include exposure to rain and snow. In addition, the use of deicing products to improve driver's safety on bridges is also a factor. As a result, various environmental exposures were considered in the study to evaluate the FRP-concrete bond durability. These exposures include: immersion in deicing agents, wet-dry cycles, freeze-thaw cycles, and immersion in water. Each exposure is described in more detail in the subsequent sections.

6.4.1 Exposure to Deicing Agents

To evaluate long-term bond durability under deicing exposure, concrete blocks and beams reinforced with CFRP were placed face down in a 0.25 in - 0.50 in (6 mm - 13 mm) depth of deicing solution. ASTM C672/C672M (2003) was used for guidance on the depth of solution needed for the

conditioning of the beams and blocks. The standard specifies the exposure procedure using a solution of calcium chloride, but for the purposes of this study, two different deicers were used: Meltdown Apex and Apogee, provided by Envirotech Services. The first one is characterized as a performance enhanced magnesium chloride solution, while the second one is described as a non-chloride deicer.

For preparation of the deicers, both products were diluted with water at a 1:1 weight ratio to achieve a concentration more representative of field conditions. Exposure was carried out for all of the testing stages described in Section 3.3. Since a constant depth was desirable, specimens were monitored to make sure a minimum depth of 0.25 in (6 mm) was maintained. When the depth was lower than the recommended 0.25 in, the plastic bins containing the specimens were refilled to the desired depth. However, all of the containers were fully covered which prevented rapid evaporation of the solution. As specified by Envirotech, concentration of the solutions is shown to decrease over time. As a result, samples of the solutions were collected and taken to the facilities at Envirotech to determine the rate at which the concentration decreased. With this rate, it was determined how often a new batch of Meltdown Apex and Apogee were needed to be mixed, in order to keep a constant concentration and avoid discontinuities in the long-term exposure.

6.4.2 Wet-Dry Cycles

A series of wet-dry cycles were applied on some specimens for all of the testing durations. One complete cycle was as follows: specimens remained soaking in a 0.25-in depth of magnesium chloride solution for 4 days, then were removed from the containers and allowed to dry for 3 days. The week-long cycles were repeated for 6 and 12 months.

6.4.3 Freeze-Thaw Cycles

Freeze-thaw exposure was applied to some of the specimens. Since there is no specific standard for testing FRP-concrete bond under freeze thaw conditions, the exposure developed by Yun and Wu (2011) was followed, and it is based on two ASTM Standards for concrete were used as guidance to develop this exposure: ASTMC666 (2003) and ASTMC672/C672M (2003). A total of four blocks

underwent freeze-thaw exposure: two for Stage 1 and two for Stage 2, resulting in a total of 6 pull-off tests per stage. No small beams for bending tests were considered for freeze-thaw exposure due to limited freezer space. Specimens were placed in the magnesium chloride solution with the FRP side down at a depth no smaller than 0.25 in (6 mm) (ASTM C672/C672M, 2003), as illustrated in Figure 6.7.

Figure 6.7. FRP reinforced concrete specimens undergoing free-thaw exposure

To ensure that the depth was kept constant, specimens were monitored often and refilled with solution to prevent considerable loss due to evaporation. One freeze-thaw cycle was characterized as follows: the temperature was held constant at 40 ^{0}F (4.4 ^{0}C) for 8 hours; the temperature was then decreased to 0 ^{0}F (-17.8 ^{0}C) in 30 min and was held constant for 15 hours. Finally, the temperature was increased back to 40 ^{0}F (4.4 ^{0}C) in 30 min. The total time for one cycle was 24 hours.

The temperature ranges were obtained from the ASTMC666/C666M Standard recommendations. However, this standard targets rapid cycles, in which it is advised that one cycle be no longer than 5 hours, with 300 being the maximum number of cycles during a test. For the purposes of this study, freeze-thaw exposure was chosen to last the same time as the other environmental scenarios, for proper comparison of the different results. For this reason, freeze-thaw exposure was continued for 183 cycles for testing Stage 1, and 365 cycles for testing Stage 2, 6 months and 12 months respectively.

6.5 Long-term Testing Stages

Three testing stages were executed in the study. Stage 0 consisted of testing 3 beams under three-point bending and 2 blocks after the application of the CFRP. With 3 pull-off tests per block, a total of 6

pull-off tests were performed during this stage. Stage 0 specimens were characterized as control, kept in dry conditions and at room temperature. These specimens provided a basis for comparison for the later testing stages. Stage 1 was the testing stage following 6 months of environmental exposure. A total of 15 blocks and 13 beams were tested during this stage. Finally, Stage 2 represented 12 months of exposure, in which 15 blocks and 13 beams were tested. Tables 6.2 and 6.3 summarize the entire testing plan, showing the different types of specimens and environmental scenarios at each stage.

Table 6.2. Stage 1 (6-month) Tests

Pull-off			**Beam Bending**		
# of Blocks	Exposure	CFRP Layers	# of Beams	Exposure	CFRP Layers
1	Dry	2	2	Dry	2
2	Water	2	2	W/D in Chloride Deicer	2
2	W/D in Chloride Deicer	2	3	Water	2
2	Non-Chloride Deicer	2	3	Non-Chloride Deicer	2
2	Non-Chloride Deicer	3	3	Chloride Deicer	2
2	Chloride Deicer	2			
2	Chloride Deicer	3			
2	F/T in Chloride Deicer	2			

Note: W/D = Wet- Dry cycles, F/T = Freeze-Thaw cycles

Table 6.3. Stage 2 (12-month) Tests

Pull-off			Beam Bending		
# of Blocks	Exposure	CFRP Layers	# of Beams	Exposure	CFRP Layers
1	Dry	2	2	Dry	2
2	Water	2	2	W/D in Chloride deicer	2
2	W/D in Chloride deicer	2	3	Water	2
2	Non-chloride deicer	2	3	Non-chloride deicer	2
2	Non-chloride deicer	3	3	Chloride deicer	2
2	Chloride deicer	2			
2	Chloride deicer	3			
2	F/T in chloride deicer	2			

Note: W/D = Wet- Dry cycles, F/T = Freeze-Thaw cycles

6.6 Fabrication and Testing of Specimens

With pull-off and three-point flexural tests chosen for testing the bond, two types of concrete specimens were manufactured according to the quantities shown in Tables 6.2 and 6.3. The concrete specimens were then reinforced with the carbon fiber fabrics and finally exposed to their respective environmental exposures. Sections 6.5.1 through 6.5.4 explain in detail the procedure for the concrete casting, CFRP application, and specifics for the pull-off and bending tests.

6.6.1 Concrete Specimens

The concrete mix was obtained from Lafarge North America, located north of Fort Collins. Specifications for the concrete were taken from the Colorado Department of Transportation 2011 Specifications Book, Section 601: Structural Concrete. For the purposes of this study, Class D concrete was chosen. Class D concrete was chosen to represent a common concrete type that is used in bridges. The mix specifications included a slump of 4 inches, air entrainment of 5-8%, a water to cement ratio of 0.45, and a 28-day compressive strength of 4500psi (31.0 MPa). As stated in the specifications book, Class D concrete is a dense medium strength structural concrete, required to be made with AASHTO M 43 sizes No. 57, or No. 67 coarse aggregate.

Wooden molds were fabricated prior to casting the concrete. Once the forms were finished, the mixing truck arrived at the Colorado State University Engineering Research Center to proceed with the

pouring of concrete. A total of 45 blocks for pull-off tests, 42 beams for bending tests, and 17 cylinders for compressive strength tests were cast, as shown in Figure 6.8. The details on these specimens (including dimensions) are specified in the following sections. The concrete specimens were allowed to cure for 5 days before removal from the forms. During this 5-day period, curing was aided by sprinkling water on the surface and covering them with sheets of transparent polyethylene plastic to help prevent water from evaporating.

Figure 6.8. Casting of concrete specimens

Following the removal of the blocks and beams from the forms, it was observed that some of the small beams showed a considerable amount of voids/ air pockets on the sides. Since Class D concrete has a significant amount of large aggregate, the workability of the mix was low which made it difficult to achieve proper compaction in small molds. Such behavior was not anticipated as previous related studies did not specify the maximum aggregate size used in their concrete samples. As a result, a total of 9 beams were repaired and patched using Class S mortar mix, and allowed to harden for 30 minutes before they were placed in water containers with the other specimens for curing. Figure 6.9 shows the characteristics of the specimens before and after mortar patching. All specimens were fully submerged in water for the remaining 23 days of the curing stage to provide them with as much moisture as possible and prevent cracking during this period.

Figure 6.9. Concrete beams before (left) and shortly after (right) patching

6.6.2 Application of CFRP to Concrete Specimens

Following proper curing of all the blocks and beams, the CFRP was applied. The carbon fiber fabrics were obtained from HJ3 Composite Technologies, characterized as unidirectional fabrics with design strength of nearly 119 ksi (821 MPa). Table 6.4 presents the physical properties of the composite provided by HJ3.

Table 6.4. Composite Properties from HJ3

	Typical Values	**Design Values**
Tensile Strength, ksi (MPa)	150 (1,034)	118.6 (814)
Modulus of Elasticity, ksi (MPa)	12,380 (85,357)	10,433 (71,933)
Ply Thickness, in (mm)	0.047 (1.194)	
Strain at Rupture	0.0117	

All of the specimens were first sandblasted to the level of aggregate using 30 Grit silica based sand. The purpose of sandblasting was to eliminate any loose particles, debris, and uneven surfaces. Specimens were then air blasted to remove any dust and dirt accumulation from the surface. A surface that is sandblasted and air blasted ensures improved bonding of the carbon fabrics to the concrete. Figure 6.10 illustrates the concrete surface before and after sandblasting.

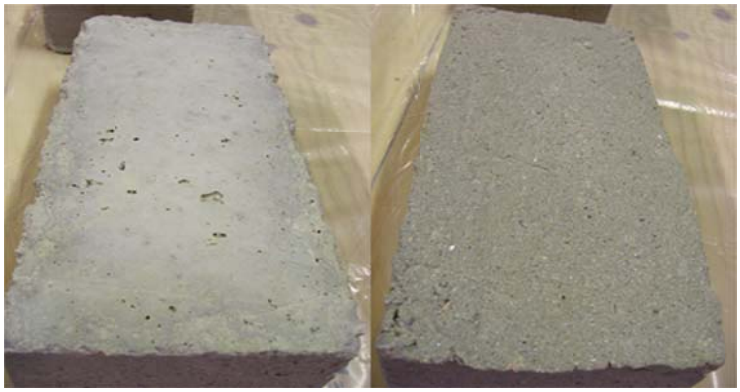

Figure 6.10. Concrete surface before (left) and after (right) sandblasting

Following proper cleanup of the surfaces, a primer coat provided by HJ3 Composite Technologies was applied on the surface of the specimens using a roller, spreading uniformly along the entire surface to avoid any excessive buildup. The goal of the primer as stated by the manufacturer was to promote higher bond strength between the CFRP and the concrete. The primer was allowed to cure for 48 hours and then a wet-layup process was used to manufacture the composite directly on the surface of the concrete, following the steps suggested by the manufacturer. The process consisted of first saturating the fabrics with the two-component epoxy and then pressing the carbon fiber strips onto the concrete surface. SRW-400 was the saturating epoxy used in the application of the CFRP. This two-part epoxy contained a resin and a hardener that were thoroughly mixed at a 2:1 ratio by volume. Rollers were used to ensure uniform pressure during CFRP application and to remove significant air pockets. Finally, any minor air pockets were removed by smoothly but firmly applying pressure on the specimens, starting from the center and moving towards the edges. The wet-layup procedure was repeated on the appropriate specimens to complete the double-layer and triple-layer CFRP reinforcement. Figure 6.11 shows the concrete blocks and beams reinforced with CFRP.

Figure 6.11. Concrete specimens reinforced with CFRP for pull-off (left) and flexural (right) tests

6.6.3 Pull-off Test Specimens and Test

For the pull-off strength tests a total of 45 concrete blocks were cast. With three pull-off tests per block, this resulted in a total of 135 pull-off tests for the entire study. The blocks were 14 in x 6 in x 3.5 in (356 mm x 152 mm x 89 mm). These dimensions allowed a clear spacing of 2 in (50 mm), equivalent to the diameter of one dolly, between each pull-off. This allowed enough space between dollies to prevent any influence on one test from adjacent tests on the same block (Karbhari and Ghosh, 2009). The blocks were reinforced with carbon fiber fabric cut into sheets with dimensions of 13 in x 5 in (330 mm x 127 mm). Figure 6.12 illustrates the specimen dimensions and dolly spacing.

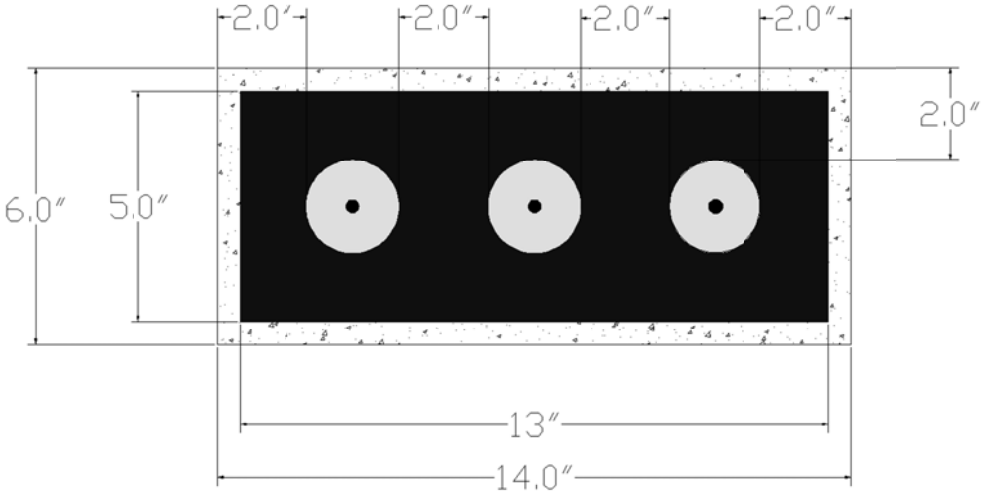

Figure 6.12. Specimen dimensions and dolly spacing

Two layers of CFRP were applied on 33 blocks. The remaining 12 blocks were reinforced with three layers of fabric. After environmental conditioning and shortly before testing, three 2 in (50 mm) diameter cores were made at the location where the dollies were going to be placed in each concrete block. The depth of the core cut was no less than 0.25 in (6 mm) but no more than 0.50 in (12 mm), as recommended by ASTM D7522. When using a core drill, it was likely that the drill bit would rapidly skip off the desired cut area and cause damage to the surface. A fixed wooden frame with three holes at the desired locations was built in order to keep the drill under control. Following the cutting of the cores and prior to adhesion of the dollies, both the CFRP surface and the dollies were roughened with medium-grit sandpaper, then cleaned with water and isopropyl alcohol, and allowed to dry for 24 hours. A roughened surface allows for improved bonding of the dollies on the FRP material. The dollies were then fixed onto the specimens using a Devcon high strength epoxy, with strength of 1500 psi (10.34 MPa). This was a two part epoxy containing a resin and a hardener with a curing time of 5 minutes. As a result, the dollies needed to be placed on the surface rapidly after the mixed epoxy was applied on the dollies. This epoxy was advertised as reaching maximum strength one hour following application. To ensure that the dollies were properly fixed to the surface, the epoxy was allowed to cure for a minimum of 24 hours before performing pull-off tests. Figure 6.13 shows the dollies adhered to the concrete specimens.

Figure 6.13. Concrete specimens following adhesion of dollies

Once the dollies were fully adhered, pull-off testing took place using a Proceq pull-off tester, model: Dyna Z16. The load was applied at the ASTM D7522 recommended rate of less than 150 psi/min

(1 MPa/min) by slowly rotating the crank of the pull-off tester until the maximum force was reached. The machine contained a digital force indicator that displayed the pull-off strength as the crank was being rotated, until failure. Maximum strength was recorded, and failure modes were reported. Figure 6.14 shows the setup for the pull-off testing.

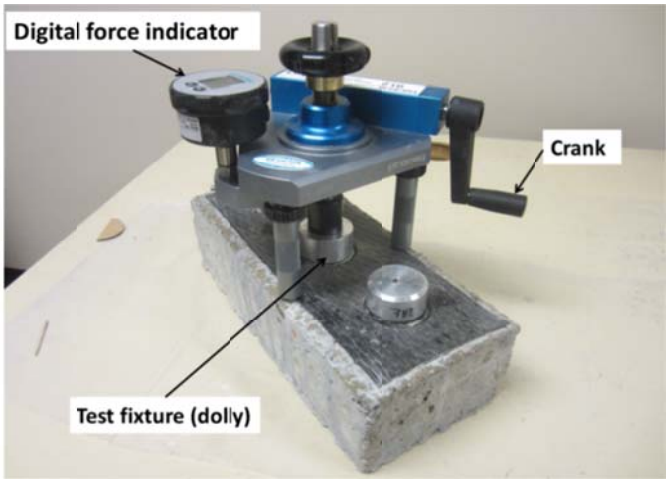

Figure 6.14. Pull-off testing setup

6.6.4 Beam Specimen and Tests

For the beam bending tests a total of 42 small beams were cast, with dimensions of 14 in x 4 in x 4 in (356 mm x 102 mm x 102 mm). Following the 28-day cure, the beams were saw cut at midspan on the tension face to a depth of 2 in (50 mm), equivalent to half of the beam height. Prior to beam reinforcement, the fabrics were cut into strips of 8 in x 1 in (203 mm x 25 mm). Two layers of CFRP sheets were applied on all 42 specimens to evaluate the possibility of failure not only between the concrete and the fibers, but also in between the sheets. Prior to CFRP reinforcement, the surface was prepared using sandblasting and air blasting procedures, as previously described.

Figure 6.15. Concrete beams reinforced with CFRP

For the purposes of testing, the loading rate was set at 0.01 in/min (0.25 mm/min) in order to follow the study by Gartner, Douglas, Dolan and Hamilton (2011). Their research indicated that this loading rate allowed for failure 1-2 min after half capacity was achieved. The main parameters recorded were peak load and cross head position. Peak load, as well as the geometrical properties of the specimens allowed for calculation of the bond shear strength. This is the stress developed on the CFRP-concrete interface during loading. Since the saw cut is equivalent to half the depth of the beam, compression during loading was shown on the upper half of the beam. Assuming a linear stress distribution in the concrete, the resultant of this compression stress distribution is located one-sixth of the total beam depth, which leaves a distance of five-sixths the depth of the beam between the compression and the tension resultant at the level of the FRP, or 5h/6. The tensile force T was found to be 3PL/5h, which is then divided by the CFRP area to determine the bond shear strength.

Equation 6.2 demonstrates the derivation of the bond shear strength (τ), derivation obtained from Gartner et. al. (2011):

Equation 6.2

$$T = \frac{\frac{PL}{2}}{\frac{5h}{6}} = \frac{3PL}{5h}, \qquad so\ \tau = \frac{T}{wS} = \boldsymbol{\frac{3PL}{5hwS}}$$

Where:

τ = Bond shear strength (ksi)
T = Tensile force (kips)
P = Peak load (kips)
L = Span under testing = 12 in
h = Height of specimen = 4 in
w = Width of CFRP reinforcement = 1 in
S = Length of CFRP reinforcement = 8 in

A United Testing Machine Model SFM – 300 kN was used to conduct the flexural tests. The main parameters recorded by the testing machine were time, force, and crosshead position. In order to be able to place the beams on the machine properly for testing, a loading fixture was built. This fixture consisted of a 13.5 in x 6 in x 2 in (343 mm x 152 mm x 50 mm) steel plate with a 3 in x 2 in x 0.5 in (76 mm x 50 mm x 13 mm) steel plate welded at the bottom in the shape of a "T" to allow proper gripping in the machine. Two smooth bars were welded along the 6 in length which served as simple supports of the beam. These bars were separated by 12 in, equivalent to the span under analysis. Figure 6.16 shows the fixture in the machine, and the beam setup for testing.

Figure 6.16. Beam fixture and specimen

6.7 Test Results

6.7.1 Stage 0 Cylinder Tests

A total of four cylinders were tested in compression during Stage 0. Cylinders were of the standard size of 6 in x 12 in (15.2 cm x 30.4 cm). A high average strength of 6.26 ksi (43.16 MPa) was seen in this group. Table 6.5 shows the individual and average values for compressive load and compressive strength. Figure 6.17 shows the characteristic failure corresponding to the four specimens.

Table 6.5. Cylinder tests for Stage 0

Cylinder	Load		Compressive Strength	
	kip	kN	ksi	MPa
1	180	801	6.37	43.89
2	178	792	6.30	43.41
3	176	783	6.22	42.92
4	174	774	6.15	42.43
Average	**177**	**787**	**6.26**	**43.16**

Figure 6.17. Characteristic failure for compression tests

6.7.2 Stage 0 Pull-off Tests

A total of six pull-off tests were conducted for stage zero. Block #1, equivalent to test labels 1, 2, and 3 showed results of 374 psi (2.58 MPa), 442 psi (3.05 MPa), and 391 psi (2.70 MPa), respectively. Out of the three pull-off tests planned on Block #1, test 1 showed an adhesive failure between the dolly

and the CFRP, labeled as failure Mode A by ASTM D7522/D7522M (2009), not an acceptable failure for statistical validation. Figure 6.18 below illustrates the adhesive failure mode from test 1.

Figure 6.18. Pull-off Mode A failure

As illustrated in Figure 6.19, the dollies from tests #2 and #3 show mostly concrete failure but with some black spots in which the CFRP did not adhere to the concrete during the reinforcement process. In the case of block #2, equivalent to tests 4, 5, and 6, all three showed a Mode A failure, with strengths of 444 psi (3.06 MPa), 270 psi (1.86 MPa), and 266 psi (1.83 MPa).

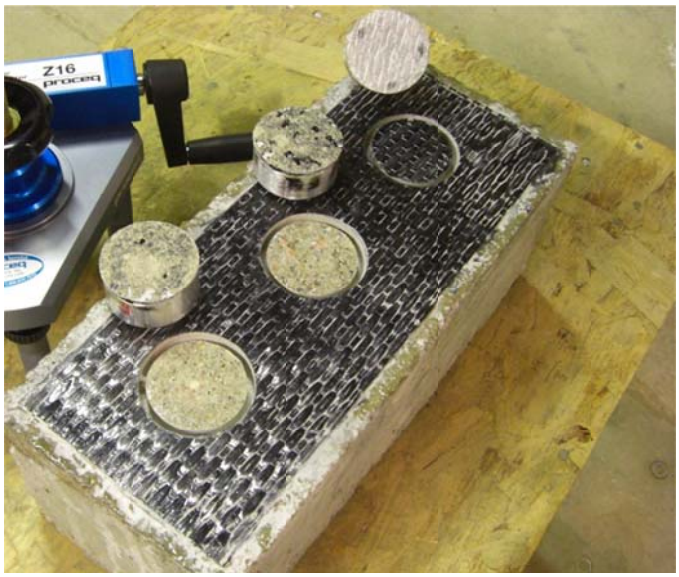

Figure 6.19. Pull-off tests 1, 2, and 3 failure modes

Out of the six pull-off tests performed, four showed a fully adhesive failure. As a result, four additional core circles were drilled, two for each block, with the purpose of performing four more pull-off

tests for statistical validation. Tests 7 and 8 were performed on block #1. The same procedure was followed in the adhesion, including the sanding and cleaning of the surface and dollies. The Devcon high strength epoxy was applied on the dollies for adhesion and allowed to cure for 24 hours before testing. Even though strength was shown to be 405 psi (2.79 MPa) and 401 psi (2.76 MPa), failure still occurred in the adhesive layer.

The persistence of the adhesive failure modes was attributed to two main reasons. Twisting of the dolly during adhesion could have caused minor air voids in the dolly-CFRP interface which decreased the suitability of the bond. The second possibility for adhesive failure could be the curing time of the Devcon epoxy. For all previous tests the epoxy was allowed to cure for 24 hours, and failure Mode A was still showing. Therefore, tests 9 and 10 on block #2 were allowed to cure for 5 days to ensure that the epoxy was fully cured. For these last two tests the dollies were not twisted, they were slowly placed on the surface uniform pressure was applied for 30-90 seconds to avoid slippage. As a result, tests 9 and 10 showed strengths of 433 psi (2.98 MPa) and 439 psi (3.03 MPa), respectively, with acceptable Mode F failures. Figures 6.20 and 6.21 illustrate the strengths and failure modes of all the pull-off tests performed during Stage 0. The notations on Figures 6.20 and 6.21 represent the test number, the ASTM D7522/D7522M failure mode letter, and the strength in psi. These results are also summarized in Table 6.6.

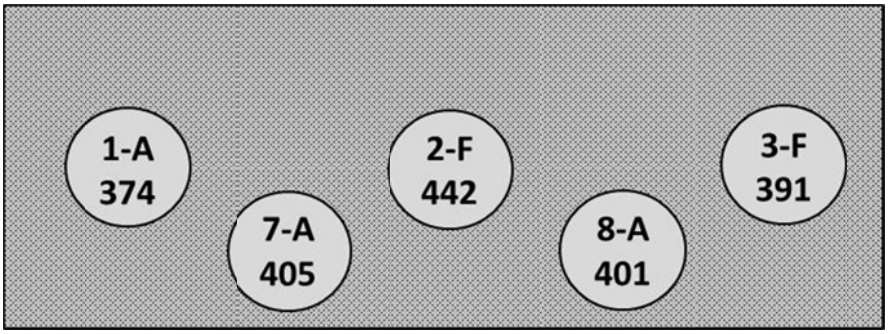

Figure 6.20. Block #1 Results

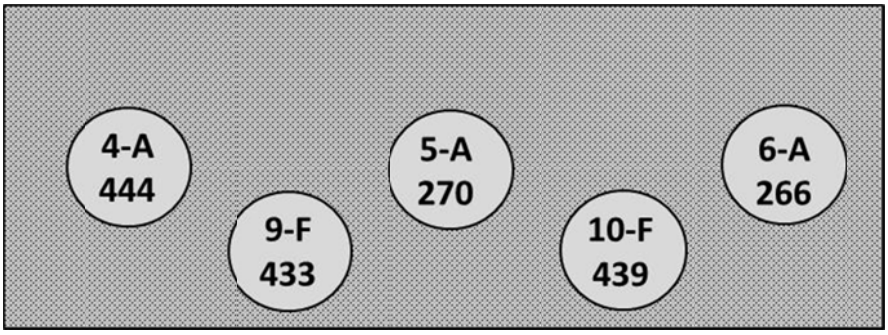

Figure 6.21. Block #2 Results

Table 6.6. Stage 0 Test Results

Test Label	Pull-off Strength		Failure Mode
	psi	Mpa	(ASTM D7522)
1	2.58	374	A
2	3.05	442	F
3	2.70	391	F
4	3.06	444	A
5	1.86	270	A
6	1.83	266	A
7	2.79	405	A
8	2.76	401	A
9	2.98	433	F
10	3.03	439	F

6.7.3 Stage 0 Beam Tests

Stage 0 contained three small beams to be tested under three-point flexure. Due to an error with the testing machine, one specimen was prematurely damaged so the remaining two were used as the control specimens. As previously mentioned, a United Testing Machine Model SFM- 300 kN was used and the parameters recorded were time, force, and deflection as measured by the crosshead position. Figure 6.22 shows failure of one of the beams and how a single flexural crack was developed at the top of the saw cut, as desired.

Figure 6.22. Beam following crack failure

Both beams from this stage showed a fairly similar failure behavior, in which one side of the beam debonded before the other. However, the peak force witnessed on beam 1 was considerably higher, 0.563 kips (2.50 kN) greater than for beam 2. The larger force resisted by beam 1 also resulted in a displacement of 0.029 in (0.74 mm) greater than for beam 2. One possible reason for Beam 2 having a lower peak force is a weaker CFRP-concrete bond coming from the CFRP application. The darker spots on the failure surface for Beam 2 show that the CFRP did not completely adhere to the concrete substrate during application. Beam 1 contained little to no adhesive layer on top of the concrete surface after failure, which indicates that the CFRP was fully bonded to the concrete. Figure 6.23 shows the failure surfaces for both specimens and it is noticeable how beam 2 contained a significantly higher amount of adhesive on the concrete.

Figure 6.23. Beam 1 (left) and beam 2 (right) following testing

A Force vs. Displacement plot was created and labeled as Figure 6.24.

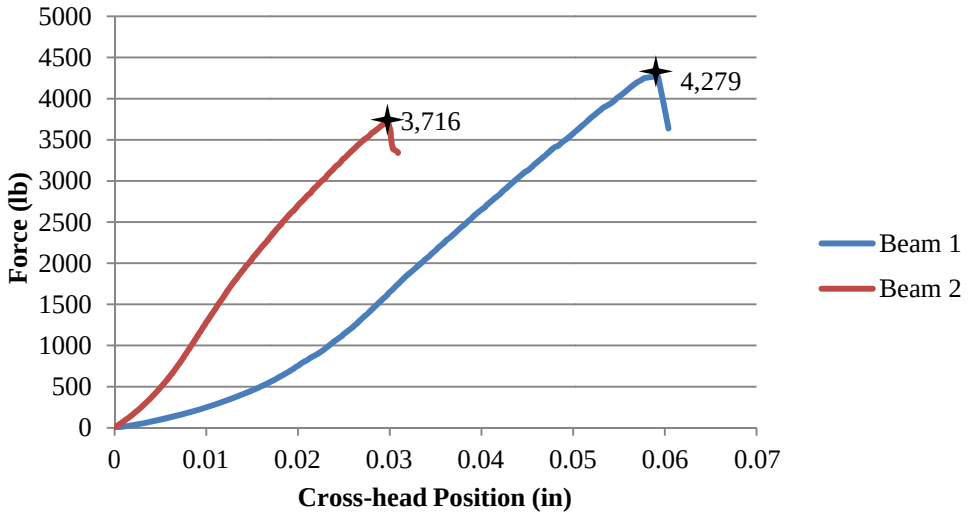

Figure 6.24. Force vs. displacement graphs for Stage 0 beams

With the parameters recorded by the testing machine and the geometric properties of the specimens, the bond shear stress was calculated using Equation 6.3. A sample calculation is provided below. All variables in the equation are fixed values for all specimens, except for the peak load. The peak load used in the following calculation is from beam 1. Finally, Table 6.7 summarizes the results obtained from the Stage 0 specimens.

Table 6.7. Stage 0 Beam Results

Beam	Maximum Load		Bond Shear Stress	
	Kip	kN	ksi	MPa
1	4.28	19.04	0.963	6.64
2	3.72	16.55	0.837	5.77

6.8 Stage 1 Results

6.8.1 Stage 1 Cylinder Tests

A total of four cylinders were tested under compression during this stage. With an average load of 155 kips (690 kN) and average strength of 5.49 ksi (37.83 MPa), these cylinders were weaker by approximately 12% than those tested 6 months prior. These lower values were unexpected and may have been due to calibration of the machine that was made prior to Stage 1 testing. Failure modes for the four specimens were similar to those from Stage 0. See Table 6.8 for the summarized results of the four cylinders.

Table 6.8. Cylinder Tests for Stage 1

Cylinder	Load		Compressive Strength	
	kip	kN	ksi	Mpa
1	161	716	5.69	39.26
2	151	672	5.34	36.82
3	151	672	5.34	36.82
4	158	701	5.57	38.41
Average	**155**	**690**	**5.49**	**37.83**

6.8.2 Stage 1 Pull-off Tests

Forty five pull-off tests were performed during this stage. Environmental exposures included water immersion, wet-dry (W/D) cycles in Chloride- based deicer (Apex), immersions in both chloride and non-chloride based deicers (Apex and Apogee), and freeze-thaw cycles on chloride-based deicer (Apex). All specimens that underwent conditioning were pulled out of their respective containers and left in dry conditions and room temperature for 5 days to allow for proper air drying before the adhesion of the dollies. In addition, a cloth was used every day for the 5-day period to help increase drying speed.

Once fully dried, the specimens were prepared as previously described, including the core drilling and adhesion of the dollies. Table 6.9 shows the results obtained from the forty five pull-off tests.

Table 6.9. Stage 1 Pull-off Test Results

Block	Dolly	Exposure	CFRP Layers	Pull-Off Strength psi	Pull-Off Strength MPa	Average Strength psi	Average Strength Mpa	Failure Mode (ASTM D7522)
	1			226	1.56			F
1	2	Dry	2	152	1.05	172	1.19	F
	3			139	0.96			F
	4			528	3.64			A
2	5			513	3.54			A
	6	Immersion in	2	408	2.81	372	2.57	A
	7	Water		308	2.12			A
3	8			304	2.10			A
	9			173	1.19			F
	10			89	0.61			F
4	11	Wet-Dry		132	0.91			F
	12	in Chloride	2	133	0.92	292	2.02	F
	13	Deicer		291	2.01			F
5	14			579	3.99			F
	15			530	3.65			F
	16			179	1.23			F
6	17	Immersion in		458	3.16			F
	18	Non- Chloride	2	432	2.98	450	3.10	F
	19	Deicer		579	3.99			F
7	20			475	3.28			F
	21			575	3.96			F
	22			101	0.7			F
8	23	Immersion in		403	2.78			G
	24	Non- Chloride	3	294	2.03	208	1.43	F
	25	Deicer		82	0.57			F
9	26			142	0.98			F
	27			224	1.54			F
	28			408	2.81			F
10	29			405	2.79			F
	30	Immersion in	2	528	3.64	385	2.65	A
	31	Chloride Deicer		375	2.59			A
11	32			355	2.45			F
	33			237	1.63			F
	34			467	3.22			F
12	35			627	4.32			G
	36	Immersion in	3	522	3.6	417	2.87	F
	37	Chloride Deicer		389	2.68			F
13	38			80	0.55			F
	39			defective				-
	40			313	2.16			F
14	41	Freeze-Thaw		296	2.04			A
	42	in Chloride	2	287	1.98	327	2.25	A
	43	Deicer		422	2.91			F
15	44			351	2.42			F
	45			291	2.01			A

The most common failure was identified by Mode **F** as labeled by ASTM D7522. Thirty three from the 45 dollies tested showed this type of failure, in which a partial adhesive failure of the FRP-concrete interface, combined with a partial concrete failure is seen. Figure 6.25 below shows a typical failure Mode F encountered during testing. The figure illustrates how the CFRP did not fully adhere to the concrete, and it is noticeable by the black spots of CFRP that are still visible, especially on the middle dolly.

Figure 6.25. Mode F failures (ASTM D7522) during Stage 1 testing

The three pull-off tests corresponding to the dry block showed a representative Mode F failure, with forces ranging from 139 psi to 226 psi (0.96 MPa to 1.56 MPa). These results were used as control to be able to compare dry, room temperature environment with the remaining scenarios. In the case of the two blocks immersed in water for the 6-month period, 5 of the 6 pull-off tests resulted in a fully adhesive Mode A failure. These forces ranged from 173 psi to 528 psi (1.19 MPa to 3.64 MPa), with the lower limit being the only failure in this group characterized as Mode F. A potential reason for which failure Mode A was predominant on the water-exposed blocks could be due to continued curing of the concrete when it was placed in water for six months, making the specimens stronger and forcing the pucks to detach at the adhesive level. The two specimens that underwent wet-dry cycles were more consistent in their failure characteristics, as all six pull-off tests failed at a Mode F level. However, the pull-off force

variation was quite large, with forces ranging from 89 psi up to 579 psi (0.61 MPa to 3.99 MPa) among the two blocks. Potential causes for these large discrepancies among the forces will be explained later on in this section.

The next specimens that underwent exposure were those immersed in a non-chloride based deicer. A total of four blocks were exposed, two reinforced with two layers of CFRP and two reinforced with three layers. Eleven of the twelve pull-off tests in this group showed a Mode F failure, with the remaining failure being identified as Mode G. However, in this case, the use of an extra CFRP layer did not demonstrate any improvements to the bond strength. In fact, the average pull-off strength for the six pull-offs performed on the double- CFRP layer specimens was 450 psi (3.10 MPa), which turned out to be 242 psi higher than the average pull-off strength seen on the two blocks reinforced with three CFRP layers.

The next group of specimens consisted of four blocks immersed in a chloride-based deicer. Similar to the previous group, this one consisted on two blocks reinforced with two layers of CFRP and two blocks strengthened with three layers, with a total of 12 pull-off tests. From these twelve tests, eight showed a Mode F failure, two showed a Mode A failure, one showed a full concrete failure Mode G, and the remaining one was categorized as defective due to thread malfunction of the dolly. The average pull-off strength for the double-layer specimens was 385 psi (2.65 MPa), this force being 32 psi (0.220 MPa) lower than those reinforced with three layers of composite.

The last group of specimens consisted of those exposed to lower temperatures. Freeze-thaw cycles were applied on specimens reinforced with two layers of CFRP. Two blocks, or six pull-off tests were conducted in this group. Three pull-offs showed a Mode F failure, and the remaining three failed at the adhesive layer. Forces ranged from 287 psi (1.98 MPa) to 422 psi (2.91 MPa), with an average bond strength of 328 psi among the six pull-offs. ASTM D7522 does not consider failure Mode A as an acceptable mode. For this reason, if these adhesive failures are not taken into consideration, the average

strength increases to 365 psi among the three dollies that failed partly at the concrete and partly at the FRP-concrete interface.

There are large variances in the results from the pull-off tests. A special concern is the fact that the control specimens showed the lowest strengths in relation to the other groups. Exact reasons why strengths can vary to this magnitude among specimens that underwent similar conditioning are unknown, but it gives an idea of the extremely localized behavior that pull-off tests can exhibit.

While firm conclusions are difficult, listed below are several potential reasons why such discrepancies in the results would be created:

- Inconsistencies in the depth of the core drilling prior to puck adhesion. The recommended depth per ASTM D7522 is 0.25 in. (6 mm) to 0.50 in. (12 mm). A core drill depth of 0.50 in. could present much different results than a core that is 0.25 in. deep.
- Varying volumes of epoxy used per dolly. Since the dollies are manually adhered onto the surface one by one, a slight difference in the volume of epoxy used per dolly could potentially decrease precision of results.
- Irregularities on the surface of the specimen that would prevent a fully flat adhesion. If a surface is not completely flat, more epoxy would have to be used on the side that is not in contact with the dolly. This would lead to variations in thickness across a bond surface.
- Twisting of the dollies when adhering to the FRP surface. Such twisting during adhesion could create minor air voids and decrease adhesion performance. Therefore, a uniform pressure with no rotation of the dolly is recommended.
- Inconsistencies in the mixing of epoxy. Since the type of epoxy used is only workable for 5-7 minutes, and there was a large number of dollies that needed to be adhered, several mixes of epoxy had to be performed separately. As this is all done by hand, occasions in which an ideal 1:1 ratio of resin to hardener is not used, may decrease the performance of the epoxy and deviate results.

- Improper cleaning and sanding of the FRP surface and/or the aluminum dollies. Accumulation of dust or dirt, as well as a non-roughened, smooth surface would considerably decrease adhesion performance.

All of these sources of error, however, were carefully considered prior to preparation of the specimens for testing and significant effort was made to prevent them. Another cause that may have influenced the results has to do with the type of concrete. Since pull-offs are such a small scale testing procedure, having a strong concrete with large amounts of coarse aggregate can vary pull-off strengths within the same block.

Finally, throughout testing the forty five pull-offs, three special cases were encountered. A special note worth discussing in the chloride based deicer group with triple layer reinforcement is the large discrepancy encountered within the six pull-offs. Test #38 resulted in the absolute lowest value for the entire stage, with a strength of 80 psi (0.55 MPa). On the other hand, Test #35 resulted in the absolute highest value among the 45 pull-off tests performed in this stage, with a strength of 627 psi (4.32 MPa). This particular pull-off was characterized as an ideal concrete failure, Mode G in ASTM D7522. It is believed that the reasons for the extremely large discrepancies among the specimens that underwent the exact same conditioning is due to the large aggregate present on test #35, as well as the presence of moisture within the concrete-FRP interface on test #38. This moisture was noticed because of the lighter color of the concrete, as well as a softer and more clayey feel to the touch. Notice in Figure 6.26 the large aggregate on test #35, as well as the lighter color and thinner layer of concrete on test #38.

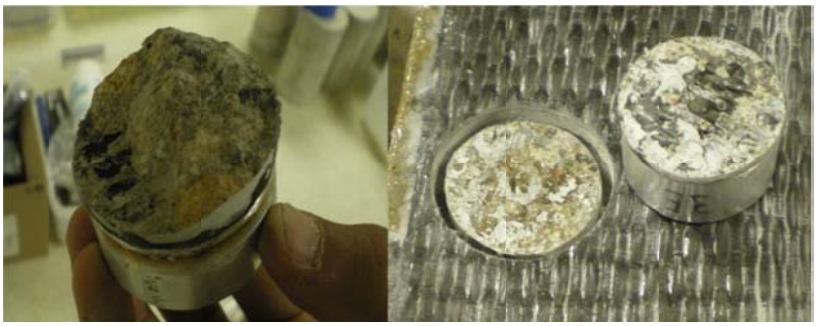

Figure 6.26. Test #35 (left) vs. test #38 (right)

The second special case encountered during testing has some relation to test # 38 above. The presence of moisture in the CFRP-concrete interface on Blocks #4, #9, and #13. This moisture was not present at the time of fabrication of specimens. Therefore, the deicing solution that these blocks were exposed to actually infiltrated into the bond either through the FRP or the concrete. This moisture was noticed in the specimens with different tonalities of gray in the concrete, as well as a softer, more clayey feel to the touch. It was determined that such moisture did decrease strength considerably. In the case of block #4 corresponding to wet-dry cycles, dollies #10, #11 and #12 showed moisture and did result in the ones with weaker strengths out of the whole group. In addition, dolly # 16 from the non-chloride based deicer group showed a strength of 271 psi (1.868 MPa) lower than the remaining dollies in that group, and it was the only pull-off that exhibited levels of moisture within that group.

The same moisture level – strength relationship was witnessed in dollies #25, #26, and #27 (Block 9) within the non-chloride based deicer group, as well as dollies #33 from Block 11, and dollies #37 and #38 from Block 13. With these patterns identified, one can draw the conclusion that the presence of moisture does in fact reduce the pull-strength. However, reasons why some dollies within the same group may or may not have exhibited moisture are unknown. A characteristic example of a dolly showing sign of moisture is illustrated in Figure 6.27.

Figure 6.27. Presence of moisture at CFRP-concrete interface

The last special case consisted of having a mixed failure mode between Mode A and Mode F. In this special case, the CFRP fibers may not have been fully saturated during application, causing

separation of the bundles. Figure 6.28 shows how half of the dolly completely detached from the concrete at an adhesive level on the dolly-FRP interface, whereas the second half was seen as an adhesive failure on the concrete-FRP interface.

Figure 6.28. Combined Mode A and Mode F failure

6.8.3 Stage 1 Beam Tests

Following completion of the pull-off tests, three-point flexural tests on thirteen beams were conducted in this stage. Due to improper handling of testing machine, beam # 7 corresponding to water exposure was characterized as defective. Peak forces ranged from 1.562 kips (6.95 kN) to 4.242 kips (18.87 kN). With the maximum load values and the geometrical properties of the beams, Equation 6.2 was used to calculate the bond shear stress in a similar fashion. Results are summarized in Table 6.10

Table 6.10. Stage 1 Beam Results

Beam	Exposure	Maximum Load		Bond Shear Stress	
		Kip	kN	ksi	Mpa
1	Dry	4.242	18.87	0.95	6.58
2		3.843	17.09	0.86	5.96
3	W/D in chloride	3.799	16.90	0.85	5.89
4	deicer	3.345	14.88	0.75	5.19
5	Water	3.696	16.44	0.83	5.73
6		2.057	9.15	0.46	3.19
7		Defective	-	-	-
8	Non-chloride	1.562	6.95	0.35	2.42
9	deicer	3.644	16.21	0.82	5.65
10		3.203	14.25	0.72	4.97
11	Chloride deicer	3.353	14.91	0.75	5.20
12		1.718	7.64	0.39	2.67
13		2.586	11.50	0.58	4.01

Two control specimens were kept at dry conditions and room temperature. From the thirteen beams tested, these two possessed the highest peak load values at 4.242 kip (18.87 kN) and 3.843 kips (17.09 kN). The absolute lowest load experienced on the beams was identified on beam #8, corresponding to immersion in non-chloride based deicer. Figure 6.29 below clearly demonstrates the major differences in the bond between one of the control specimens (beam #1) and beam #8. The larger area of darker spots on the concrete surface where the CFRP failed was found noticeable. The dark spots correspond to the cured epoxy adhesive that did not fully bond with the CFRP strip. Although it is possible that the non-chloride deicer may have contributed to degradation of the bond, the other potential cause for this behavior is improper adhesion of the CFRP onto the concrete during preparation.

Figure 6.29. Beam #1 (left) vs. beam #8 (right) failure

Table 6.11 shows the results summarized by exposure. The wet-dry exposure was identified as the group of beams that degraded the least in terms peak load values, with a load of 88% of the control beams. On the other hand, the chloride-based deicer was found to be the exposure that corresponded to the highest strength degradation, with the peak load being 63% of the control specimens.

Table 6.11. Stage 1 Average Results for Beams

	Average Peak Load		Average Bond shear Stress		% of
Exposure	**Kip**	**kN**	**ksi**	**Mpa**	**Control**
Dry	4.043	17.98	0.910	6.271	100.0%
W/D in chlorde deicer	3.572	15.89	0.804	5.541	88.4%
Water	2.876	12.79	0.647	4.462	71.2%
Non-chlorde deicer	2.803	12.47	0.631	4.348	69.3%
Chloride deicer	2.552	11.35	0.574	3.959	63.1%

6.9 Stage 2 Results

6.9.1 Stage 2 Cylinder Tests

A total of four cylinders were tested in compression during Stage 2. The average strength for this group was 5.14 ksi (35.44 MPa). These cylinders turned out to be 6.5% weaker than those tested six months prior, and 18% than the ones tested twelve months prior. The failure mode, however, was similar to those tested in the previous stages. Table 6.12 summarizes the results for these cylinders.

Table 6.12. Cylinder Tests for Stage 2

Cylinder	Load		Compressive Strength	
	kip	**kN**	**ksi**	**Mpa**
1	147.5	656	5.22	35.97
2	137.5	612	4.86	33.53
3	141	627	4.99	34.38
4	155	689	5.48	37.80
Average	**145**	**646**	**5.14**	**35.42**

6.9.2 Stage 2 Pull-off Tests

A total of forty five pull-off tests were conducted during Stage 2. The specimens were subject to the same environmental conditioning as Stage 1. One block was left at room temperature to be used as control. For this stage, all specimens undergoing conditioning were pulled out of the containers seven

days prior testing. Specimens were again prepared following procedures previously explained. Table 6.13 shows the results for the forty five pull-offs, including their average strength per group, and failure mode per ASTM D7522.

Table 6.13. Stage 2 Pull-off Test Results

Block	Dolly	Exposure	CFRP Layers	Pull-Off Strength psi	Pull-Off Strength MPa	Average Strength psi	Average Strength Mpa	Failure Mode (ASTM D7522)
	1			245	1.69			F
1	2	Dry	2	249	1.72	286	1.97	F
	3			365	2.52			F
	4			382	2.63			A
2	5			353	2.43			A
	6	Immersion in	2	367	2.53	356	2.45	A
	7	Water		209	1.44			F
3	8			399	2.75			F
	9			425	2.93			F
	10			192	1.32			F
4	11	Wet-Dry		152	1.05			F
	12	in Chloride	2	334	2.30	222	1.53	F
	13	Deicer		275	1.90			F
5	14			313	2.16			F
	15			66	0.46			F
	16			340	2.34			A
6	17	Immersion in		308	2.12			A
	18	Non- Chloride	2	311	2.14	357	2.46	F
	19	Deicer		372	2.56			F
7	20			425	2.93			G
	21			386	2.66			F
	22			330	2.28			F
8	23	Immersion in		310	2.14			F
	24	Non- Chloride	3	306	2.11	260	1.79	A
	25	Deicer		131	0.90			F
9	26			239	1.65			F
	27			241	1.66			F
	28			95	0.66			F
10	29			154	1.06			F
	30	Immersion in	2	329	2.27	203	1.40	F
	31	Chloride Deicer		289	1.99			A
11	32			163	1.12			F
	33			190	1.31			F
	34			139	0.96			F
12	35			329	2.27			F
	36	Immersion in	3	270	1.86	257	1.77	F
	37	Chloride Deicer		281	1.94			F
13	38			273	1.88			A
	39			251	1.73			F
	40			330	2.28			F
14	41	Freeze-Thaw		283	1.95			F
	42	in Chloride	2	348	2.40	352	2.42	A
	43	Deicer		344	2.37			A
15	44			311	2.14			A
	45			494	3.41			A

Once again, the most common failure type corresponds to Mode F. Thirty two of the forty five pull-off tests resulted in this failure mode, equivalent to 71% of the total. Figure 6.30 below shows a representative failure for these thirty two dollies. The black spots on the dolly correspond to sections where the CFRP did not fully adhere to the concrete, followed by partial concrete detachment within the same dolly.

Figure 6.30. Representative Mode F failure for Stage 2

All three pull-offs conducted on the control specimen were Mode F failures. With strength values ranging from 245psi to 365 psi (1.69 MPa to 2.52MPa), the average strength for this group was 286 psi (1.97 MPa). When comparing these tests to the rest of the groups within Stage 2, the control specimens were not the highest in strength but were not the weakest either. The specimens that were immersed in water for twelve months had pull-off forces approximately 24.5% higher than the control specimen. The forces ranged from 209 psi to 425 psi (1.44 MPa to 2.93 MPa), with an average of 356 psi (2.45 MPa). From the six pull-offs conducted in this group, half were Mode A and half were Mode F. The next group of specimens was subjected to wet-dry cycles. These two blocks contained higher variances in the results, with forces ranging from 66 psi to 334 psi (0.46 MPa to 2.30 MPa). The average strength in this group was 222 psi (1.53 MPa). However, there was consistency as far as failure modes go, where all six dollies exhibited a Mode F failure.

Four blocks were exposed to a non-chloride based deicer, equivalent to a total of twelve pull-off tests. Two of these blocks were reinforced with two layers of CFRP, and the remaining two blocks with three layers of CFRP. Failure modes varied from Mode A in three pull-offs, Mode F in eight dollies, and the last one corresponded to an ideal Mode G failure. Figure 6.31 shows the Mode G failure that was witnessed on dolly #20 from this stage, corresponding to one of the blocks reinforced with two layers of CFRP.

Figure 6.31. Mode G failure in dolly #20

One observation worth mentioning within this group is the fact that the specimens reinforced with three layers of CFRP turned out to be weaker than those reinforced with two layers by a difference of 37.3%. The average strength for the double-layer reinforced blocks was 357 psi (2.46 MPa), compared to the average strength of 260 psi (1.79 MPa) in the ones reinforced with three layers of CFRP. Reasons for this are unknown, but it gives an idea of the further discrepancies in results that may be found when conducting pull-offs.

The next specimens are those exposed to a chloride based deicer. In this group, forces ranged from 95 psi to 329 psi (0.66 MPa to 2.27 MPa) in those with double-layer reinforcement, and from 139 psi to 329 psi (0.96 MPa to 2.27 MPa) in those with triple-layer FRP reinforcement. This group showed a more logical behavior as far as average strengths, since there was a 26.7% increase in strength when

adding an extra layer of FRP. However, the high variances among individual results make it difficult to draw solid conclusions as to what the values actually mean. As far as failure modes go, ten of the twelve showed a Mode F failure, and the remaining two were adhesive Mode A failures. The next and final group of specimens corresponded to two blocks that underwent freeze-thaw cycles in a chloride-based deicer for twelve months. In this case, forces ranged from 283 psi to 494 psi (1.95 MPa to 3.41 MPa). Failure modes, however, were controlled by Mode A. Out of the six pull-offs, only two showed a Mode F failure and the remaining detached at the adhesive level.

In this stage, the presence of moisture in some of the dollies was also witnessed. Two of the dollies within the water exposure group, three within the wet-dry cycle group, three within the non-chloride based deicer group, and nine within the chloride-based deicer group, were the specimens that showed moisture between the concrete and FRP. Once again, the different tonalities of gray as well as a softer more clayey feel to the touch helped identify which dollies showed levels of moisture. The amount of moisture ranged from very small spots around the edges, to larger areas within the dolly. Figure 6.32 shows a characteristic image of the presence of moisture in the specimens. As far as moisture – strength relationship in the water group, no logical pattern was found. In fact, dollies #8 and #9 resulted in the highest bond strength in the group, even though these were the ones that showed some moisture within the group. However, dollies #25, #26, and #27 did turn out to be weakest ones within the non – chloride based deicer group. For the chloride based deicer group, the moisture-strength relationship makes sense in the double-layer reinforcement ones, where dollies #28, #29, #32, and #33 showed the lowest strengths as oppose to the drier ones. These patterns, however, are difficult to interpret, as the moisture was not present within individual blocks, but rather within individual dollies.

Figure 6.32. Presence of moisture on dollies

Finally, the special case in which a combined Mode A and Mode G failure was witnessed in dolly # 31 from Stage 1, was also seen in Stage 2 in dolly #42. Figure 6.33 shows dolly #42 with this particular failure. The cause may have been once again due to improper adhesion of the fabric, causing separation of the bundles, or due to a weak pattern of concrete on one side.

Figure 6.33. Combined Mode A and Mode F failure in dolly #42

6.9.3 Stage 2 Beam Tests

Thirteen beams were tested to failure in this stage. The beams were classified in the same manner as those from Stage 1. Failure loads ranged from 2.104 kips (9.36 kN) to 4.181 kips (18.60 kN). On average, the control specimens showed the highest strength, as expected. All beams showed a similar failure mode, wherein a single flexural crack is started at the top of the saw cut and shear failure

debonding on one of the FRP-concrete interfaces is witnessed. The lowest strength corresponded to beam #4, in the wet-dry group. It is unknown if that specific environmental exposure might have been the main cause of strength degradation. However, it was observed that those beams exhibiting lower strengths were the ones that showed more adhesive marks on the concrete, meaning the FRP strip did not fully adhere to the surface. Figure 6.34 illustrates the significant difference there is between a proper bond and an improper one. This clearly had an effect in strength, especially in beams #4, #5, #6, and #12. Table 6.14 shows the peak loads with respect to each environmental conditioning. Table 6.14 also shows the values for the bond shear stress.

Table 6.14. Stage 2 Beam Results

Beam	Exposure	Maximum Load		Bond Shear Stress	
		Kip	kN	ksi	Mpa
1	Dry	4.181	18.60	0.94	4.18
2		3.656	16.26	0.82	3.66
3	W/D in chloride	3.704	16.48	0.83	3.71
4	deicer	2.104	9.36	0.47	2.11
5	Water	2.928	13.02	0.66	2.93
6		2.295	10.21	0.52	2.30
7		4.317	19.20	0.97	4.32
8	Non-chloride	3.895	17.33	0.88	3.90
9	deicer	3.780	16.81	0.85	3.78
10		3.927	17.47	0.88	3.93
11	Chloride deicer	3.640	16.19	0.82	3.64
12		2.303	10.24	0.52	2.30
13		4.106	18.26	0.92	4.11

Note: W/D = Wet-dry cycles

Figure 6.34. Beam #6 (left) vs. beam #1 (right)

As far as degradation in relation to the control beams, no significant pattern was encountered compared to the results from Stage 1. In this stage, the beams that underwent wet-dry cycles turned out to be the weakest, whereas in Stage 1 these turned out to be the second strongest, right after the control beams. As a result, it is difficult to draw comparative conclusions among stages, as no clear pattern was seen in relation to strength degradation. See Table 6.15 for a summary of results and the percentage of strength relatively to the dry beams.

Table 6.15. Stage 2 Beam Average Results

	Average Peak Load		Average Bond shear Stress		% of
Exposure	**Kip**	**kN**	**ksi**	**Mpa**	**Control**
Dry	3.919	17.43	0.882	6.079	100.0%
W/D in chlorde deicer	2.904	12.92	0.653	4.505	74.1%
Water	3.180	14.15	0.716	4.933	81.2%
Non-chlorde deicer	3.867	17.20	0.870	5.999	98.7%
Chloride deicer	3.350	14.90	0.754	5.196	85.5%

6.10 Durability

Figure 6.35 illustrates the average results from the 6-month and 12-month exposures for the pull-off tests, classified per conditioning. For the most part, there was a strength degradation observed in the specimens exposed for an additional six months. The only exceptions were in the groups of freeze-thaw, and the non-chloride specimens with three FRP layers. Also, there was a decrease in strength in the control specimens between 0 and 6 months, but it increased at the end of the twelve month period.

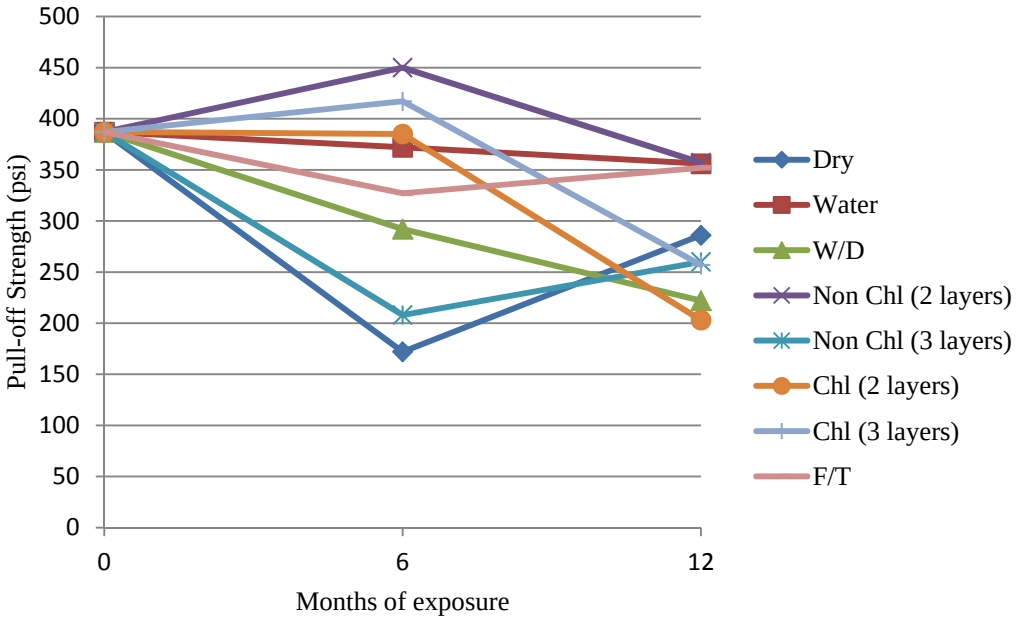

Figure 6.35. Average pull-off results for the 6-month and 12-month exposure

Figure 6.36 shows a comparison plot of the beams tested at all stages. As expected, the dry (control) beams were the strongest ones throughout the entire durability study. In addition, a decrease in strength was witnessed in the water group. However, for unknown reason there was an increase in strength during the last six months of exposure for the rest of the groups. This may have been due to an increase in the concrete strength during conditioning.

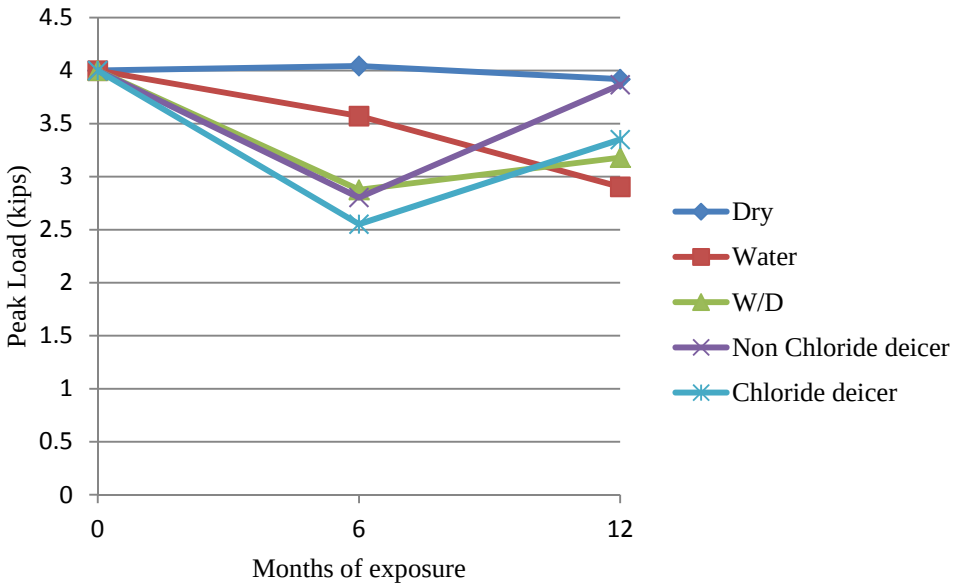

Figure 6.36. Average beam results for the 6-month and 12-month exposure

Due to these unexpected results it is impossible to draw any conclusions regarding the effect of the conditioning. From what was seen in all of the results previously discussed, high variability was witnessed, especially in the pull-offs. Factors such as an increase in strength over time, as well as inconsistencies in failure modes within the same specimens make interpretation of results challenging. It is difficult to know if the type of exposure has any influence in strength degradation. Therefore, the next section will be focused on evaluating pull-offs, by examining the challenges that may be encountered when analyzing the data obtained during testing, including the high variances pull-off test results can exhibit in the field and laboratory.

7.0 EVALUATING PULL-OFF TESTS

7.1 Pull-off Tests Limitations Overview

In effect of obtaining variations in results from both the field study in the Castlewood Canyon Bridge, as explained in Section 3.0, and from the durability study conducted in the lab as described in Section 6.0, pull-off tests were researched more in depth in this section. Over the years, various tests have been created in the laboratory and the field in order to characterize the bond behavior. Due to their low cost, small scale, and convenient method of testing bond. Although convenient, this test method does contain certain limitations affecting consistency and interpretation of results. For one, in a direct tension test, load is applied perpendicular to the surface. When the FRP repair is in service, perfectly perpendicular loads are never experienced by an FRP-concrete bond, meaning it can be difficult to understand what the test results actually mean in terms of structural performance. Also, due to the small scale of the testing procedure, drastic variations among results within the same test group can occur. The strength of the concrete substrate plays a large role in the bond strength that an FRP-concrete system can show. However, when bond strength is controlled by the strength of the pre-existing concrete, test results may not necessarily be indicative of the quality of the actual repair. In addition, preparation of the testing surface can introduce factors that may potentially increase variability of results, such as the presence of water as well as torsional and thermal stresses applied during the core drilling process. Finally, variations in the depth of the core cut must be paid close attention, as certain guidelines specify different depths, which could potentially alter the results. In light of these limitations, this chapter seeks to evaluate direct tension tests as a tool for understanding FRP-concrete bond in both the laboratory and the field.

7.2 Variations in the Depth of Cut

In addition to the specifications and procedures described by ASTM D7522, there are additional guidelines that focus on pull-off tests, and the depth of the core cut depths must be paid special attention. Guideline No. 03739 by the International Concrete Repair Institute (ICRI) also targets pull-off tests as a way to evaluate the tensile strength of a concrete surface repair. However, when looking at these different

guidelines, the depth of the core cut was found to be inconsistent. The ICRI Technical Guideline No. 03739 (2004) recommends a minimum depth of core drill to be 1 in (25 mm) for a 2 in (50 mm) dolly. On the other hand, ASTM D7522 (2009) recommends for the same size dolly, a core depth of 0.25 in (6 mm) to 0.50 in (12 mm). Finally, ACI 503R (1993) advises to barely core drill into the substrate. As a result, variations in these figures make it quite difficult to determine which depth would be the most appropriate for use in any field or laboratory setting.

7.3 Previous Laboratory Studies involving Direct Tension Pull-off Tests

In this section, previous research laboratory studies regarding pull-off tests were summarized. Karbhari and Ghosh (2009) used pull-off tests to study the long-term bond durability of CFRP adhered to concrete under various environmental conditions such as immersion in salt water, immersion in water, exposure to freezing conditions, and different humidity levels. A total of 250 pull-off tests were conducted, which were split among the various environmental exposures. The tests were conducted at 6 month intervals for a total of 24 months. In general, results were fairly consistent, with a gradual increase in the level of deterioration for those specimens immersed for a longer period. They concluded that the specimens immersed in salt water exhibited the largest degree of deterioration, possibly due to infiltration of the sodium chloride into the CFRP-concrete interface.

A recent study conducted by Eveslage et. al. (2009) investigated the effect of variations in the use of ASTM D7522 as a standard pull-off test for FRP-concrete systems. The study included variables such as depth of core cut, shape of loading fixture or specimen, and the effects of retesting specimens that showed an unacceptable failure mode initially (Mode A per ASTM D7522). The experimental program involved a total of 75 pull-off tests. The specimens were prepared in accordance with instructions from the standard. For the specimens that exhibited a Mode A adhesive failure initially, it was determined that, even though the retests did show a Mode G failure, the average strengths were in fact lower, which indicated the possibility that damage to the specimens occurred during the initial testing. However, consistency in results from this group of specimens was witnessed, with a coefficient of variation of about 16%, similar to those that did not require retests. Three different cut depths were investigated: 0.10 in (2.5

mm), 0.25 in (6 mm), and 0.75 in (19 mm), with a total of 5, 21, and 5 pull-off tests conducted, respectively. From the test results, no change in strength was witnessed among the 0.10 in (2.5 mm) and 0.25 in (6 mm) core depths. However, the deeper core cut of 0.75 in (19 mm) showed a decrease in strength of up to 26%. A possible explanation for this lower strength is the likelihood of larger torsional and thermal stresses induced by drilling, as compared to the lower cuts. Table 7.1 shows statistics of pull-off results for each cut depth.

Table 7.1. Pull-off Strength Results (Eveslage et. al., 2009)

Depth of	Sample	Mean Bond Strength		Standard Deviation		COV
Cut, mm	Size	Mpa	psi	MPa	psi	%
0	31	2.72	395	0.141	20.5	20
2.5	5	2.78	403	0.094	13.6	13
6	21	2.78	403	0.110	15.9	16
19	5	2.06	299	0.125	18.2	22

7.4 Previous Field Studies Involving Direct Tension Pull-off Tests

Banthia, Abdolrahimzadeh, and Boulfiza (2009) conducted a field study in which four bridges in Canada were investigated to assess the durability of the FRP repairs applied on the bridges after several years of service. Four structures were selected to represent a range of environmental conditions, lengths of service, and types of FRP reinforcement. Table7.2 summarizes some of the characteristics of these structures.

Table 7.2. Bridges Characteristics (Banthia, Abdolrahimzadeh, and Boulfiza, 2009)

Structure	Location	Year of Construction	Year of FRP Repair	Type of FRP Repair
SafeBridge	Youbou, BC	1955	2001	Sprayed GFRP
St-Ètienne Bridge	Quebec	1962	1996	GFRP and CFRP column wraps
Leslie Street Bridge	Ontario	1960s	1996	CFRP column wraps
Maryland Bridge	Manitoba	1969	1999	CFRP sheets at girder ends

Pull-off tests were conducted on specific sections of these repairs in order to determine the condition of the bond. These tests were conducted following ASTM C1583-04, titled “Standard Test Method for Tensile Strength of Concrete Surfaces and the Bond Strength or Tensile Strength of Concrete Repair and Overlay Materials by Direct Tension (Pull-off Method)”. Similar to ASTM D7522, this

standard is suitable for both laboratory and field tests and is used to determine the bond strength of the repair. The testing procedures are similar for both standards, requiring core drilling, attachment of the dolly, and tensile load application until failure.

The locations of the pull-off tests on these bridges were randomly chosen, except in the case of the girders of the Maryland Bridge, where the cores were made at locations near the supports where maximum shear is witnessed. The depth of the cores was 0.40 in (10 mm) and diameter of the dollies used was 2 in (50 mm), as specified by ASTM C1583. Results from the pull-off tests showed significant variability. The average pull-off bond strength for all four structures ranged from 104 psi (0.72 MPa) to 522 psi (3.60 MPa), both values obtained on different columns of the same bridge. For all structures the COV is very large, where values ranged from 27.7% for the Maryland Bridge, up to 154.2% for column 1 of the St-Etienne Bridge.

Interpretation of these results is challenging for several reasons. Failure modes were not specified in this study. Therefore, it is unknown what material controlled the bond strength; whether it was a concrete substrate failure or an FRP failure. In addition, the strength of concrete at the time of testing, which most likely varied among the different bridges, has significant influence on results and is important to interpret them. Finally, the lack of baseline or control values makes it difficult to understand whether low strengths represent poor application of the repair or degradation of bond strength over time. Figure 7.1 shows a plot of the values obtained for each structure.

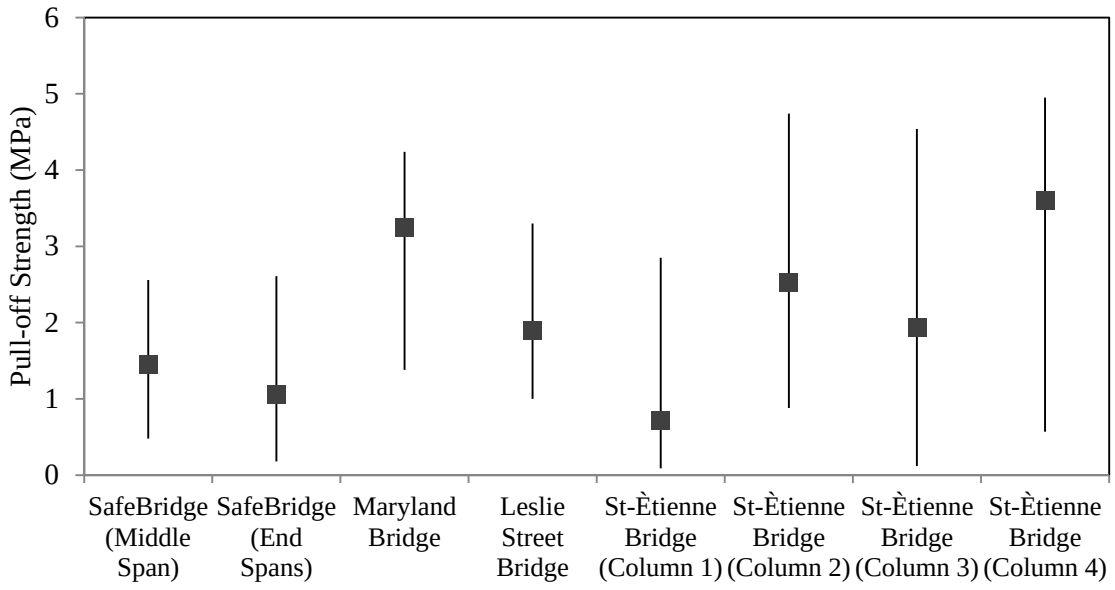

Figure 7.1. Pull-off Strength Results (Banthia, Abdolrahimzadeh, and Boulfiza, 2009). The ends of the vertical lines represent the lowest and highest values, and the boxes represent the mean values.

Another example involving pull-off tests in the field consisted of a recent quality control procedure focused on the evaluation of an FRP repair. The repair was made on the pier caps and columns of an Interstate bridge in Colorado. A total of seven pull-off tests were completed in 2011, using steel dollies with 3 in (76 mm) diameters, as opposed to the commonly used 2 in (50 mm) diameter aluminum dollies. Once again, large variations in the bond strength results were witnessed, as seen in Table 7.3. Strengths ranged from as low as 99 psi (0.683 MPa) to as high as 424 psi (2.92 MPa). The predominant failure mode was a cohesive concrete failure, also known as Mode 6, as labeled by the ICRI Technical Guideline No. 03739, equivalent to Mode G per ASTM D7522.

Table 7.3. Bond Strength Results (CTL Thompson Materials Engineers, Inc., 2011)

Location	Load		Pull-off Strength		Failure Mode	
	kN	lbs	MPa	psi	(ICRI No. 03739)	ASTM D7522
Pier 4 West side Pier Cap North	6.23	1400	1.37	198	6	G
Pier 4 West side Column North	9.34	2100	2.05	297	6	G
Pier 6 East Side Pier Cap North	3.11	700	0.68	99	5	F
Pier 6 East Side Column South	8.01	1800	1.75	254	6	G
Pier 6 West Side Pier Cap North	3.56	800	0.78	113	5	F
Pier 5 East Side Pier Cap North	9.34	2100	2.05	297	3	C
Pier 5 East Side Pier Cap South	13.34	3000	2.92	424	6	G

This example is limited by the small number of tests conducted, only one pull-off per bridge section, which makes statistical validation impossible. When conducting pull-off tests as a quality control procedure in the field, the tests are in fact destructive and repair of the surface is needed. Even though these tests are fairly simple to prepare, in the long run they can take time to complete if the amount of pull-offs becomes large. Therefore, pull-off tests do not become very practical if used as quality control.

8.0 CONCLUSIONS

This project investigated the long-term performance of FRP strengthening materials in the field and in laboratory durability tests. Special attention was paid to the bond between the FRP and concrete because it is vital to the successful function of a FRP repair. The field evaluation of the Castlewood Canyon Bridge indicated that debonding seemed to be occurring at more locations on the bridge over time. The strength of the FRP materials removed from the bridge was lower than the manufacturer provided values, but it was difficult to draw strong conclusions without more baseline data regarding the original quality of the material application. While the FRP seems to be holding up pretty well, it is recommended that if CDOT continues to use FRPs for strengthening existing bridges, the need to collect durability data should be considered at the time of the repair and provision made for establishing baseline values and a periodic testing/evaluation plan.

The laboratory component of this project was not successful at determining the durability of the FRP concrete bond when subject to common deicing chemicals due to limitations of the testing process. The direct tension pull-off test was used because it is simple and compact, but the results of this research made it apparent that the test method is very sensitive to localized conditions and can produce results with high variability. Pull-off tests are typically specified as a quality control measure by CDOT. CDOT engineers should understand the limitations of this test. Based on this research it is recommended that CDOT require pull-offs to evaluate the underlying concrete before the FRP is applied and that supplementary tests such as acoustic sounding are used to evaluate the quality of a repair. In the longer term there may be value in trying to determine a better quality control test.

FRPs provide a valuable alternative for strengthening existing concrete structures. In many situations they are likely to be the best available option. When FRP is applied by CDOT there is great value in continuing to collect data from these field applications and in conducting targeted laboratory studies to answer specific design questions.

9.0 REFERENCES

ACI 503R-93, Use of Epoxy Compounds with Concrete (Reapproved 2008). American Concrete Institute. ACI Committee 503 and ACI Committee 548. July 1993.

ACI Committee. _1997_. "Considerations for Design of Concrete Structures Subjected to Fatigue Loading." *ACI 215R-74* _reapproved 1997_, ACI, Farmington Hills, Mich.

Aidoo, J., Harries, K.A. and Petrou, M.F. (2004) "Fatigue Behavior of Carbon Fiber-reinforced Polymer-Strengthened Reinforced Concrete Bridge Girders." *Journal of Composites for Construction*, 8(6), 501-509.

Al-Hammoud, R., Soudki, K. and Topper, T.H. (2011) "Fatigue Flexural Behavior of Corroded Reinforced Concrete Beams Repaired with CFRP Sheets," *Journal of Composites for Construction*, 15(1), 42-51.

ASTMC78/C78M. (2010). "Standard test method for flexural strength of concrete (using simple beam with third-point loading)." West Conshohocken, Pennsylvania, USA.

ASTMC666/C666M. (2003). "Standard test method for resistance of concrete to rapid freezing and thawing." West Conshohocken, Pennsylvania, USA.

ASTMC672/C672M. (2003). "Standard test method for scaling resistance of concrete surfaces exposed to deicing chemicals." West Conshohocken, Pennsylvania, USA.

ASTM D3039/D3039M-08, Standard Test Method for Tensile Properties of Polymer Matrix Composite Materials. ASTM Subcommittee D30.04. American Society for Testing and Materials. Vol 15.03.

ASTM D7522/D7522M-09, Standard Test Method for Pull-Off Strength for FRP Bonded to Concrete Structures. ASTM Subcommittee D30.05. American Society for Testing and Materials. Vol 15.03.

Banthia, N., Abdolrahimzadeh. A., and Boulfiza. M. (2009). Field Assessment of FRP Sheets-Concrete Bond Durability. 1st International Conference on Sustainable Built Environment Infrastructures in Developing Countries, 301-306. Oran, Algeria.

Barlow, P. (2005). 10 Years of Seismic and Strengthening Case Histories using FRPs in the Northwest. *Materials and Processing Technologies for Revolutionary Applications, Fall Technical Conference (37th ISTC)*. October 31-November 3, 2005, Seattle, WA.

Byars, E.A., Waldron, P., Dejke, V., Demis, S., Heddadin, S. (2003). Durability of FRP in concrete Deterioration mechanisms. *International Journal of Materials & Product Technology*, 19(1-2) 28-39.

Chen, Y., Davalos, J.F., Ray, I., Kim, H. (2007). Accelerated aging tests for evaluations of durability performance of FRP reinforcing bars for concrete structures. *Composite Structures*, 78(1) 101-111.

Colorado Department of Transportation (CDOT), (2003). "Revision of Section 602." Fiber Bonded Polymer (FRP) Surface Reinforcing, not published. Construction Specification.

Crawford, K. (2008). Evaluating long-term durability of FRP-structural systems applied to concrete bridges. *CSCE 2008 Annual Conference*. Quebec, QC Proceedings, June 10-13.

Davalos, J. F., Chen, A., Ray, I., Justice, A., and Anderson,M. (2010a). "District 3-0 investigation of fiberwrap technology for bridge repair and rehabilitation (phase-III)." FHWA-PA-2010-002-510401-014, Pennsylvania Dept. of Transportation, ⟨http://trid.trb.org/view.aspx?id=915714⟩.

Dong, J.F., Wang, Q.Y. and Guan, Z.W. (2012) "Structural Behaviour of RC Beams Externally Strengthened with FRP Sheets under Fatigue and Monotonic Loading." *Engineering Structures*, 41(1), 24-33.

Eveslage, T., Aidoo, J., Harries, K. A., and Bro, W. (2010). Effect of Variations in Practice of ASTM D7522 Standard Pull-Off Test for FRP-Concrete Interfaces. *Journal of Testing and Evaluation*, 38 (4), West Conshohocken, Pennsylvania, USA.

Fafach, D., Shing, B., Chang, S., Xi, Y. (2005). Evaluation of the FRP-Retrofitted Arches in the Castlewood Canyon Bridge. Colorado Department of Transportation Research Branch. Report No. CDOT-DTD-R-2005-01.

Gartner, A., Douglas, E. P., Dolan, C. W., Hamilton, H. R. (2011). "Small beam bond test method for CFRP composites applied to concrete." J. Compos. Constr., 15(1), 52-61.

Ghosh, K., Karbhari, V.M. (2005). Evaluation of environmental effect on FRP/concrete bond. *International SAMPE Symposium and Exhibition*, 50(Proceedings) 265-279.

Green, M.F., Bisby, L.A., Beaudoin, Y., Labossiere, P. (2000). "Effect of freeze-thaw cycles on the bond durability between fiber-reinforced polymer plate reinforcement and concrete." Can. J. Civ. Eng. 27, 949-959.

Gordon, K., and Cheng, L. (2011). "Evaluation of Empirical Fatigue Prediction Models for FRP-Strengthened RC Beams." *American Concrete Institute*, ACI Special Publication, SP-275-37, pp. 1-13.

Hag-Elsafi, O., Alampalli, S., Kunin, J. (2004). In-service evaluation of a reinforced concrete T-beam bridge FRP strengthening system. *Composite Structures*, 64(2) 179-188.

Hu, A., Ren, H., Yao, Q. (2007). Durability of Concrete Structures Strengthened with FRP Laminates. *Journal of Harbin Institute of Technology (New Series)*, 14(4) 571-576.

Karbhari, V.M., Chin, J.W., Reynaud, D. (2000). Critical gaps in durability of FRP composites in civil infrastructure. *International SAMPE Symposium and Exhibition*, 45(Proceedings, May 21-25) 549-563.

Karbhari, V. M., Ghosh, K. (2009). "Comparative durability evaluation of ambient temperature cured externally bonded CFRP and GFRP composite systems for repair of bridges." Composites: Part A 40, 1353-1363.

Kim, Y.J. and Heffernan, P.J. (2008) "Fatigue Behavior of Externally Strengthened Concrete Beams with Fiber-Reinforced Polymers: State of the Art." *Journal of Composites for Construction*, 12(3), 246-256.

Ko, H., Sato, Y. (2007). "Bond Stress-Slip Relationship between FRP Sheet and Concrete under Cyclic Load" J. Compos. Constr., 11(4), 419-426.

Meneghetti, L.C., Garcez, M.R., Silva Filho, L.C.P., and P.S.L. Gastal, F. (2011) “Fatigue Life Regression Model of Reinforced Concrete Beams Strengthened with FRP.” *Magazine of Concrete Research*, 63(7), 539-549.

Micelli, F., Myers, J.J. (2008). “Durability of FRP-confined concrete”. Institution of Civil Engineers, Construction Materials 161, 173-185.

No. 210.3-2004- Guide for Using In-Situ Tensile Pull-Off Tests to Evaluate Bond of Concrete Surface Materials (formerly No. 03739). International Concrete Repair Institute (ICRI)

Reay, J.T., Pantelides, C.P. (2006). Long-Term Durability of State Street Bridge on Interstate 80. *Journal of Bridge Engineering*, 11(2) 205-216.

Rosenboom, O. and Rizkalla, S. (2006) “Behavior of Prestressed Concrete Strengthened with Various CFRP Systems Subjected to Fatigue Loading.” *Journal of Composites for Construction*, 10(6), 492-502.

Saenz, N., Walsh, E.J., Pantelides, C.P., Adams, D.O. (2004). Long-term Durability of FRP Composites for Infrastructure Rehabilitation. *SAMPE 2004 – Long Beach, CA* May 16-20, 2004.

Tan, L., Liu, X., Zhu, M. (2011). Research on Factors Affecting Durability and Improvements for FRP Reinforced Concrete Structures. *Advanced Materials Research*, 189-193(NA) 847-852.

The Concrete Society, (2000). “Design Guidance for Strengthening Concrete Structures Using Fibre Composite Materials.” Technical Report No. 55, Cromwell Press, Trowbridge, Wiltshire, UK

Toutanji, H. A., Gomez, W. (1997). “Durability Characteristics of Concrete Beams Externally Bonded with FRP Composite Sheets.” Cement and Concrete Composites 19, 351-358.

UserCom, (2000). Interpreting DSC Curves. Information for users of Mettler Toledo thermal analysis systems.

Vaysburd, A.M., McDonald, J.E. (1999). “An Evaluation of Equipment and Procedures for Tensile Bond Testing of Concrete Repairs.” Technical Report REMR-CS-61. Army Corps of Engineers, Washington, DC

Xiao, J., Li, J., Zha, Q. (2004). “Experimental Study on bond behavior between FRP and concrete”. Construction and Building Materials 18, 745-752.

Yun, Y., Wu, Y.F. (2011). “Durability of CFRP-concrete joints under freeze-thaw cycling.” Cold Regions and Science Technology 65, 401-412.

Zhang, J.S., Karbhari, V.M., Reynaud, D. (2002). Field exposure based durability assessment of FRP column wrap systems. *Composites: Part B*, 34(1) 41-50.

APPENDIX A: VOIDS, DEFECTS, AND THERMAL IMAGES

The following appendix is an account of the size and location of all notable defects, voids, cracks, and rust stains, found on the East arch during the field assessment of 2011. This documentation is intended to be a permanent record as opposed to the temporary physical markings left directly on the bridge. Details of the defects found are tabulated below. In addition, the available photographs and thermal images of the defects are organized with regard to the "bay" in which the defects were located.

Due to circumstances during the field assessment, there were a limited amount of thermal images and photographs. In some cases there was no photograph or thermal image of a particular defect. It is possible that defects with areas smaller than 5.1 cm x 5.1 cm (2" x 2") exist on the extrados of the east arch and are not documented in the table or photographs below.

Sizes and distances were approximated in cases such as the rust spot found on the extrados in the 1NW bay, seen below in Figures A1 and A2.

Table A1. Summary of Voids on the Extradoses of the Entire East Arch and One Bay of the West Arch

Summary of Defects on the Extrados of the East Arch				Location			
Void ID #	**Bay**	**2007 Size, NS x EW Units: cm (in)**	**2011 Size, Measured : NS x EW Units: cm (in)**	**Reference Column**	**Distance from reference column Units: cm (in)**	**Edge Reference**	**Distance from edge Units: cm (in)**
1	1NE		27.9 x 50.8 (11 x 20)	1NE	91.4 (36)	East	101.6 (40)
2	1NE		5.1 x 5.1 (2 x 2)	1NE	119.4 (47)	East	58.4 (23)
3,4,5	1NE		< 5.1 x 5.1 (2 x 2)	NA	NA	NA	NA
6	2NE		22.9 x 14 (9 x 5.5)	1NE	203.2 (80)	East	52.1 (20.5)
7	2NE		12.7 x 5.1 (5 x 2)	2NE	195.6 (77)	East	43.2 (17)
8	2NE		34.3 x 7.6 (13.5 x 3)	2NE	40.6 (16)	East	40.6 (16)
9	3NE		68.6 x 20.3 (27 x 8)	2NE	Near	West	15.2 (6)
10	3NE	7.6 x 12.7 (3 x 5)	24.1 x 25.4 (9.5 x 10)	2NE	195.6 (77)	West	68.6 (27)
11	3NE		52.1 x 68.6 (20.5 x 27)	2NE	256.5 (101)	West	61 (24)
12	3NE		27.9 x 30.5 (11 x 12)	2NE	317.5 (125)	West	45.7 (18)
	3NE	20.3 x 20.3 (8 x 8)	20.3 x 68.6 (8 x 27)	2NE	Near	West	15.2 (6)
13	3NE		50.8 x 10.2 (20 x 4)	3NE	152.4 (60)	East	8.9 (3.5)
14	4NE		10.2 x 3.8 (4 x 1.5)	3NE	61 (24)	West	45.7 (18)
15	6E		8.9 x 7.6 (3.5 x 3)	5NE	61 (24)	East	45.7 (18)
16	6E		10.2 x 20.3 (4 x 8)	5NE	62 (24)	West	63.5 (25)
17	4SE		29.2 x 17.8 (11.5 x 7)	4SE	Near	East	20.3 (8)
18	4SE	17.8 x 29.2 (7 x 11.5)	35.6 x 35.6 (14 x 14)	4SE	17.8 (7)	East	45.7 (18)
19	4SE		152.4 x 64.8 (60 x 25.5)	4SE	106.7 (42)	West	71.1 (28)
20	3SE		10.2 x 10.2 (4 x 4)	2SE	30.5 (12)	West	17.8 (7)
21	3SE		10.2 x 12.7 (4 x 5)	2SE	45.7 (18)	West	96.5 (38)
22	2SE		15.2 x 16.5 (6 x 6.5)	2SE	226.1 (89)	East	61 (24)
23	2SE		12.7 x 7.6 (5 x 3)	2SE	218.4 (86)	East	91.4 (36)

Table A1. Continued

Summary of Defects on the Extrados of the East Arch				Location			
Void ID #	**Bay**	**2007 Size, NS x EW Units: cm (in)**	**2011 Size, Measured : NS x EW Units: cm (in)**	**Reference Column**	**Distance from reference column Units: cm (in)**	**Edge Reference**	**Distance from edge Units: cm (in)**
24	2SE		5.1 x 10.2 (2 x 4)	2SE	165.1 (65)	East	91.4 (36)
25	1SE		14 x 16.5(5.5 x 6.5)	1SE	68.6 (27)	West	16.5 (6.5)
26,27,28	1NW		< 5.1 x 5.1 (2 x 2)	NA	NA	NA	NA

Table A2. Summary of Cracks on the Extradoses of the Entire East Arch

Crack ID #	**Bay**	**2007 Size, NS x EW Units: cm (in)**	**2011 Size, NS x EW Units: cm (in)**	**Reference Column**	**Distance from reference column Units: cm (in)**	**Edge Reference**	**Distance from edge Units: cm (in)**
1	1NE	Crack identified, length unknown	Section removed	1NE	91.4 (36)	East	101.6 (40)
2	2NE	Crack identified, length unknown	88.9 (35)	2NE	101.6 (40)	East	88.9 (35)
3	3SE	Crack identified, length unknown	NA	NA	NA	NA	NA

Table A3. Summary of Rust on the Extradoses of the Entire East Arch and One bay of the West Arch

Rust ID #	**Bay**	**2007 Size, NS x EW Units: cm (in)**	**2011 Size, NS x EW Units: cm (in)**	**Reference Column**	**Distance from reference column Units: cm (in)**	**Edge Reference**	**Distance from edge Units: cm (in)**
1	1NW	Rust identified, Size unknown	25.4 x 45.7 (10 x 18)	1NW	101.6 (40)	East	25.4 (10)

Bay 1NW: 3 Voids, 1 Rust Spot

Figure A1. Bay 1NW, 2 of the 3 small voids and rust spot

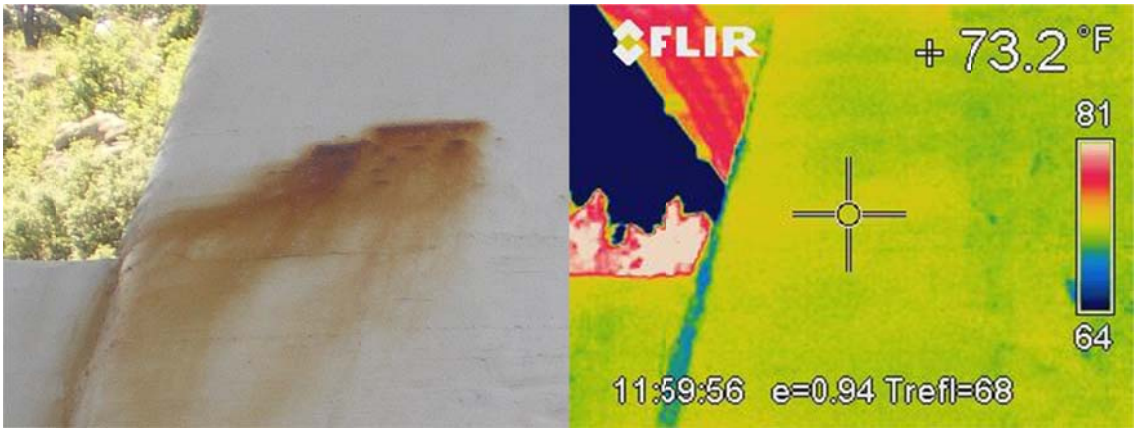

Figure A2. Photograph and thermal image of rust spot

Bay 1NE: 5 Voids, 1 Crack

Figure A3. Bay 1NE, 5 voids

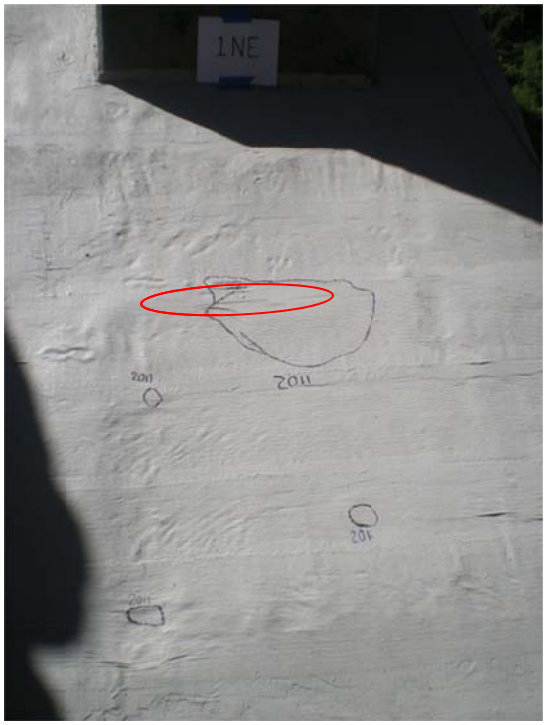

Figure A4. Bay 1NE, 4 of the 5 voids; crack exists, enclosed in red oval, in the top of the largest void

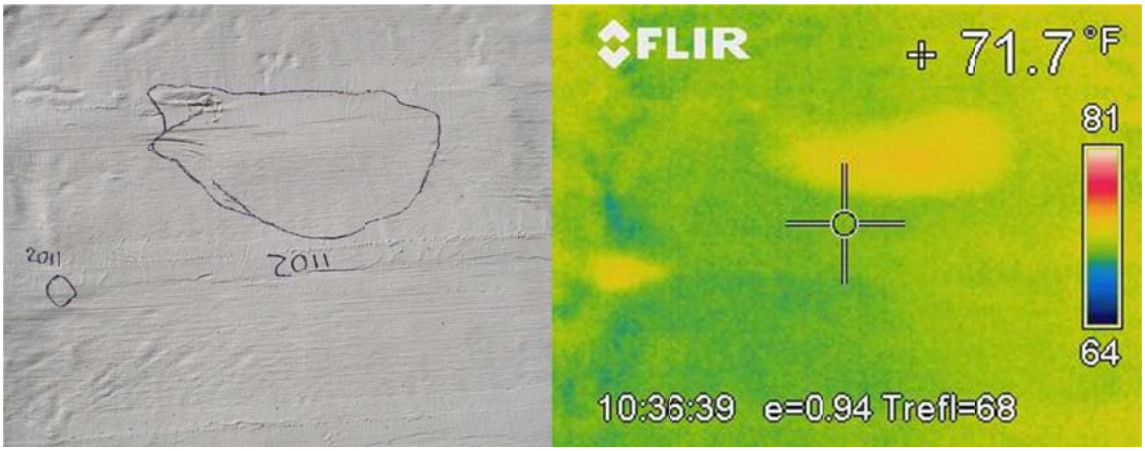

Figure A5. Photograph and thermal image of two voids in Bay 1NE

Bay 2NE: 3 Voids, 1 Crack

Figure A6. Bay 2NE, 3 voids

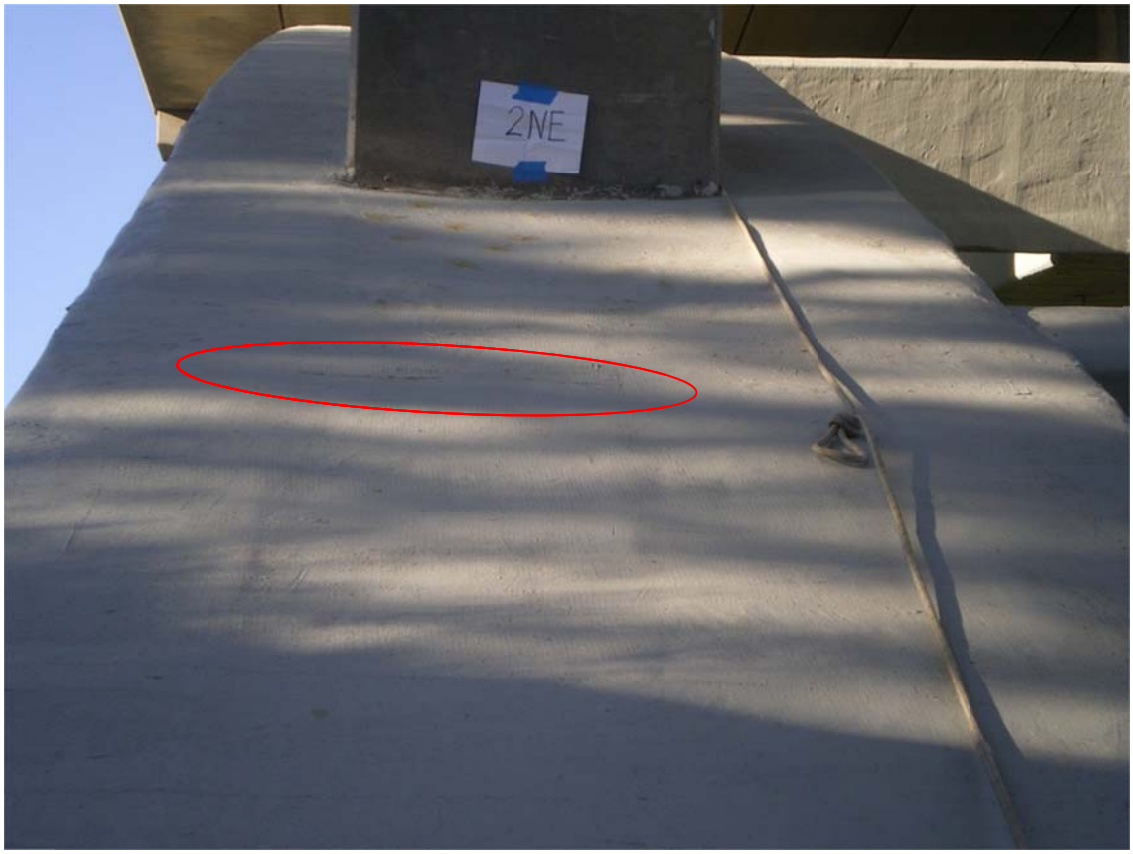

Figure A7. Bay 2NE, Crack enclosed in red oval was identified in 2007

Figure A8. Previously identified in 2007, a crack enclosed in the red oval, no debonding at the location of the crack

Bay 3NE: 5 Voids, 2 Were Identified in 2007

Figure A9. Bay 3NE with 1 of the 2 defects found in 2007 shown

Figure A10. 4 of the 5 voids found in 2011

Figure A11. Enclosed in the red circle is 1 of the 2 voids found in 2007

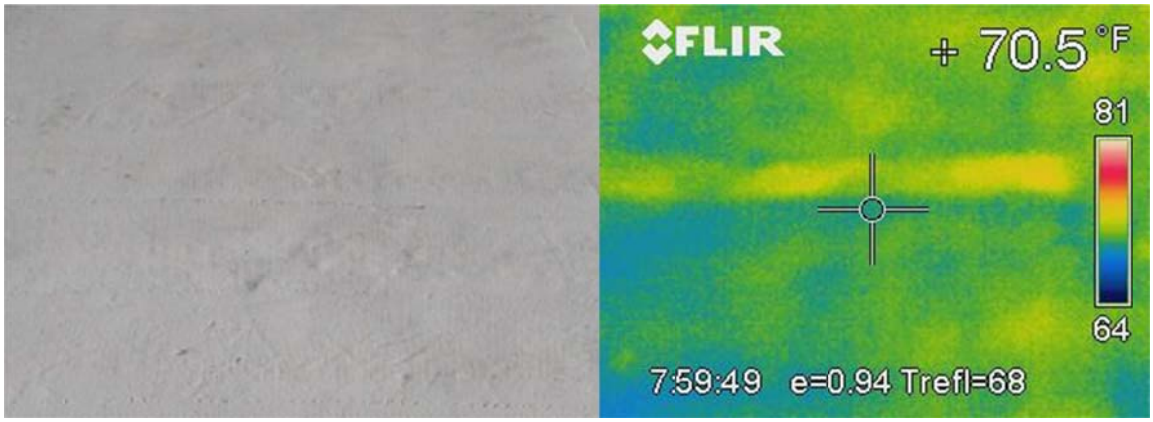

Figure A12. Photograph and thermal image of a seam in the CFRP sheets, no void present

Bay 4NE: 1 Void

Figure A13. Bay 4NE, V-shaped silicone bead water diverter

Bay 5NE: No Defects Found

Figure A14. Bay 5NE

Bay 6E: 2 Voids

No photos available

Bay 5SE: No Defects Found

Figure A15. Bay 5SE

Bay 4SE: 3 Voids, 1 Was Identified in 2007

Figure A16. Bay 4SE

Figure A17. Void from 2007 has grown and a new void developed

Bay 3SE: 2 Voids, 1 Crack

Figure A18. Bay 3SE

No photograph available for the previously identified cracks in 3SE or the two small voids, but the thermal image is below

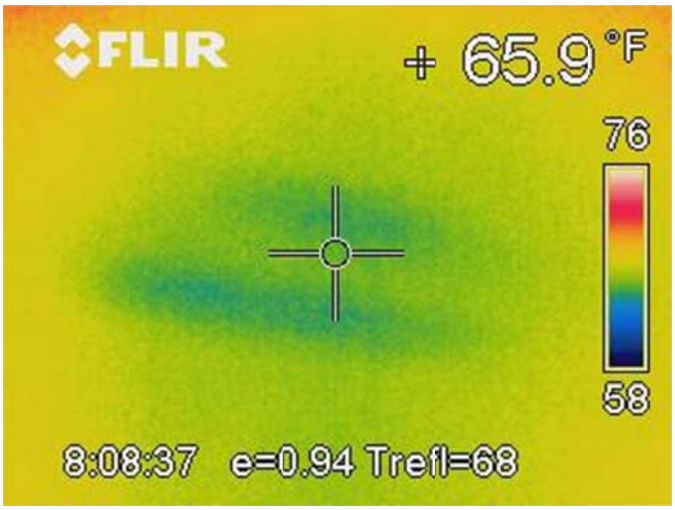

Figure A19. Thermal image of cracks previously identified in 2007

Bay 2SE: 3 Voids

Figure A20. Bay 2SE

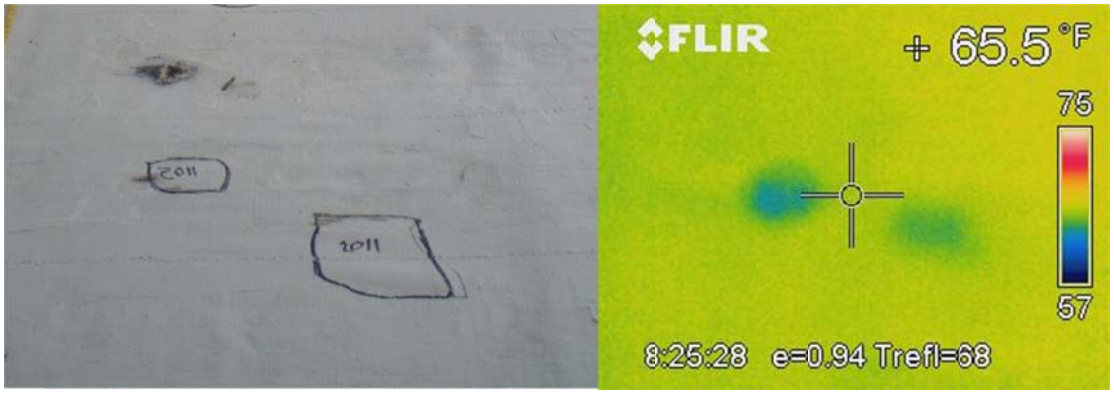

Figure A21. Photograph and thermal image of two voids

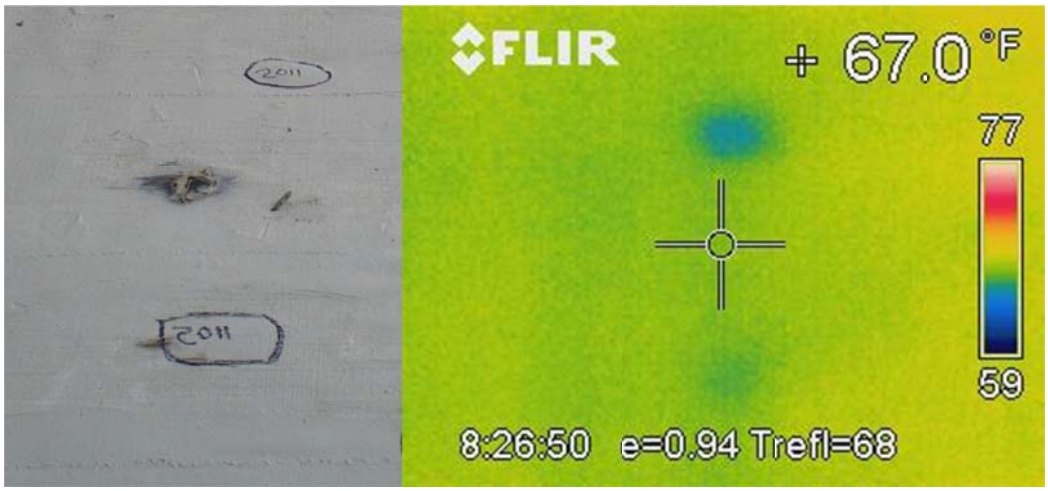

Figure A22. Photograph and thermal image of two voids, the black color in the photograph is leftover strain gauges from the work done by Colorado University of Boulder

Bay 1SE: 1 Void

Figure A23. Bay 1SE, 1 void

Bay 1SW: 1 Defect

Figure A24. Photograph and thermal image of a defect found in Bay 1SW

APPENDIX B: PULL-OFF TEST RESULTS

Table B1. Pull-off Test Results from 2011

Global Test Number	Date	Test No.	Core Diameter		Tensile Bond Strength		Failure Mode (ASTM A-G)
			mm	in	MPa	psi	
Test Location: North End of East Arch (1NE)							
1	7/11/2011	1	50	2	1.63	237	F
2	7/11/2011	2	50	2	2.07	300	A
3	7/11/2011	3	50	2	2.93	425	A
4	7/11/2011	4	50	2	1.54	224	E
5	7/12/2011	5	50	2	1.92	279	F
6	7/12/2011	6	50	2	2.39	346	F
7	7/12/2011	7	50	2	2.25	327	F
8	7/12/2011	8	50	2	1.15	167	E
9	7/12/2011	9	50	2	1.35	196	F
Test Location: North End of West Arch (1NW)							
10	7/12/2011	1	50	2	1.03	150	E
11	7/12/2011	2	50	2	NA	NA	NA
12	7/12/2011	3	50	2	1.03	150	E
13	7/12/2011	4	50	2	0.83	120	E
14	7/12/2011	5	50	2	1.15	167	E
15	7/12/2011	6	50	2	0.52	76	E
16	7/12/2011	7	50	2	NA	NA	NA
17	7/12/2011	8	50	2	3.81	553	G
18	7/12/2011	9	50	2	3.42	496	F

Table B1. Continued

Global Test Number	Date	Test No.	Core Diameter		Tensile Bond Strength		Failure Mode (ASTM A-G)
			mm	in	MPa	psi	
Test Location: Center of East Arch (6E)							
19	7/12/2011	1	50	2	3.35	486	B/F
20	7/12/2011	2	50	2	3.09	448	B/F
21	7/12/2011	3	50	2	2.55	370	G
22	7/12/2011	4	50	2	1.98	287	G
23	7/12/2011	5	50	2	0.74	108	G
24	7/12/2011	6	50	2	1.79	260	G
25	7/12/2011	7	50	2	3.08	446	G
26	7/12/2011	8	50	2	0.13	19	G
27	7/12/2011	9	50	2	2.50	363	G

Table B2. Pull-off Test Results from 2003

Global Test Number	Date	Test No.	Core Diameter		Tensile Bond Strength		Failure Mode (ASTM A-G)
			mm	in	MPa	psi	
Test Location: 1SE							
1	6/10/2003	1	50	2	2.59	375	A
2	6/10/2003	2	50	2	3.43	498	A
3	6/10/2003	3	50	2	4.12	597	G
4	6/10/2003	4	50	2	NA	NA	NA
5	6/10/2003	5	50	2	4.09	593	G
6	6/10/2003	6	50	2	3.24	470	G
Test Location: 1SW							
7	6/10/2003	1	50	2	4.07	590	G
8	6/10/2003	2	50	2	3.52	510	G
9	6/10/2003	3	50	2	3.50	508	E
10	6/10/2003	4	50	2	3.34	485	G
11	6/10/2003	5	50	2	3.03	439	A
12	6/10/2003	6	50	2	3.03	440	G

Table B2. Continued

Global Test Number	Date	Test No.	Core Diameter		Tensile Bond Strength		Failure Mode (ASTM A-G)
			mm	in	MPa	psi	
Test Location: 1NW							
13	6/13/2003	1	50	2	3.54	513	A
14	6/13/2003	2	50	2	3.54	514	G
15	6/13/2003	3	50	2	3.94	572	A
16	6/13/2003	4	50	2	3.76	545	A
17	6/13/2003	5	50	2	3.45	501	A
18	6/13/2003	6	50	2	3.25	471	A
Test Location: 6E							
19	6/30/2003	1	50	2	3.03	439	G
20	6/30/2003	2	50	2	3.12	452	G
21	6/30/2003	3	50	2	3.25	471	G
Test Location: 6W							
22	6/30/2003	1	50	2	3.30	478	G
23	6/30/2003	2	50	2	2.72	395	G
24	6/30/2003	3	50	2	2.99	433	G
Test Location: 5SE							
25	7/9/2003	1	50	2	1.32	191	A
26	7/9/2003	2	50	2	1.50	217	G
27	7/9/2003	3	50	2	1.67	242	G
Test Location: 5SW							
28	7/9/2003	1	50	2	2.81	408	E
29	7/9/2003	2	50	2	2.72	395	G
30	7/9/2003	3	50	2	2.90	420	G
Test Location: 5NE							
31	7/17/2003	1	50	2	2.94	427	G
32	7/17/2003	2	50	2	2.76	401	G
33	7/17/2003	3	50	2	NA	NA	NA
Test Location: 5NW							
34	7/17/2003	1	50	2	1.76	255	G
35	7/17/2003	2	50	2	1.89	274	G
36	7/17/2003	3	50	2	NA	NA	NA

Table B2. Continued

Global Test Number	Date	Test No.	Core Diameter		Tensile Bond Strength		Failure Mode (ASTM A-G)
			mm	in	MPa	psi	
Test Location: 4NE							
37	7/17/2003	1	50	2	2.24	325	G
38	7/17/2003	2	50	2	3.03	439	G
39	7/17/2003	3	50	2	2.19	318	G
Test Location: 4NW							
40	7/17/2003	1	50	2	2.68	389	F
41	7/17/2003	2	50	2	2.72	395	F
42	7/17/2003	3	50	2	3.56	516	F

Table B3. Average Values of Bond Strength

Averages	MPa	psi
2003 Tests	2.99	433.36
2011 Tests	1.93	280.00
% Decrease	35.4	

Corresponding photographs to the 2011 pull-off tests:

Bay 1NE

Figures B1 and B2. Tests No.1 and 2

Figure B3. Test No.3, Photograph of test No.4 is not available

Figures B4 and B5. Test No.5, note puck slid off of center while epoxy was setting, and test No. 6

Figures B6 and B7. Test No.7 and test No.8, weak bond strength

Figure B8. Test No.9, weak bond strength

Bay 1NW

Figure B9. Test No.10, weak bond strength, and test No.11 not available, cored area failed during drilling

Figures B10 and B11. Test No.12, weak bond strength, and test No.13, weak bond strength

Figures B12 and B13. Test No.14, weak bond strength, and test No.15, weak bond strength

Test No.16 not available, puck had faulty threads

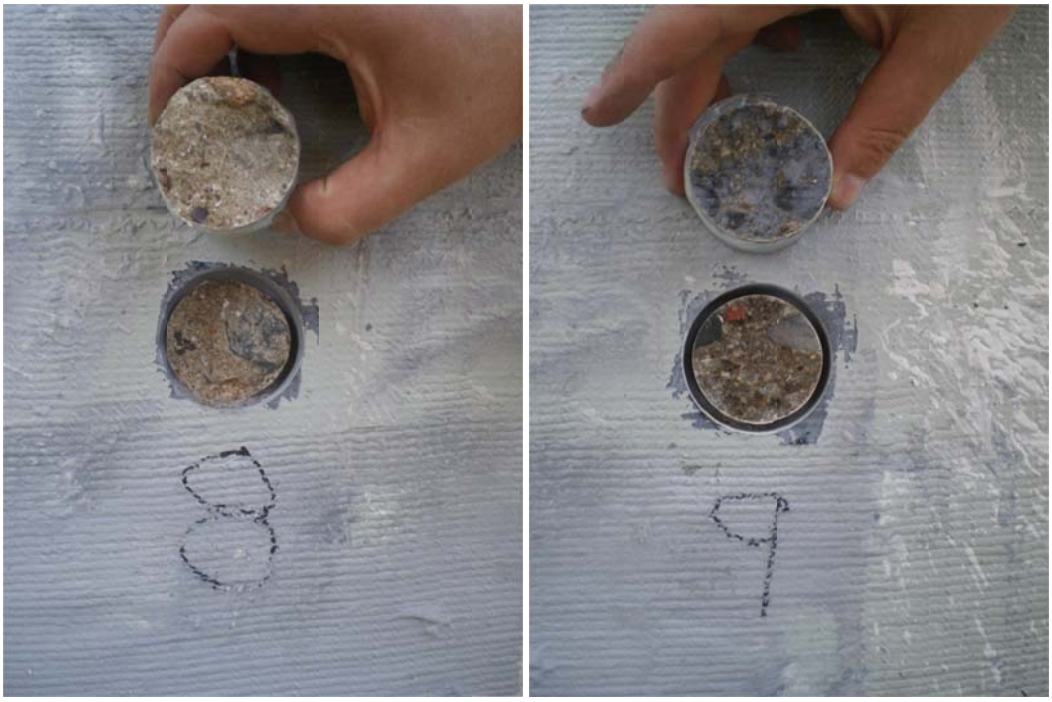

Figures B14 and B15. Tests No.17 and 18

Bay 6E

Figures B16 and B17. Tests No.19 and 20

Figures B18 and B19. Tests No.21 and 22

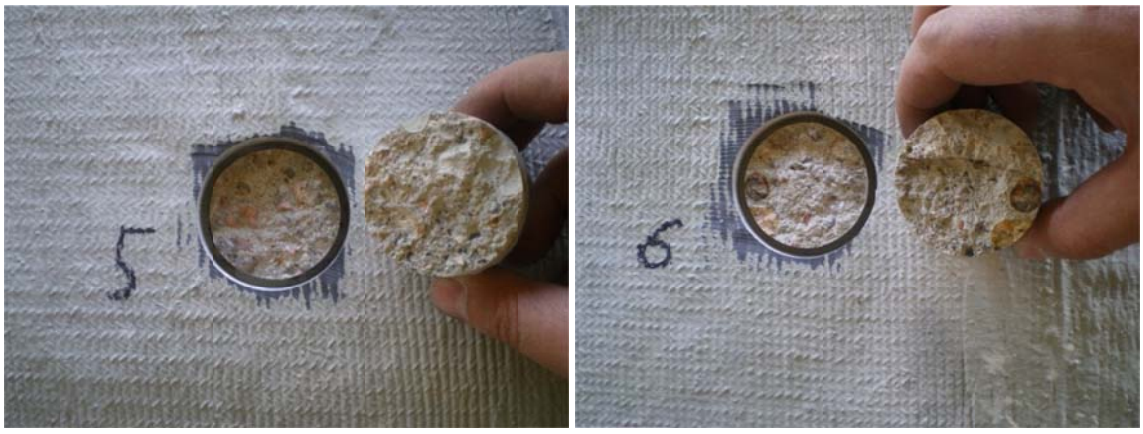

Figures B20 and B21. Test No.23, weak bond strength (poorly mixed concrete?), and test No.24

Figures B22 and B23. Test No.25 and test No.26, note very weak bond strength (poorly mixed concrete?)

Figure B24. Test No.27

APPENDIX C: TENSILE TEST RESULTS

Table C1. 2011 Tensile Tests

Specimen ID	Width		Thickness		Actual Area of 1 Layer		Normalized Area of 1 Layer	
	mm	in	mm	in	mm^2	in^2	mm^2	in^2
Small Patch from Bay 1NE								
1	25.7	1.01	2.39	0.09	61.3	0.10	26.1	0.040
2	25.9	1.02	2.95	0.12	76.2	0.12	26.3	0.041
3	27.0	1.06	3.23	0.13	87.0	0.13	27.4	0.042
4	25.9	1.02	3.20	0.13	82.9	0.13	26.3	0.041
5	25.8	1.02	2.87	0.11	74.1	0.11	26.2	0.041
6	26.0	1.02	2.79	0.11	72.6	0.11	26.4	0.041
7	25.9	1.02	2.67	0.11	69.0	0.11	26.3	0.041
8	25.9	1.02	2.54	0.10	65.7	0.10	26.3	0.041
9	25.9	1.02	3.15	0.12	81.5	0.13	26.3	0.041
10	25.2	0.99	3.63	0.14	91.6	0.14	25.6	0.040
11	25.8	1.02	3.53	0.14	91.1	0.14	26.2	0.041
12	25.9	1.02	3.11	0.12	80.5	0.12	26.3	0.041
Large Patch from Bay 3NE								
1	26.1	1.03	3.15	0.12	82.2	0.13	26.5	0.041
2	26.5	1.04	3.33	0.13	88.2	0.14	26.9	0.042
3	26.0	1.02	3.56	0.14	92.4	0.14	26.4	0.041
4	26.2	1.03	3.53	0.14	92.5	0.14	26.6	0.041
5	26.0	1.02	3.48	0.14	90.5	0.14	26.4	0.041
6	26.6	1.05	3.33	0.13	88.5	0.14	27.0	0.042
7	25.5	1.00	3.48	0.14	88.6	0.14	25.9	0.040
8	26.5	1.04	3.58	0.14	94.9	0.15	26.9	0.042
9	26.5	1.04	3.35	0.13	88.7	0.14	26.9	0.042
10	25.9	1.02	3.51	0.14	90.9	0.14	26.3	0.041
11	26.4	1.04	3.12	0.12	82.5	0.13	26.8	0.042
12	26.4	1.04	3.61	0.14	95.3	0.15	26.8	0.042
Manufacturer's Data			1.016	0.04				

Table C1. Continued

Specimen ID	Tensile Force		Normalized Tensile Strength		Normalized MoE		Rupture Strain	Failure Mode
	N	lb (f)	MPa	ksi	GPa	ksi		
Small Patch Removed from Bay 1NE								
1	1197	5324	36.7	5.3	79.3	11506	0.00046	SGM
2	1100	4892	16.9	2.4	87.7	12714	0.00019	LAT
3	1064	4732	10.9	1.6	74.8	10852	0.00015	LAB
4	1039	4621	8.0	1.2	88.2	12795	0.00009	LWB
5	939	4176	5.8	0.8	84.6	12272	0.00007	SGM
6	1123	4996	5.7	0.8	82.7	11998	0.00007	SGM
7	1305	5807	5.7	0.8	72.2	10476	0.00008	XGM
8	1115	4960	4.3	0.6				SGM
9	1106	4920	3.8	0.5	103.3	14982	0.00004	MAB
10	907	4035	2.8	0.4	66.5	9649	0.00004	LGM
11	1050	4669	2.9	0.4	71.3	10335	0.00004	LGM
12	1149	5110	2.9	0.4				AWT
Large Patch Removed from Bay 3NE								
1	878	3906	26.9	3.9				SAB
2	1115	4961	17.1	2.5	75.4	10942	0.00023	LWB
3	840	3737	8.6	1.2	61.1	8855	0.00014	LAB
4	1041	4632	8.0	1.2	69.8	10123	0.00011	LAT
5	756	3365	4.6	0.7	88.1	12779	0.00005	SGM
6	1164	5179	6.0	0.9	72.2	10477	0.00008	MGM
7	933	4151	4.1	0.6	91.4	13255	0.00004	SAT
8	1274	5666	4.9	0.7	85.5	12397	0.00006	LAT
9	960	4269	3.3	0.5	102.3	14843	0.00003	LAT
10	1078	4795	3.3	0.5	61.6	8929	0.00005	LWB
11	781	3474	2.2	0.3	54.8	7955	0.00004	LAB
12	297	1320	0.8	0.1	51.3	7437	0.00001	LAB
Manufacturer's Data			875.6	127	72.4	10500	0.01210	

Table C2. Average Values for Each Sample

Averages	Tensile Force		Normalized Tensile Strength		Normalized MoE		Rupture Strain
	N	lb(f)	MPa	ksi	GPa	ksi	
Bay 1NE	1091	4854	820	119	81	11758	0.010121
Bay 3NE	926	4121	688	100	74	10726	0.009306
Total	1009	4487	754	109	78	11242	0.009713